Development of Epitaxial Lift-off Technique for II-VI Semiconductor Heterostructures

NIROSH M ELDOSE

Submitted for the Doctorate degree of Philosophy

Heriot-Watt University

Institute of Photonics and Quantum Sciences

School of Engineering and Physical Sciences

December 2020

Abstract

In this thesis, I present current advances with Heriot Watt MBE group II-VI epitaxial lift-off (ELO) technique. Discussing potential structures and devices that can be created using this technology, structures not currently achievable by standard fabrication techniques. ELO is a post growth process which is used to lift off layers grown on the substrate and transfer them to different surfaces. The main advantage of ELO technique is that it can be used to create a new structure by stacking multiple layers and changing the relative orientations of adjacent layers. I present the stacking of ZnSe (1-5 μm) and ZnSe/ZnCdSe single quantum well (QW) structure grown on GaAs (100) and GaAs (211) B substrates. The QW grown structure was lifted off using the highly reactive MgS layer as the sacrificial layer, with etch rate difference of ZnSe of approximately 10^8:1 in dilute HCl (30%). The lifted layers were transferred onto a glass plate and stacked 15 layers on top of each other forming a multi quantum well (MQW) structure. The optical characterization was done by photoluminescence (PL) spectroscopy showing no obvious degradation after ELO. Also, the range of structures which can be lifted has been extended further with ZB MgS growth on GaAs (211) B substrates, allowing ELO of (211) ZnSe. This can be used for generating II-VI non-linear quasi phase matched (QPM) devices.

Acknowledgement

I offer my sincere gratitude to my supervisor Dr. Ajoy K Kar, who helped me sail through my journey in PhD with his patience and knowledge, at the same time gave me the freedom and space to work in my own way. I am extremely lucky to have a supervisor who cared much throughout my research.

I also thank Dr. Kevin Prior for all his guidance during my PhD. He retired early during the beginning of my PhD, nevertheless he was very resourceful and helped me to think beyond the surface level by challenging and instigating thought-provoking ideas.

A special thanks to Dr. Richard Moug, for all those stimulating conversations and thoughts. The technical support from Dr. Richard Moug helped me troubleshoot in the lab and we shared many research ideas.

I thank my office mates, Harikumar K, Vikram Kamaljith and David Carvalho for sharing a wonderful time with me. I am eternally grateful to my family, especially my mother for her constant support, both morally and financially. Thanks to my sister Neethu M. Eldose for all the support.

Research Thesis Submission

Please note this form should be bound into the submitted thesis.

Name:	NIROSH M ELDOSE		
School:	EPS		
Version: *(i.e. First, Resubmission, Final)*	Final	Degree Sought:	PhD (Physics)

Declaration

In accordance with the appropriate regulations I hereby submit my thesis and I declare that:

1. The thesis embodies the results of my own work and has been composed by myself
2. Where appropriate, I have made acknowledgement of the work of others
3. The thesis is the correct version for submission and is the same version as any electronic versions submitted*.
4. My thesis for the award referred to, deposited in the Heriot-Watt University Library, should be made available for loan or photocopying and be available via the Institutional Repository, subject to such conditions as the Librarian may require
5. I understand that as a student of the University I am required to abide by the Regulations of the University and to conform to its discipline.
6. I confirm that the thesis has been verified against plagiarism via an approved plagiarism detection application e.g. Turnitin.

ONLY for submissions including published works

Please note you are only required to complete the Inclusion of Published Works Form (page 2) if your thesis contains published works)

7. Where the thesis contains published outputs under Regulation 6 (9.1.2) or Regulation 43 (9) these are accompanied by a critical review which accurately describes my contribution to the research and, for multi-author outputs, a signed declaration indicating the contribution of each author (complete)
8. Inclusion of published outputs under Regulation 6 (9.1.2) or Regulation 43 (9) shall not constitute plagiarism.

* *Please note that it is the responsibility of the candidate to ensure that the correct version of the thesis is submitted.*

Signature of Candidate:		Date:	20/12/2020

Submission

Submitted By *(name in capitals):*	NIROSH M ELDOSE
Signature of Individual Submitting:	
Date Submitted:	20/12/2020

For Completion in the Student Service Centre (SSC)

Limited Access	Requested	Yes		No		Approved	Yes		No	
*E-thesis Submitted (**mandatory for final theses**)*										
Received in the SSC by *(name in capitals):*						Date:				

TABLE OF CONTENTS

List of Figures

List of Tables

LIST OF PUBLICATIONS

1. N.M. Eldose, J Zhu, N. Mavridi, K.A. Prior, R.T. Moug, Molecular beam epitaxial growth of zinc blende MgS on GaAs (211) B substrates, Journal of Crystal Growth **485** (2018) 86–89.

2. N.M. Eldose, J. Zhu, N. Mavridi, K.A. Prior and R.T. Moug, Stacking of ZnSe/ZnCdSe Multi-Quantum Wells on GaAs (100) by Epitaxial Lift-Off, Journal of Electronic Materials **47**, (2018) 4366-4369.

3. N. Mavridi, N.M. Eldose, J Zhu, K.A. Prior and R.T. Moug, Adhesion Measurements of Epitaxially Lifted MBE-Grown ZnSe Journal of Electronic Materials **47** (2018) 4394-4398.

4. N. Mavridi, N.M. Eldose, K.A. Prior, R.T. Moug, Optimization of the MBE growth of metastable zinc blende MnS on GaAs (100) substrates using ZnS as sulphur source Journal of Crystal Growth **511** (2019) 61–64

CHAPTER 1

1.1 Introduction

The study of ZnSe-based II-VI semiconductors grown by Molecular Beam Epitaxy (MBE) has been ongoing for more than forty years since the first growth of ZnSe layers on GaAs substrates by Yao in 1977 [1]. The commercial motivation for this research was a desire to emulate the success of GaAs based III-V semiconductor materials in producing orange, red and near-infrared wavelength light emitting devices (LEDs) and laser diodes (LDs). ZnSe based materials have larger bandgaps than GaAs based materials and paves the way to deliver LEDs and LDs in the green, blue and near- ultraviolet (UV) wavelength regions. The research into ZnSe-based materials was thus based on a desire for devices which would facilitate the production of full-colour display and, because of their shorter wavelength, allow for a large density of data storage on optically-addressed compact discs [2].

II-VI semiconductor material has wide range of band gap energy from HgTe (0eV) to BeSe (6eV). This wide range of band gap II-VI materials can interact with wavelengths in the visible and UV region of the electromagnetic spectrum. Interest in these materials originally stemmed from the development of solar cells [3] and electroluminescent phosphors [4], and the wish to fabricate long wavelength IR sensors-based HgCdTe [5] and blue laser diodes on ZnSe [6]. Although the outstanding success of the GaN devices has reduced interest in the development of ZnSe based blue laser diodes. Even though research in the field of IR detectors and solar cells still continues. Another active area of interest for this group of materials is the investigation of dilute magnetic semiconductors (DMS) [7].

One of the principal limitations in the development of II-VI semiconductor compounds is the necessity to grow II-VI material on III-V substrate [8]. This is due to the high cost and

poor quality of commercially available the II-VI substrate. The lattice mismatch of the substrate and epilayers cause strain between two layers, which leads to the formation of large dislocation density, resulting degradation of material quality [9]. As a consequence, the lifetime of active devices such as LEDs and lasers has been reduced [10]. The use of II-VI epitaxial layers for optoelectronic devices is also depends on the realisation of p and n type doping in the same material [11], it also proved difficult to p-type dope II-VI material, leading to non-ohmic contact and subsequent increasing in operating voltage and temperature which hastened the degradation of devices [12].

1.2 Fabrication Technology

Fabrication technology plays a crucial part in the development of any semiconductor material. Both molecular beam epitaxy (MBE) [13] and metal-organic chemical vapour deposition (MOCVD) [14] offer nanometre precision on epitaxial layer thickness, composition, interface quality and uniformity during growth of compound semiconductors. These fabrication techniques will give the advantage of altering the band gap of the materials by changing the growth parameters and doping with other materials [15], which can create structure such as quantum well (QW) and quantum dot (QD) [16][17]

1.3 II-VI material research at Heriot Watt

The MBE group at Heriot Watt University was established in 1988 and the first high quality ZnSe epitaxial layers were grown in May 1989 [18]. Research in the first few years was devoted to issues concerning II-VI laser development, which culminated in 1992 with the first demonstration of a blue QW ZnSe/$Zn_{0.8}Cd_{0.2}Se$ laser in Europe [19]. Following the shift away from blue laser development, the group continues with various different topics related to the structural properties and fundamental spectroscopy of II-VI semiconductors [20]. Later, the group has developed ZnS based layers on both GaAs and

GaP which has resulted in the fabrication of ZnS/ZnCdS lattice matched QW structures [21].

The group has been also exploring novel growth techniques, with the aim of finding new materials which exhibit very large exciton binding energies. The growth of MgS in zinc blende (ZB) crystal structure was successfully demonstrated for the first time and grown thick layer up to 130 nm thick [22]. MgS has a potential wide bandgap of ~5 eV and it opened up the possibilities of epitaxial lift- off (ELO) technique [23]. The other ongoing research include studies of ferromagnetic and antiferromagnetic properties by growing transition metal sulphides such MnS, CrS, and MnCrS [25]. For the first time, I have demonstrated that ELO can combine thin films of dissimilar materials to create structures that are not currently achievable by standard growth and processing techniques [24].

1.4 Overview of thesis

The growth of ZB MgS for the development of ELO technique has discussed in this thesis. ELO is a post growth process enables the separation of II-VI layers from GaAs substrate and manipulated as freestanding films. ELO layers have been successfully transferred to alternative substrates such as glass, laser diodes [26], distributed Bragg reflectors (DBRs)[27], $LiNbO_3$[28]. ELO layers can be assembled into complex structures with many different types of materials to generate devices, not currently possible by normal thin film growth techniques due to fundamental material limitation.

The chapter 2 contains description of Heriot Watt MBE system with *in situ* monitoring technique, Reflection High Energy Electron Diffraction (RHEED). Also, the various characterisation technique including Photoluminescence (PL) and X ray diffraction (XRD) explained in detail with some background theory and experimental setup.

The crystal structure of MgS in bulk is rocksalt and it is quite difficult to grow in ZB structure. The growth of ZB MgS on GaAs (100) substrate using MBE is discussed in

chapter 3. Pyrometer and thermocouple measurements are used to monitor the accuracy in substrate temperature during the ZB MgS growth. The growth of ZB MgS on GaAs substrate is investigated by XRD and RHEED. Double Crystal X-ray Rocking Curves (DCXRC) were used to determine growth rate of epitaxial layer. Intense PL measurements, details of the procedures used, and the results obtained will be presented.

Chapter 4 discusses the use of ZB MgS as a sacrificial layer for ELO process. An MBE QW structure is grown and lifted using ELO technique and which was then transferred onto glass plate. The multiple ELO layers were then stacked on top of each other to form a triple QW structure. This stacked structure was compared to an MBE grown multi quantum well (MQW) structure of similar design. The quality of these structures was compared with PL measurements, there was no shift in the PL peak position and less degradation of the sample. The structural quality of the lifted layer was maintained after lift-off. There was increase in PL intensity observed in stacked layers compared with grown MBE structure which will be discussed in detail.

In chapter 5, the growth of ZB MgS on GaAs (211) B substrate is presented for the first time. When the strained layers are grown on low symmetry surfaces such as (211), there is a large polarisation field due to the internal piezoelectric effect. Also, there is a refractive index dependence for the transmitted light related to the surface orientation of the epilayer which is the focus of the current work on (211) oriented layers. RHEED patterns were monitored during the growth. XRD and PL was used to characterise the grown structure.

If the II-VI layer can be removed from the GaAs (211) B substrate, by technique such as ELO and stacking in different crystal orientations with period (1 μm), then these (h11) oriented layers allow devices to be constructed which optimize second harmonic generation. In chapter 6, presents the stacking of ZnSe layers with a period of 20 μm per crystal orientation. Considering normal growth rates for single crystal ZnSe range from

0.2-1μ/h growing each period via MBE would take an impractical amount of time. Stacked layer thickness was measured by using DEKTAK thickness profiler.

Chapter 7 includes the summary of the results presented in this thesis along with the conclusions drawn from the collected data. Information about future research related to the MgS material and devices will be discussed.

REFERENCES

[1] T. Yao, Y. Miyoshi, Y. Makita and S. Maekawa, "Growth rate and sticking coefficient of ZnSe and ZnTe grown by Molecular Beam Epitaxy," Japanese Journal of Applied Physics, vol. 16, pp. 369-373, 1977.

[2] S. Tanaguchi, T. Hino, S. Itoh, K. Nakano, N. Nakayama, A. Ishibashi and M. Ikeda, "100h II-VI blue-green laser diode," Electronics Letters , vol. 32, pp. 552 - 553, 1996.

[3] M. Yamaguchi, "Present status and prospects of photovoltaic technologies in Japan," Renewable and Sustainable Energy Reviews, vol. 5, pp. 113-135, 2001.

[4] P. D. Rack and P. H. Holloway, "The structure, device physics, and material properties of thin film electroluminescent displays," Materials Science and Engineering: R: Reports, vol. 21, pp. 171-219, 1998.

[5] R.K.Willardson, Semiconductors and Semimetals, New York : Academic Publishers, 1982.

[6] K. A. Prior, "The development of II–VI semiconductors for blue diode lasers," Contempororary Physics, vol. 37, pp. 345-358, 2006.

[7] T. Dietl, "Magnetic Semiconductors," in Handbook on Semiconductors, T. Moss and S. Mahajan, North Holland, 1992, pp. III 5 1-5.

[8] H. H. Farrell, M. C. Tamargo and J. L. de Miguel, "Optimal GaAs(100) substrate terminations for heteroepitaxy," Applied Physics Letters, vol. 58, pp. 355-357, 1991.

[9] G. Horsburgh, K. A. Prior, W. Meredith, I. Galbraith, B. C. Cavenett, C. R. Whitehouse, G. Lacey, A. G. Cullis, P. J. Parbrook, P.M¨ock and K. Mizuno, "Topography measurements of the critical thickness of ZnSe grown on GaAs," Applied Physics Letters, vol. 72, pp. 3148-3150, 1998.

[10] M. Fukuda, Reliability and Degradation of Semiconductor Lasers and LEDs, Artech House, 1991.

[11] R. N. Bhargava, "Compact blue lasers in the near future," Journal of Crystal Growth, vol. 117, pp. 894-901, 1992.

[12] Y. Fan, J. Han, L. He, J. Saraie, R. L. Gunshor, M. Hagerott, H. Jeon, A. V. Nurmikko, G. C. Hua and N. Otsuka, "Graded band gap ohmic contact to p-ZnSe," Applied Physics Letters, vol. 61, pp. 3160-3162, 1992.

[13] E. H. C. Parker, The Technology and Physics of Molecular Beam Epitaxy, Plenum Press, 1985.

[14] M. Razeghi, MOCVD Technology and its Applications, Institute of Physics Publishing, 1992.

[15] S. Mahajan and K. S. Sree Harsha, Principles of growth and processing of semiconductors, McGraw-Hill, 1998.

[16] T. Wenckebach, Essentials of Semiconductor Physics, J. Wiley and Sons, 1999.

[17] D. Bimberg, M. Grundmann and N. N. Ledenstov, Quantum dots Heterostrucutures, J. Wiley and Sons, 1999.

[18] K.A.Prior, J.M.Wallace, J.J.Hunter, S.J.A.Adams, M.J.L.S.Haines, M.Saoudi and B.C.Cavenett, "Growth of MBE ZnSxSe1−x using a novel electrochemical sulphur source," Journal of Crystal Growth, vol. 101, pp. 176-179, 1990.

[19] I. S. Hauksson, S. Y. Wang, J. Simpson, M. R. Taghizadeh, K. A. Prior and B. C. Cavenett, "Development and characterization of II–VI blue-green diode lasers," Physica B: Condensed Matter, vol. 191, pp. 124-129, 1993.

[20] J. S. Milnes, C. Morhain, S. A. Telfer, W. Meridith, T. A. Steele, K. A. Prior and B. C. Cavenett, "A spectroscopic study of the piezoelectric effect in ZnSe/ZnCdSe

single quantum wells grown on (2 1 1)B GaAs," Journal of Crystal Growth, vol. 184, pp. 714-717, 1998.

[21] S. A. Telfer, C. Morhain, B. Urbaszek, C. O'Donnell, P. Tomasini, A. Balocchi, K. A. Prior and B. C. Cavenett, "MBE growth of ZnS and ZnCdS layers on GaP," Journal of Crystal Growth, Vols. 214-215, pp. 197-201, 2000.

[22] B. C, C. B. O'Donnell, B. Urbaszek, A. Balocchi, C. Morhain, K. A. Prior and B. C. Cavenett, "Growth of zinc blende MgS/ZnSe single quantum wells by molecular-beam epitaxy using ZnS as a sulphur source," Applied Physics Letters, vol. 76, pp. 3929-3931, 2000.

[23] C. Bradford, A. Currran, A. Balocchi, B. C. Cavenett, K. A. Prior and R. J. Warburton, "Epitaxial lift-off of MBE grown II–VI heterostructures using a novel MgS release layer," Journal of Crystal Growth, vol. 278, pp. 325-328, 2005.

[24] J. Zhu, N. M. Eldose, N. Mavridi, K. A. Prior and R. T. Moug, "Molecular beam epitaxial growth of zinc blende MgS on GaAs (211) B substrates," Journal of crystal growth, vol. 485, pp. 86-89, 2018.

[25] L. David and K. A. Prior , "Determination of the lattice constant of CrS from Mn1–xCrxS MBE epitaxial layers," Phys. Stat. sol., vol. 4, pp. 778-781, 2006.

CHAPTER 2

Heriot Watt MBE system and Characterisation Techniques

2.1 Introduction

There are many different crystal growth techniques used to produce high quality semiconductors. The technique used in this thesis is molecular beam epitaxy (MBE), which was developed in late 1960s [1]. MBE is crystal growth technique that allows high quality compound semiconductor layers to be grown with monolayer precision.

This chapter outlines the operation of Heriot Watt MBE system, discusses the *in situ* monitoring technique and characterisation technique used for the optical and electronic properties of the growth materials is explained.

2.2 MBE System Design

All the samples analysed in this thesis were grown in a Vacuum Generators V80H MBE system shown in figure 2.1. The V80H consists of four vacuum chambers, which are isolated by gate valves. There are two similar growth chambers, HWA and HWC both accessible through a preparation chamber and a fast entry lock, which allows samples to be quickly introduced into the vacuum environment. The entry lock has its own rotary and turbo molecular pump, which allows it to be brought up to atmosphere and back down to a pressure of 10^{-6} mbar. A pulley driven railway system located in preparation chamber facilities the transport of samples via a trolley to and from the growth chamber.

In the growth chamber, working pressure of around 10^{-9} to 10^{-10} mbar are required to minimise contaminants. Such low pressure also means that the mean free path of the molecules effusing from the cells is larger than the dimensions of the chamber. Therefore, only collisions between molecules and solid surfaces occur, rather than inter-molecular collisions which would cause scattering from the beam.

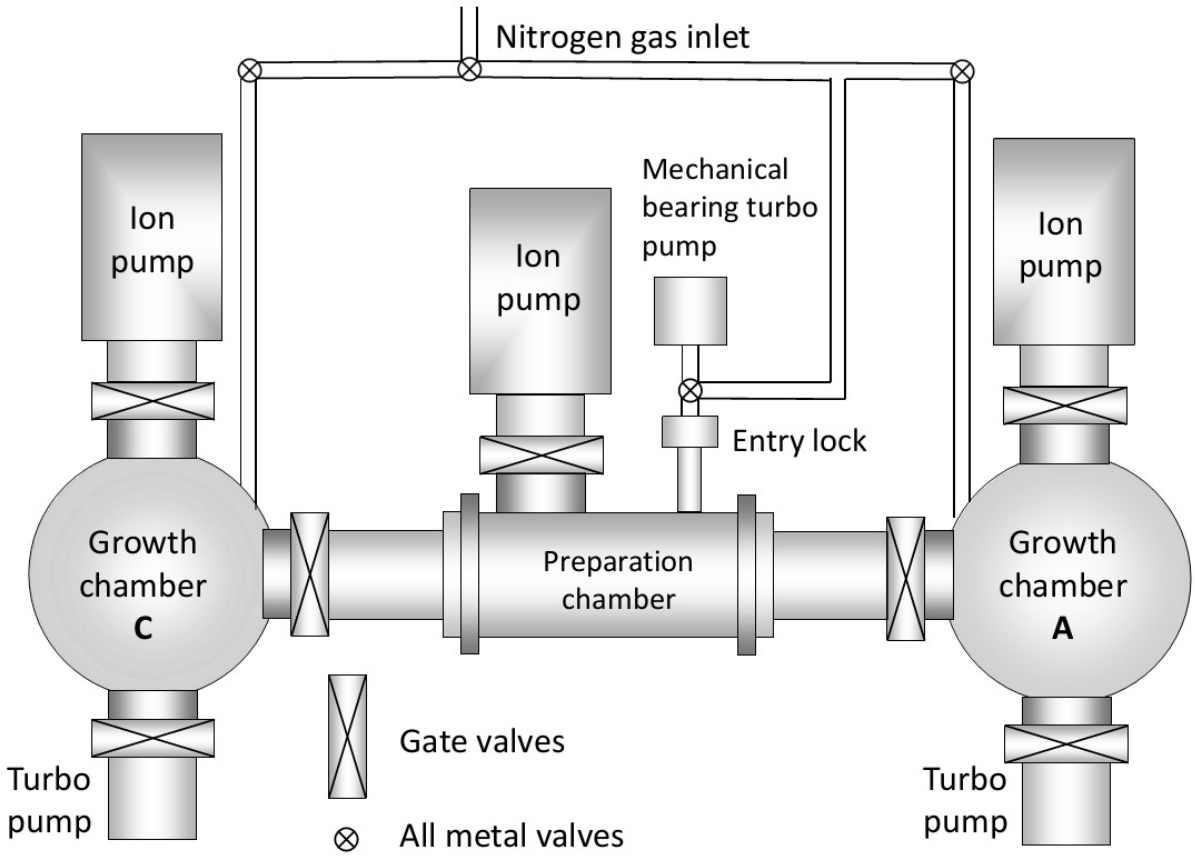

Figure 2.1: Heriot-Watt MBE system with highlighting the external components. This figure is adapted from [2]

The vacuum is maintained using several pumps. Oil sealed rotary vane pumps are used to pump down ~10^{-3} mbar, turbo molecular pumps reduce the pressure still further. Below 10^{-6} mbar, ionisation pumps are used to achieve pressures in the low 10^{-9} mbar region.

Accurate pressure measurement is a fundamental requirement for vacuum systems. At Heriot Watt two types of pressure measurement gauges are used. Pirani gauges are used to monitoring the pressure in the main chambers as well as in the backing line between the turbo and rotary pumps. The operational range of this type of gauge is from atmospheric pressure to 10^{-3} mbar. The ultra-high vacuum (UHV) in the preparation and growth chambers is measured by Bayard-Alpert ionisation gauges.

In ion gauges, electrons are emitted by a cathode or filament and accelerated towards an anode grid. These ions may collide with and ionise molecules in this journey. A collector held at the earth potential attracts the ions. The collector current depends on the number of ions reaching it, which is dependent on the pressure. Ion gauges operate in the range of 10^{-4} mbar to 10^{-11} mbar and so its ideal for pressure measurement in the UHV chambers. The upper limit is reached when pressure is high enough for an electron to ionise more than one molecule after emission by the filament. The lower limit comes from photoelectrons leaving collector due to the X-rays emitted when electrons strike the anode grid. During growth, the normal operating pressure is ~10^{-10} mbar.

2.3 Heriot Watt MBE

All the samples detailed in this thesis were grown in the HWC Chamber of the V80H system shown schematically in Figure 2.2. MBE is performed under ultra-high vacuum conditions where the pressure is typically in the range 10^{-8} to 10^{-10} mbar. Ultra-pure solid source materials (99.9999% (6N)) pure materials are used in this thesis) are heated in thermal effusion (Knudsen) cells generating the molecular beams that then react with a crystalline substrate. These molecular beams can stop by rapid action shutters that are placed directly in front of the cell and this provides one of the main advantages of the MBE growth technique. It allows precise control of the molecular beams so that epilayer thickness can be controlled to within an atomic layer. The ultra-high vacuum conditions and the design of components inside the growth chamber ensure that the substrate surface and any subsequent growth are clean from contamination.

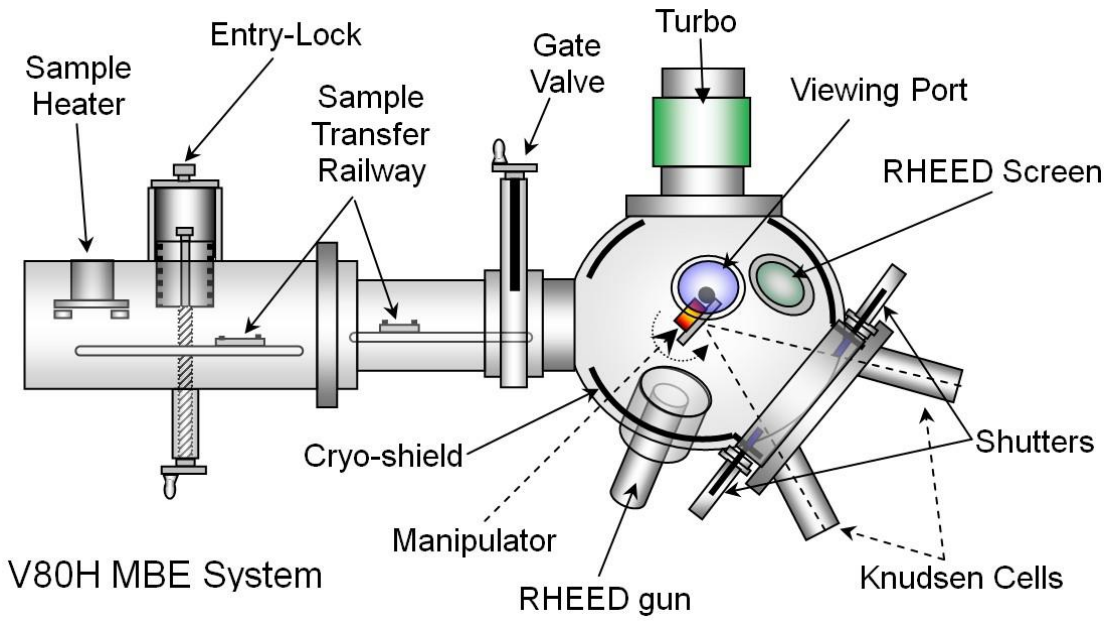

Figure 2.2. Schematic diagram of the side elevation of the V80H MBE system at Heriot Watt MBE facility. This figure is adapted from [3]

2.3.1 Knudsen Cells

In order to reduce contamination of the source materials, the crucibles housed in the K-cells shown in Figure 2.3 are made from Pyrolytic Boron Nitride (PBN), an inert material capable of withstanding temperatures up to 1400°C. PBN's directional thermal conductivity [4] provides a good means of spreading heat, leading to improved temperature uniformity. Accurate temperature control is essential in order to maintain a steady material flux. To achieve this, each cell is independently heated by radiation from a resistively heated filament. Thermocouples, in contact with the crucible, monitor the temperature of the K-cell.

Proportional Integral Derivative (PID) temperature controllers measure the emf generated by each thermocouple and power the heating filaments accordingly. This feedback system can accurately control and maintain temperatures to ±1K. The PID parameters of each cell can be individually tuned to minimise any oscillations and overshoots of the heater temperature. A water-cooling system round the source flange ports assists in keeping the

thermal crosstalk between K-cells to a minimum. For the high temperature K-cell, ZnS the water is also directed through an internal water-cooling system.

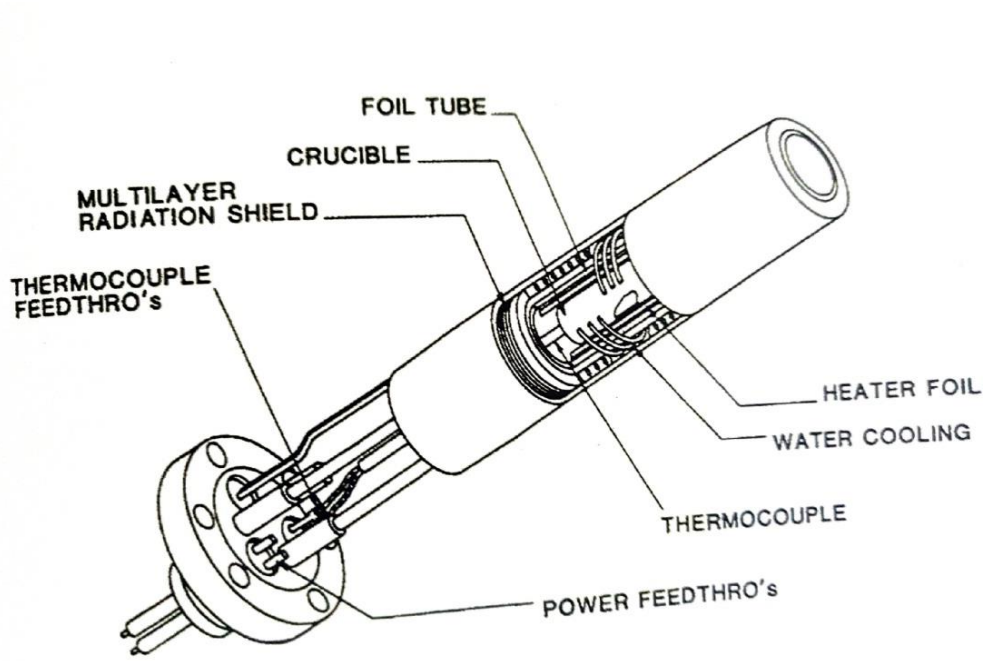

Figure 2.3: Diagram of Knudsen cell. The internal water-cooling pipes can be seen in the cut-away section. This type of cell is used for the ZnS, Mg sources. This figure is adapted from [5].

2.4 Substrate measurement, control and stability

The steady temperature control of the substrate is required for constant growth rate and to ensure the high crystal quality of the sample produced. The substrate temperature is measured by two means, a thermocouple and the use of high and low temperature pyrometers.

2.4.1 Thermocouple measurements

The thermocouple is made of tungsten/rhenium alloys, which can withstand the high temperatures used in the MBE system. A feedback system similar to that used in the operation of the K-cells is used to achieve the desired temperature of the substrate. Since the substrate needs to be rotated during the growth, it not possible for the thermocouple

to be in the ideal position (which is in direct contact with the substrate). The thermocouple is placed behind the substrate heater, which produces a temperature offset of -50°C with respect to the substrate surface. This offset can be affected by various factors, including the thickness and finish of the molybdenum substrate holder and the emissivity of the surface of the sample. The use of infrared pyrometer as the second means of temperature measurement counteracts the problem of the temperature offset.

2.4.2 Pyrometer measurement

Optical Pyrometer provide a non-contact temperature measuring facility. Basically, the temperature is measured indirectly by measuring the infrared energy radiated by the object under observation. Since the infrared intensity emitted by a body varies with temperature, pyrometer provides an effective means of temperature measurement. Because of the various temperature regimes required for the growth of different semiconductor systems, a pyrometer must be selected with its wavelength sensitivity in the appropriated range.

Two Iron Mirage optical pyrometers were used in Heriot Watt MBE machine to measure substrate temperature. The low temperature pyrometer used to measure the growth temperature of the samples which covers the range from 120°- 310°C. The high temperature pyrometer used to monitor temperature during oxide removal of the substrate which has a range of 250°-700°C.

A common failing for the pyrometer is that the temperature readings can be affected by the deposition of Zinc and Selenium related compounds on the pyrometer window. This problem was reduced by using a shutter to protect the pyrometer window when not in use, even though frequent cleaning of the window was still undertaken as a precaution.

2.5 RHEED

Reflection high energy electron diffraction (RHEED) is a useful *in situ*, analytical tool used during growth by MBE. It can provide useful information including observation of the removal of oxides from the surface, calibration of the surface temperature, monitoring the surface reconstruction and indication of the material flux [6]. The phase conversion of the metastable sulphides can also be observed with RHEED [7].

The measurement system at Heriot Watt consists of:

- A VG LEG 110 electron gun, positioned at the back of the chamber, which emits high energy electrons in the range of 10- 15keV. The inelastic scattering mean free paths of these beams are relatively long (~100-1000Å) and so the elastic scattering is strongly peaked in the forward direction with very little back scattering. At glancing angles of incidence (<5°), total external reflection of the beam occurs. The beam is thus diffracted out of the crystal after penetrating only a few atomic layers, resulting in a diffraction pattern that is determined by the periodicity of the crystal surface.
- A phosphor coated lead glass screen located opposite to the electron gun. This fluorescent screen converts the intensity of the diffracted RHEED pattern into visible light. It is mounted behind a shutter to help limit the coating of the screen when not in use. The schematic diagram of RHEED is shown in Figure 2.4.

The RHEED measurement technique is ideally suited to MBE growth. Both the incident and reflected electron beams travel almost parallel to the substrate surface. The geometry of the trajectory ensures that it is perpendicular to the molecular beams and free from any obstructions in the chamber. The small glancing angle to the substrate surface (~1°), causes the component of the electron momentum normal to the surface to be small, resulting in shallow penetration of the surface. These two factors enable the build-up of

the substrate surface to be monitored during growth making it an invaluable analytical tool unique to MBE [8].

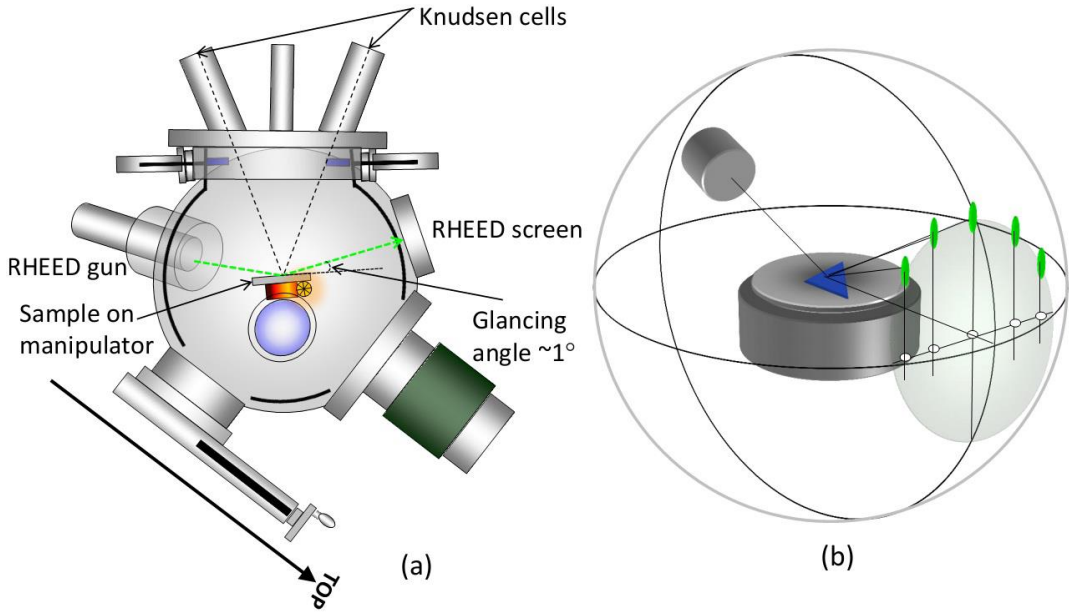

Figure 2.4: Schematic diagram of (a) RHEEED gun inside an MBE chamber and (b) diffracted RHEED pattern on phosphor screen. This figure is adapted from [2].

2.5.1 Electron Diffraction

When the electron beam hits the sample surface, it is scattered by the atoms in the periodic structure, generating spherical scattering waves. Diffraction in real space occurs when there is constructive interference between successive planes of atoms. In reciprocal space, it can be determined where constructive interference will occur by applying conservation of momentum [9]. This is done by using a geometrical construction called the Ewald sphere.

The Ewald sphere is a circle of radius, the incident electro wavevector, the origin of which is the centre of the circle and the tip of k_i is the origin of reciprocal space, see figure 2.5. The scattering of the electrons is assumed to be elastic, therefore the magnitude of the diffracted wave vector. Diffraction occurs when the Laue conditions are satisfied, i.e. the

wave vector of electron collides with the reciprocal lattice vector of a set of planes in the crystal as described by the Ewald sphere.

The diffraction pattern produced is determined by the periodicity of the crystal surface, since the electron beam only penetrates the upper few monolayers of the crystal, there is no periodicity in the direction normal to the surface. This means the diffraction from the surface is the result of 2-D crystal interaction not 3-D, i.e., there is a relaxation of the third Laue condition. Due to this relaxation the reciprocal lattice points become rods and where the rod crosses the Ewald sphere, diffraction may take place [10].

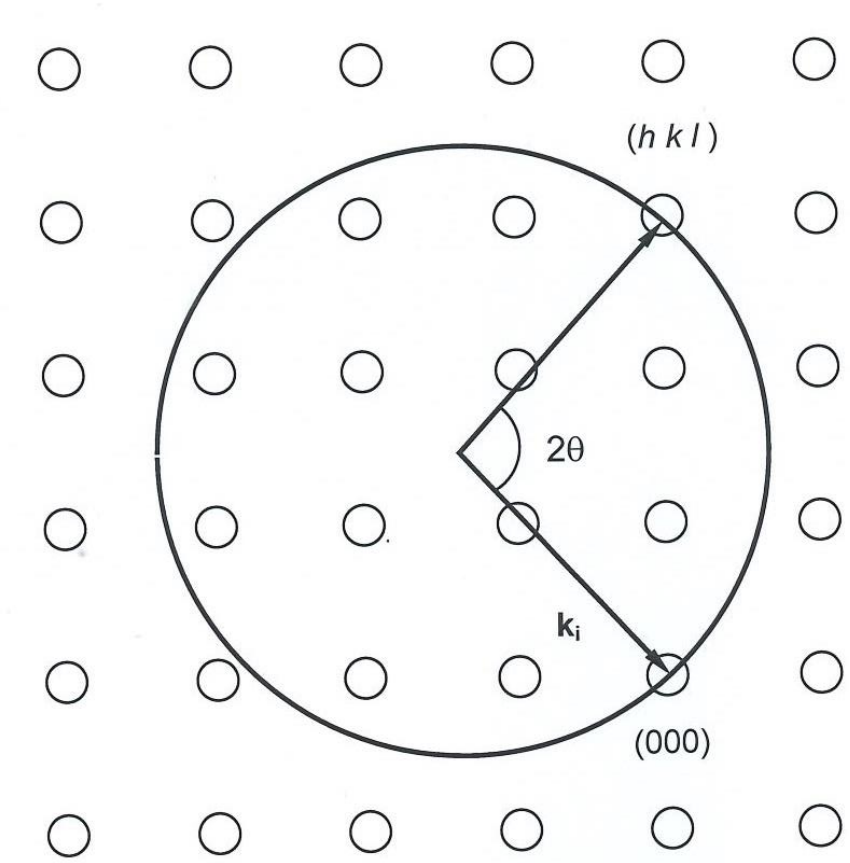

Figure 2.5: Ewald sphere, K_i is the incident wave vector. Diffraction occurs when reciprocal lattice intersects the Ewald sphere. This figure is adapted from [6]

2.5.2 RHEED Pattern

RHEED patterns, typically seen during the growth of II-VI semiconductor materials are shown in figure 2.6. A series of concentric semicircle diffraction pattern are seen in amorphous surface (a). This RHEED pattern is normally seen prior to the heat clean procedure starts.

A perfectly flat two-dimensional surface gives a diffraction pattern consisting of sharp spots lying on a Laue zone, however many RHEED patterns displays steaks, see figure 2.6 (b).

During growth, these spots tend to become elongated, forming streaks. This broadening into streaks may be due to the surface irregularities which causes the reciprocal lattice rods to have a finite width. There are number of reasons for streaks being observed instead of spots such as surface morphology, disorder, topography, phonon scattering and refraction from the surface, see figure 2.6 (c).

No surface is perfectly ordered, and so real surfaces have some degree of disorder. A surface can be considered to consist of domains and the domain can be structurally perfect or disordered. The RHEED pattern of an imperfect surface is shown in figure 2.6 (d). The streaks that have replaced by discrete spots are as result of surface non-uniformities.

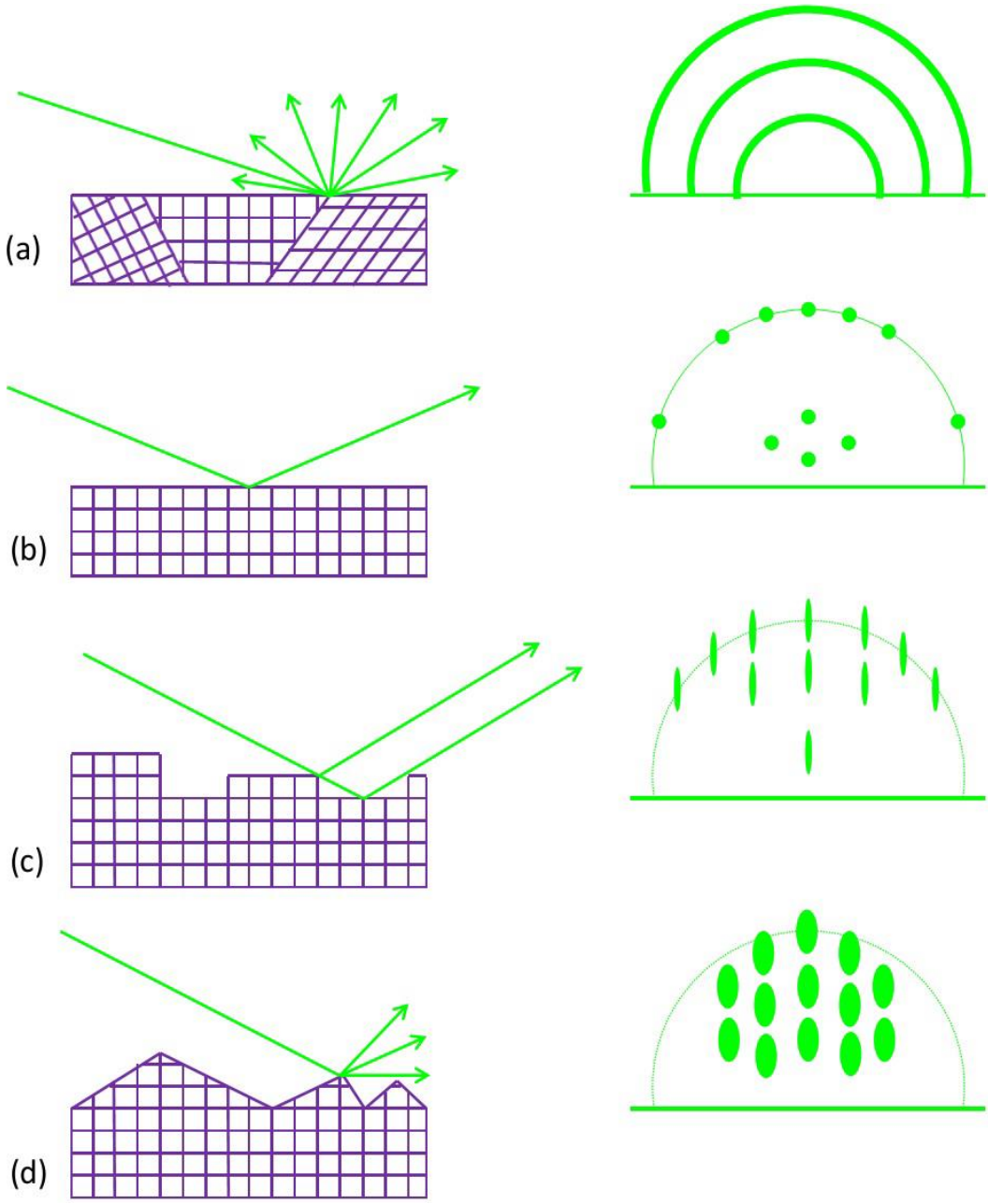

Figure 2.6: RHEED diffraction patterns for surfaces with varying degrees of roughness (a) amorphous surface (b) flat surface (c) stepped surface (d) rough surface with 3D features. This figure is adapted from [2].

2.5.3 Surface Reconstruction

When growth of II-VI semiconductor is initiated on a GaAs (100) substrate, the surface reconstructs with surface atoms bonding with other surface atoms in a regular sequence known as a surface mesh to give the lowest energy configuration [12]. The observed pattern is usually more complex than that of the bulk, since the reconstruction pattern is superimposed upon the bulk pattern, leading to the fractional streaks being visible.

A (2x1) reconstruction on a GaAs (100) is seen during ZnSe growth, see in figure 2.7 (b). The surface mesh spacing in the direction is twice that of the substrate spacing. The reconstruction is dependent of the surface stoichiometry. For example, the observed RHEED pattern from ZnSe growth is dependent on the Se/Zn flux ratio. A (2x1) pattern is observed when the ratio is >1, at ratios <1 a c (2x2) pattern is seen. A combination of both patterns is observed when the ratio is approximately 1.

Pictures of typical RHEED pattern are shown in Figure 2.7. The diffraction pattern from a GaAs (100) surface can be seen in Figure 2.7(a), the 4x reconstruction along the azimuth shows that the surface oxide layer has been removed. The streaks are the result of surface irregularities which cause the reciprocal lattice rod to have finite width [13]. Figure 2.7(b) shows the RHEED diffraction pattern that is observed, along the azimuth, during the growth of ZnSe. A rough (3-D) surface is depicted in the RHEED as series of spots shown in Figure 2.7(c).

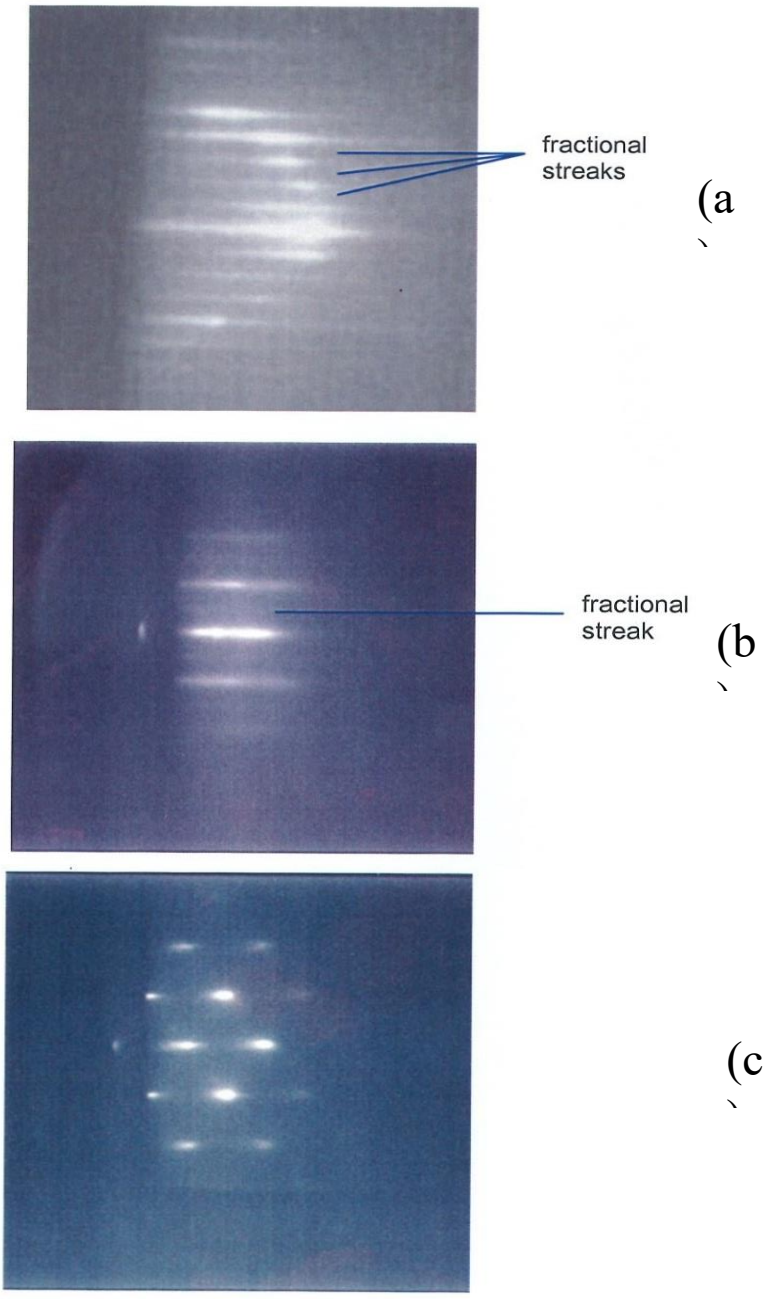

Figure 2.7: RHEED diffraction patterns (a) 4x reconstruction indicating that the surface oxide layer has been removed from the GaAs (100) substrate (b) 2x reconstruction observed during the growth of ZnSe (c) Spotty RHEED pattern indicating the onset of 3D growth.

2.6 *Ex situ* characterisation technique

Analysis of elemental, structural, optical, topographical and electrical properties give a complete picture of the characteristics of a semiconductor. Many different techniques are used to characterise the different aspects of a material. X-ray diffraction is non-destructive technique and can provide detailed information about the structural characteristics, such as composition, thickness and quality of grown layer. Optical spectroscopy techniques are sensitive enough to reveal some details of the electronic structure of low dimensional semiconductor materials. DEKTAK thickness profiler gives information about the thickness of the epitaxial lift off layers stacked on different surface.

2.7 X-ray diffraction

X-ray Diffraction (XRD) is a non-destructive characterisation technique which obtains structural information from the sample under study. The XRD technique used at Heriot-Watt is the Double Crystal X-ray Diffraction (DCXRD) method. This has been widely used to determine the lattice parameter, relaxation and composition of structures [14].

Diffraction of X-rays occurs when a plane wave front of X-ray photons collides with matter. Electrons in the material interact with the X-rays, re-emitting an electromagnetic photon, which travels outwards with a spherical wave front. This process normally takes place without any energy losses and is known as coherent scattering [15].

Bragg's law forms the foundation of XRD and states that it can be viewed as the reflection of plane waves off successive crystal planes [16].Incident X-ray strike the crystal planes at a glancing angle θ and strong diffraction will occur when they are scattered with an angle of reflection, which is also equal to θ shown in Figure 2.8. Constructive interference will occur when the path length difference between rays diffracting from consecutive parallel planes is an integral number of wavelengths. If the crystal planes are separated by a distance d, then the path length must be 2d sinθ, leading to the Bragg equation (2.1):

$$\lambda = 2d\sin\theta \qquad \text{Equation (2.1)}$$

where λ is the wavelength of the incident X-rays, d is the crystal spacing and θ is the incident angle of X-rays.

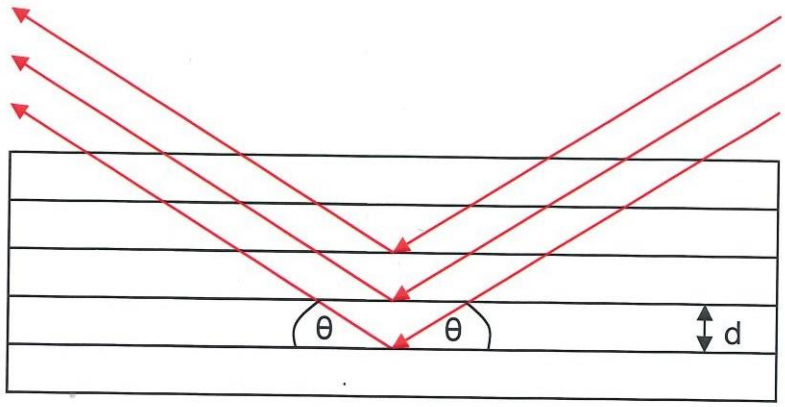

Figure 2.8: Bragg angle of X-ray diffraction. This picture is adapted from [16].

There are two different theories that can be used to describe X-ray diffraction: Kinematical and Dynamical which is described here briefly:

2.7.1 Kinematical theory

The Kinematical theory of XRD treats the scattering from each volume element in a crystal as independent, therefore the incident and diffracted beams are neither attenuated nor rediffracted. However, this does not apply for a perfect or near perfect crystal with a larger volume, as the summation of the scattering gives a diffracted intensity greater than the incident beam. Energy conservation laws require different theory.

2.7.2 Dynamical theory of X-rays

The dynamical theory considers the wave field in a crystal during diffraction as a single entity [17] [18]. The incident and diffracted beams in a crystal are coupled and continually exchanging energy, so they are considered together. An example for the need for a dynamical theory is the phenomenon of anomalous transmission. In this X-rays are detected emerging from a thick crystal, when the absorption of the crystal should have

reduced transmission to almost zero. This cannot be explained by the kinematical theory where all absorption effects are ignored or by calculating absorption merely as a function of crystal thickness. The dynamical theory predicts that a standing wave pattern occurs within the crystal resulting from the oppositely directed incident and diffracted waves. When the nodes of this pattern coincide with atomic sheets in crystals of relatively simple structure, very little photoelectric absorption can take place and so anomalous transmission can occur through very thick crystals.

2.7.3. Rocking curve

The dynamical theory can predict the position of rocking curve peaks, their intensity and width take account of absorption and rediffraction. A simulated rocking curve using Bede RADS (Rocking curve analysis by dynamical simulation) from a thin ZnSe epilayer grown on GaAs (100) substrate is shown in figure 2.9. The largest peak is due to the substrate. The second largest is from ZnSe epilyer. The subsidary peaks are thickness fringes or Pendellösung fringes of the epilayer.

The rocking curve gives a plot of diffracted intensity versus angular position (θ) of the sample [19]. The sample stage has four degree of rotation and by changing small angles in both vertical and tilt axis will give the roxking curve, see figure 2.10 (b). A (θ-2 θ) scans of the x-ray data are presented in this thesis, see figure 2.10 (a). During the scan, sample stage and detector are aligned in certain angle with 1:2 ratio and the aperture of detector has a slit to reduce background noise and scattered radiation.

The analysis of rocking curve can be simplified by the aid of simulation software, such as Bede RADS. The simulation software uses the Takagi [20] and Taupin equations [21] to compare with experimental scan. These simulations can then be compared with experimental scans and collect information about strain, thickness of lair and elemental composition can be determined.

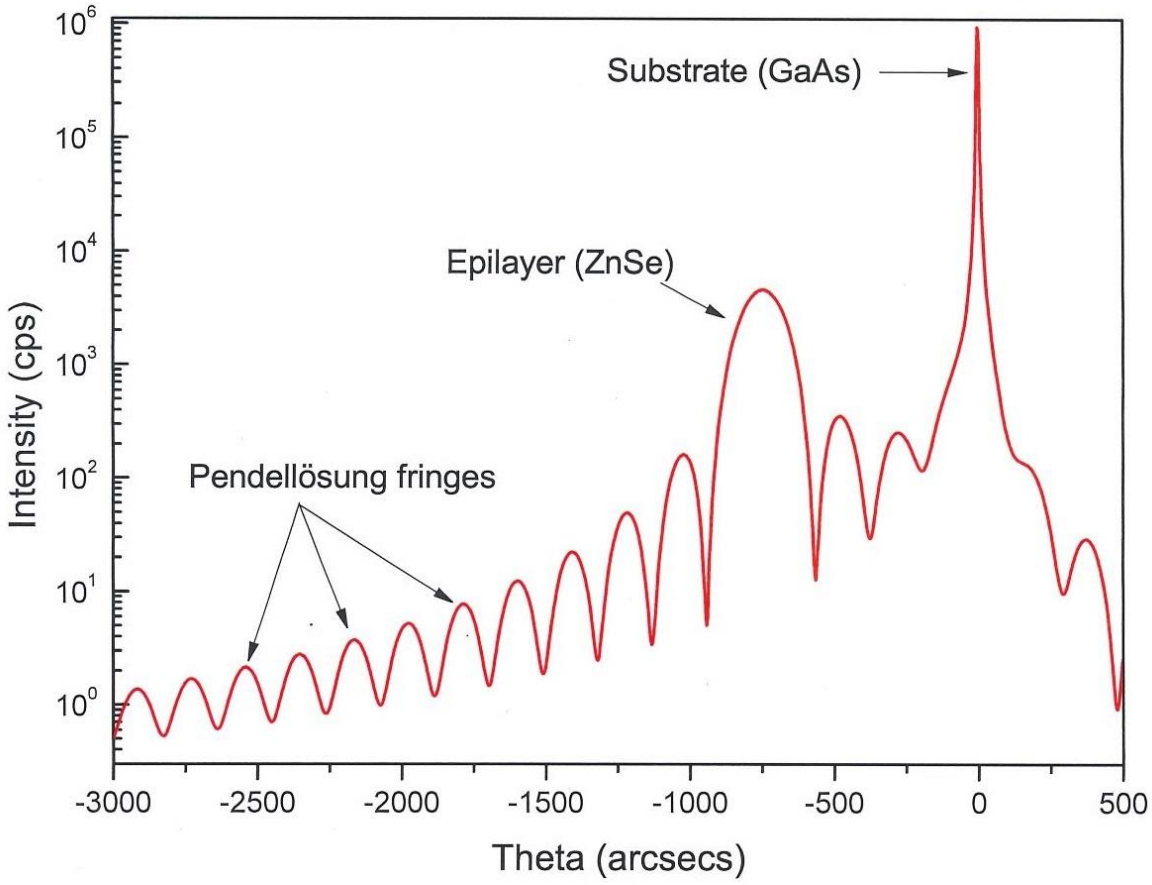

Figure 2.9: Typical 004 rocking curve for ZnSe layer grown on GaAs (100) substrate. This picture is adapted from [19]

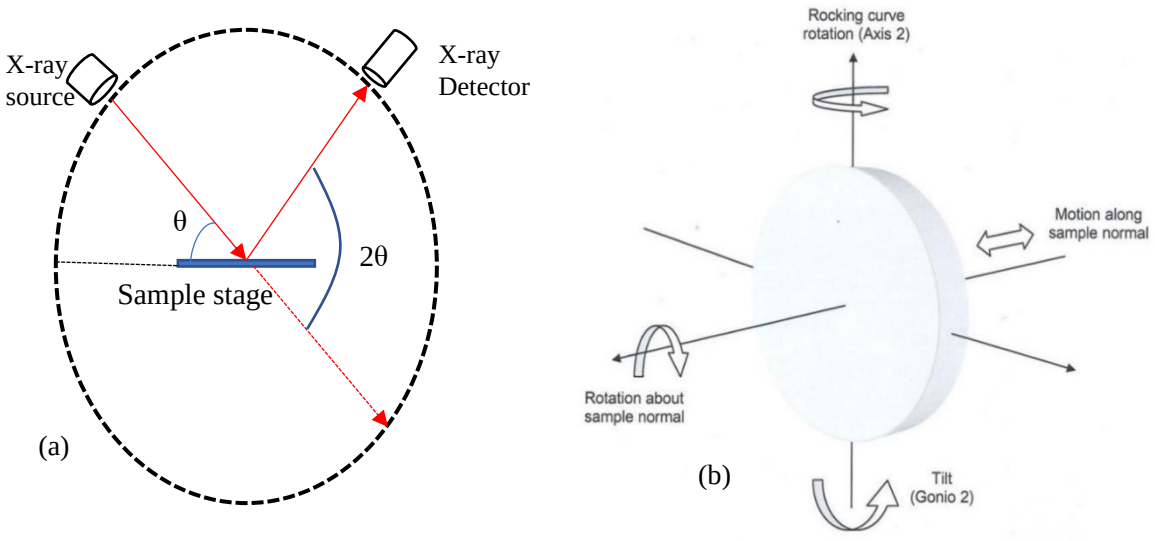

Figure 2.10: Schematic of (a) θ-2 θ scan and (b) sample stage indicating four degree of freedom. This picture is adapted from [19]

2.7.4 Experimental Setup

A schematic diagram of the Heriot Watt XRD apparatus is shown in Figure 2.10. It consists of an X-ray source, containing a copper target. The most intense radiation is the Cu $K\alpha_1$ line (1.506Å). The radiation is randomly directed and is only allowed to escape through a small (~2 cm diameter) circular beryllium window.

On leaving the source, the radiation is incident on a silicon crystal. This crystal has a channel cut into it to collimate the radiation [22]. Only X-rays impinging at the correct angle will be diffracted through the channel and emerge from the crystal, all others are absorbed by the Si crystal.

The collimated X-rays are then incident on another (111) oriented silicon crystal, to monochromate the radiation. Since the X-rays are well collimated at this point, the Bragg condition is only satisfied for one wavelength for any given orientation of the monochromate crystal.

The collimated, monochromate X-rays are then incident on the sample. The sample stage is rotated about the Axis 2 shown in Figure 2.11 until the substrate peak is found. The substrate peak is the most intense peak unless the epilayers are over a micron thick. The sample stage and detector are rotated to optimize the diffracted peaks.

The sample stage has four degrees of freedom shown in Figure 2.10. The stage can be rotated around the incident beam so that the Bragg angle can be varied, and rocking curve data taken. Since the samples under study are mounted for growth using indium, there can be uneven distribution of indium on the back of the sample. Although great care is taken when removing the sample from the molybdenum substrate holder after growth, occasionally the sample is not mounted flat on the stage. Rotating the stage around Gonio 2 axis in Figure 2.12 corrects for the uneven mounting. The stage can also be moved backwards and forwards along the normal of the surface, this is important for maintaining

sample position at the axis of rotation for samples with different thicknesses. It is also possible to rotate the sample about the normal to the surface, this can be used to determine any tilting of the epilayers.

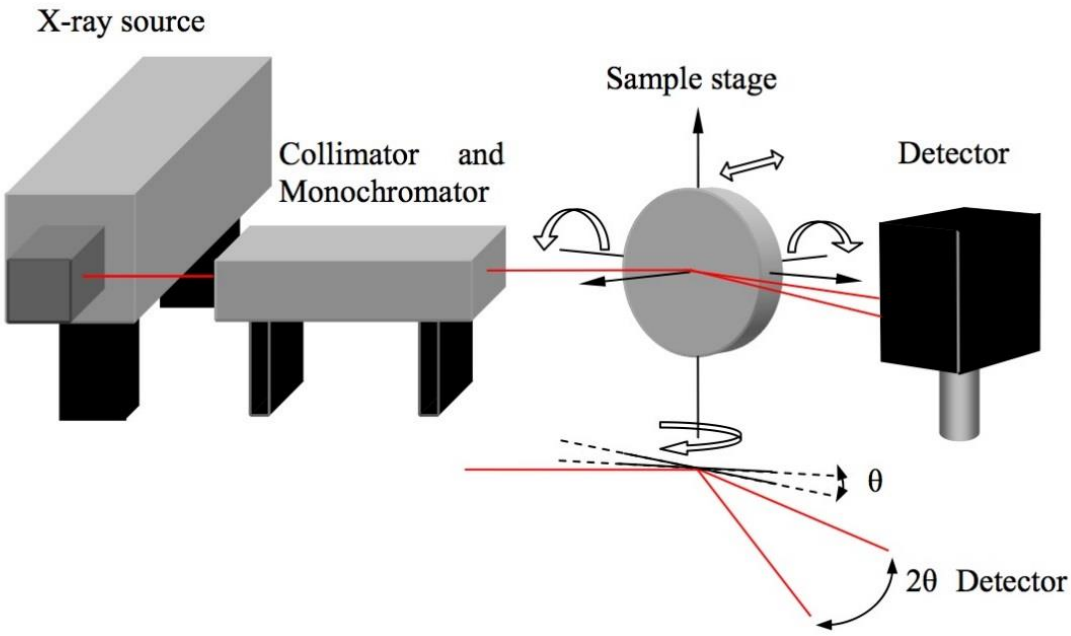

Figure 2.11: Experimental setup of DCXRD at Heriot Watt. This figure is adapted from [23]

2.8 Photoluminescence Spectroscopy

Photoluminescence spectroscopy (PL) is an established technique for assessing the quality of epitaxially grown semiconductors. Using this method, optical transitions from excited electronic states to lower states can be investigated. A transition that is detected can provide the following information, which can be used to improve material quality. It can indicate the presence of crystal imperfections such as impurities, and native crystal defects, however, there are defects that do not interact radiatively. Changes in the growth conditions of a sample will alter the structure of the crystal, which can be detected in the

PL spectrum of the sample. The PL spectrum can then be used as feedback, so that the quality can be improved by altering one growth variable and observing the resulting effect.

In photoluminescence spectroscopy, samples are excited with light that has energy greater than the bandgap of that semiconductor. This results in the promotion of electrons from the valence band to a higher energy state in the conduction band leaving a net positive charge or holes in the valence band [24], see figure 2.12. The promoted electrons eventually drop down to the lowest unfilled states in the conduction band. While the electrons are still excited, they can interact with the holes in valence band via the columbic attraction forming an electron-hole pair, which can be considered to act as one particle. The electron-hole pair is known as the exciton and it may undergo a variety of interactions before the electron and hole recombine producing a photon

The exciton binding energy for a state n is given by:

$$E_n^x = -13.6\frac{\mu}{\varepsilon_r^2 n^2} eV \qquad \text{Equation (2.2)}$$

where, ε_r is the bulk dielectric constant and μ is the equivalent mass.

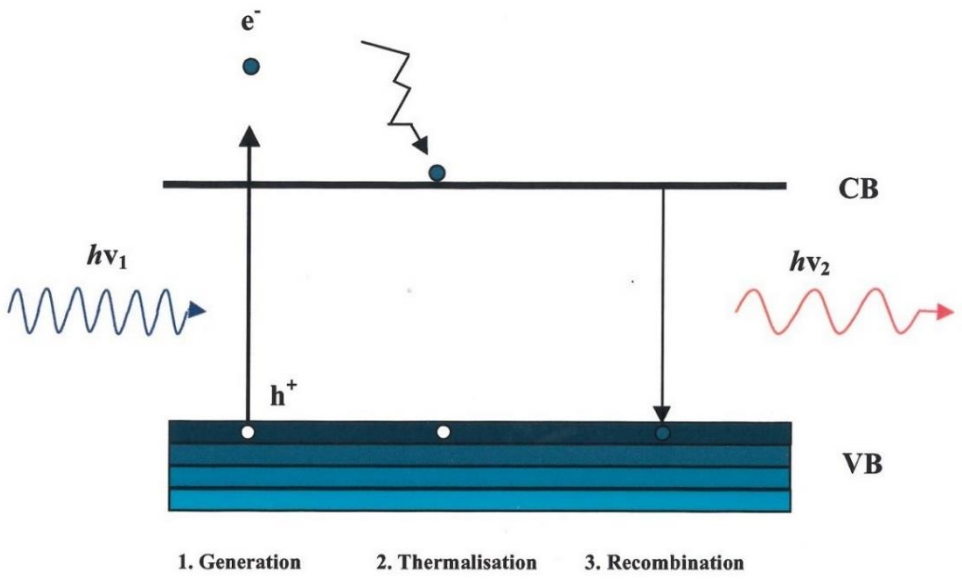

Figure 2.12: Schematic of exciton generation, thermalisation and recombination. This picture is adapted from [24].

The energy of the photon emitted depends on the lowest energy-state available. Where impurities are present, there are energy states available within the forbidden gap between the conduction and valence band [25]. A free exciton that is not captured by impurities or native crystals defects, i.e. in a semiconductor with a low number of radiative defects, wanders freely through the crystal lattice until recombination. The energy of the photon emitted after recombination is given by the following relationship that applies for a direct band-gap semiconductor, shown in equation 2.3 below:

$$h\nu = E_g - E_x \qquad \text{Equation (2.3)}$$

where E_x is the binding energy of the exciton and E_g is the semiconductor band gap.

Where a semiconductor has impurities, an exciton can be captured by those impurities and near-edge (shallow) transitions or deep level transitions can be observed [26] [27]. If it is captured by shallow donors or acceptors (neutral or ionised) it forms a bound exciton, that emits a photon with energy:

$$h\nu = E_g - E_x - E_B \qquad \text{Equation (2. 4)}$$

where E_B is the binding energy of the exciton to the donor or the acceptor.

It should be noted that strain in an epilayer shifts the PL features. The lattice constant of a layer is changed by strain which alters the band gap and hence moves the PL peaks. Also, a strained epilayer has reduced crystal symmetry which acts to remove the degeneracy of the light and heavy holes in the valence band. This produces a doublet where there was previously a singlet line. This shifting and splitting makes PL an effective probe of strain in a layer.

PL typically takes place at cryogenic temperatures and low excitation power densities. At higher excitation densities excited state emission can become significant and the presence of large numbers of carriers can screen the excitonic Coulomb interaction and break up excitons. At high temperatures thermal dissociation of excitons can occur depending on the binding energy of the exciton. Also, at low temperatures peak broadening of PL features by lattice vibrations is minimised.

Epilayers need to be relatively thick (several hundred nano metres) to produce enough e-h pairs to give a strong PL signal. This is not the case for a quantum well (QW) or other reduced dimensional structure of low band gap in the material. Optically generated e-h pairs in barrier materials have a good chance of being captured by the QW and then recombining. The quality of the barrier material is important, if it is inhomogeneous or has large defect concentrations, recombination in the barrier is more likely.

Excitonic transition energies in quantum wells are governed by many factors. The energy levels in a quantum well are given by straightforward solutions of the Schrödinger equation. The eigenvalues for an infinitely deep well are,

$$E = \frac{\hbar^2}{2m}\left(kx^2 + ky^2 + kz^2\right) \qquad \text{Equation (2.5)}$$

where $k=\pi n/L$ and L is the crystal length in the appropriate direction. In a quantum well we get quantisation for L_z but not for L_x and L_y. The energy levels in the z direction become,

$$E_n = \frac{\hbar^2}{2m}\left(\frac{n\pi}{L_z}\right)^2 \qquad \text{Equation (2.6)}$$

where n=1,2… are the ground and excited states. Therefore, the emission energy of the exciton increases as the well narrows and the band gap increases.

Interfacial roughness at the quantum well effectively leads to the formation of several quantum wells of slightly varying thickness. This results in several excitonic emissions of slightly varying

energy which manifests itself as a broadening or even splitting of the exciton peak in the PL spectrum.

The other main factors governing quantum well exciton emission energies are well depth and strain. For an infinitely deep well the exciton binding energy increases monotonically from its bulk value, R, the Rydberg energy, to 4 times this value as the well width decreases from infinity to zero. For a well of zero depth the binding energy does not change. The Heriot Watt PL apparatus, which is shown in figure 2.13, records PL spectra at a temperature of 77K using the 325 nm GaN diode laser focused onto sample and collected *via* CDD spectrometer.

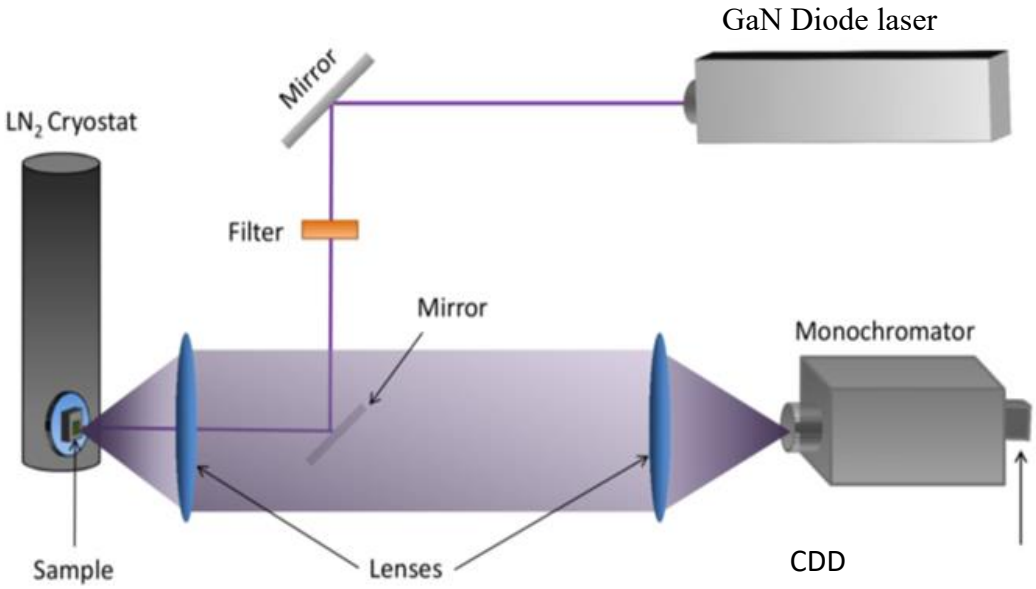

Figure 2.13: Schematic of the optical setup used for photoluminescence measurements. This picture is adopted from [23]

2.9 Summary

A detailed account on the working and structure of the MBE machine as well as the growth mechanism is given in this chapter. Similarly an overview of the most important characterization process used throughout this thesis is also presented, with emphasis on the X-ray, RHEED and PL methods as they are the prominent techniques used and provide

the most comprehensive data for growth development. Individually each technique has its merits but together they provide a more detailed description of the materials.

REFERENCES

[1] A.Y.Cho and J.R.Arthur, "Molecular beam epitaxy," Progres in solid state chemistry, vol. 10, pp. 157-191, 1975.

[2] A. Rajan, "MBE growth, processing and stability of zinc blende MgS based heterostrucutures," PhD Thesis, Heriot Watt University, 2013.

[3] Ian. A. Davidson, "The growth, processing and characterisation of II-VI semiconductor structures," PhD Thesis, Heriot Watt University, 2012.

[4] A.W.Moore, "Characterization of pyrolytic boron nitride for semiconductor materials processing," Journal of Crystal Growth, vol. 106, pp. 6-15, 1990.

[5] R.F.C. Farrow, Molecular Beam Epitaxy: Applications to key technologies, Noyes Publications, 1995.

[6] P. J. Dobson, An Introduction to RHEED, Philips research Labs, 1988.

[7] C. Bradford, K.A. Prior and B.C. Cavenett, "Temperature dependent photoluminescence of CdSe quantum dots grown in MgS and ZnSe," Physica Status Solidi (c), vol. 1, pp. 755-758, 2004.

[8] Thomas F. Kuech, Principles of Molecular Beam Epitaxy, Elsevier, 2015.

[9] P.A.Maksym and J.L.Beeby, "A theory of rheed," Surface Science, vol. 110, pp. 423-428, 1981.

[10] D. J. O'Connor, B. A. Sexton and R. S. C. Smart, Surface Analysis Methods in Material Science, Springer-Verlag, 1992.

[11] J.Massies, P.Etienne, F.Dezaly and N.T.Linh, "Stoichiometry effects on surface properties of GaAs{100} grown in situ by MBE," Surface Science, vol. 99, pp. 121-131, 1980.

[12] A. Y. Cho, “Growth of III–V semiconductors by molecular beam epitaxy and their properties,” Thin Solid Films, vol. 100, p. 291–317, 1983.

[13] J. H. NeaveB, A. Joyce and P. J. Dobson, “Dynamic RHEED observations of the MBE growth of GaAs,” Applied Physics A Materials Science and Engineering, vol. 34, pp. 179-184, 1984.

[14] B. E. Warren, X- ray Diffraction, Dover Publications, 2012.

[15] V Holy, T Baumbach and U Pietsch, High resolution X-ray scattering from thin films and multilayers, Springer-Verlag, 1999.

[16] W. H. Bragg, “The Reflection of X-rays by Crystals. (II.),” in Proceedings of the Royal Society of London. Series A, Containing Papers of a Mathematical and Physical Character (Vol) 89 , 1913.

[17] R.W. James, The Optical Principles of the Diffraction of X-rays, OX Bow Press , 1982.

[18] Z.G. Pinsker, Dynamical Scattering of X-rays in Crystals, Springer-Verlag, 1978.

[19] D. K. Bowen and B. K. Tanner, High Resolution X-ray Diffractometry and Topography, Taylor and Francis, 1998.

[20] S. Takagi, “Dynamical theory of diffraction applicable to crystals with any kind of small distortion,” Acta. Cryst., vol. 15, pp. 1311-1312, 1962.

[21] D. Taupin, “Théorie dynamique de la diffraction des rayons X par les cristaux déformés,” Bull. Soc. Fr. Mineral. Crystallography, vol. 87, pp. 469-511, 1964.

[22] N. Loxley, D.K. Bowen and B.K. Tanner, “presented at 1990 Fall MRS meeting,” Channel Cut Collimator Reference and Instruction Manual.

[23] R. T. Moug, II/VI metastable sulphides: Fundamental studies of MBE growth, characterization and nanostructure formation., PhD Thesis Heriot Watt University, 2009.

[24] A. Gustafsson, M.E. Pistol, L. Montelius and L. Samuelson, “Local probe techniques for luminescence studies of low-dimensional semiconductor structures,” Journal of Applied Physics, vol. 84, pp. 1715-1775, 1998.

[25] Kaufmann, Elton N and Toney, James E, Characterization of materials: Photoluminescence Spectroscopy, John Wiley & Sons, 2002.

[26] T. Yao, M. Ogura, S. Matsuoka and T. Morishita, “Electrical and Photo-luminescence Properties of ZnSe Thin Films Grown by Molecular Beam Epitaxy: Substrate Temperature Effect,” Japan Journal of Applied Physics, vol. 22, p. L144, 1983.

[27] T. Yao, Y. Okada, S. Matsui, K. Ishida and I. Fujimoto, “The effect of lattice deformation on optical properties and lattice parameters of ZnSe grown on (100)GaAs,” Journal of Crystal Growth, vol. 81, pp. 518-523, 1987.

This page is intentionally left blank

CHAPTER 3

Growth and characterisation of Zinc blende Magnesium Sulphide layers used in the Epitaxial Lift-off process

3.1 Introduction

When a thin film is deposited on a substrate it is not apparent whether the deposited layer will adopt the lowest energy crystal structure, that of the underlying substrate or something completely different. There are numerous examples where the growth occurs in a higher energy metastable crystal structure. It is normally found that III-V and II-VI semiconductor films deposited on a substrate adopt the crystal structure of the substrate even when it is not the lowest energy structure, giving epitaxial growth. There are however exceptions, such as CdSe [1] which grows in either wurtzite or zincblende (ZB) crystal structure depending on the orientation of the substrate.

The following chapter details the growth of ZB magnesium sulphide (MgS), which in the past has proved very difficult to grow epitaxially other than in the lowest energy rocksalt (RS) structure. A novel technique that utilises ZnS and Mg sources has been used successfully to grow high quality ZB MgS. Details of the growth method will be described, together with those improvements which have enabled to use as sacrificial layer for the epitaxial lift-off (ELO) process detailed in chapter 4.The structural characterisation of the layers has been determined by double crystal x-ray rocking curves (DCXRC) and will be discussed in detail. Photoluminescence (PL) spectroscopy is used to compare the optical emission of the samples.

3.2 Magnesium Sulphide overview

MgS is an unusual II-VI semiconductor with a number of interesting properties, in particular, its huge bandgap, ~5eV. As a result, thin (<20 nm) layers of ZB MgS have found several uses [2].

Although its stable crystal structure is the RS phase, the Phillip's iconicity of MgS is 0.786, which is modified, simulated and calculated for conductors and it is close to the boundary between the regions of stability for RS and ZB phases. It has been shown by Navrotsky and Philips [3] that the free energy for the transformation between RS and ZB phases is close to zero.

Using thin film growth technique like molecular beam epitaxy (MBE), it is possible to grow compound and alloys in the ZB phase when it is not their stable crystal structure. MgS can be grown epitaxially in the metastable ZB structure if grown on a (001) ZnSe layer, and is lattice matched to both ZnSe and GaAs [4]. When grown in the ZB crystal structure on GaAs, MgS has a tensile strain of only 0.55% compared to ZnSe which has a compressive strain of -0.27%. Hence strain symmetrised structures are therefore possible with ZnSe/MgS multilayers [5].

Prior to the attempted epitaxial growth of MgS, the material was grown as a low purity polycrystalline powder using various techniques based on the reduction of Magnesium sulphate [6]. There were many attempts by different groups to grow layers of MgS in the ZB phase using both MBE and metalorganic vapour phase epitaxy (MOVPE). The ZB MgS of 0.96 nm thickness were grown initially before changing the RHEED pattern from 2D to 3D transition. This phase transition from 2D to 3D is due to the change in crystalline structure of epilayer [7]. Failure to successfully grow thick MgS layers by MBE in the past is due to problems related to the use of elemental sulphur.

Previously in Heriot Watt MBE system, layers of good crystalline quality ZB MgS is grown using ZnS and Mg sources [8] [9]. When MgS grow directly on a GaAs substrate or on a ZnSe buffer layer it undergoes the phase transition to RS after an amount referred to as critical thickness. The thickest layer of MgS grown about 200 nm with ZnSe as buffer layer [10].

3.3 Growth of Magnesium Sulphide

The MgS and ZnSe structures presented in this thesis were grown using 6N (99.9999%) elemental sources of Mg, Zn and Se and a 6N ZnS compound source. In order to reduce substantially the amount of ZnS leaking around the shutter when the cell is at growth temperature [11], a liquid nitrogen cooled shutter was fitted between the shutter and the cell. This considerably reduced the possibility of contamination of the chamber by sulphur-containing species. Problems were, however, encountered in the preliminary stages of the project, where it was found that the ZnS flux would drop very rapidly after ~ 30 growths. This was probably due to a combination of problems, one of which was the build-up of material on the liquid nitrogen cooled shutter. At worst, this build-up could effectively halve the exit area, causing rapid reduction of the material effusing from the cell.

To counteract this effect, the Knudsen cell was replacing with a new EPI hot-lip cell. This is a single filament cell, which provides extra heating at the crucible orifice. Its purpose is to reduce the level of condensation in the crucible, thereby reducing the build-up of materials on the shutter as well as the crucible lip.

A second problem thought to be responsible for the rapid reduction in the flux rate, was associated with the ZnS crystal size of the source material placed in the crucible. It was noticed after removal of the crucible that large ZnS crystals in the top section remained intact, effectively acting as a plug and restricting the material flux from behind. ZnS is

known to be a bad thermal conductor and poor contact with the crucible wall would lead to this result. This problem was reduced by careful choice of ZnS crystal size (<10mm diameter) when refilling the cell.

3.4 GaAs substrate preparation

The MgS structures were grown on GaAs (100) substrates supplied by American Crystal Technology (AXT). Before transfer into the MBE system the substrate was etched in a 2:2:20 solution of H_2O_2: H_2O:H_2SO_4 at 60°C for 90 seconds. The substrate was then rinsed in 18MΩ deionised water and quickly dried with a jet of dry nitrogen gas. The wafers were then bonded to a molybdenum block using molten indium as a bonding agent. It has been shown by Massies *et al.* [16] that the bonding process produces a surface that is highly oxidised. The oxide layer thickness is typically 2-3 nm and is strongly dependent on the temperature and time taken during bonding.

Once the sample is mounted, the molybdenum block is placed upside down in a holder inside the fast entry lock of V80H molecular beam epitaxy machine, which prevents dust or other contamination landing on the substrate surface. The sample is then transferred to preparation chamber via fast entry lock. The oxide removal of substrate surface will be done in growth chamber by rapidly heating to ~580ºC. GaAs (100) oxide desorption explained detailed in chapter 2 section 2.5. With the cooled shutter fitted, the GaAs substrates can be reproducibly cleaned and cooled to below 300ºC under a Zn flux, while maintaining the 4x reconstruction along the [110] azimuth. This ensures that there is no significant contamination by sulphur in the growth chamber.

All MgS growths were attempted on a thin ZnSe buffer layer (~50 nm) grown on a GaAs (100) substrates. The ZnSe buffer is essential, because not only does it gives a well characterised surface on which to initiate the growth of MgS, but it also prevents sulphur from reacting with the GaAs substrate which can form a layer of Ga_2S_3, a compound

which does not have the ZB crystal structure. Typically, RHEED shows that the first stage of the ZnSe growth is 3D, which subsequently transforms to the usual (2x1) streaky RHEED pattern [17], indicative of a flat surface after the growth of 10 nm.

3.5 Challenges in initial ZB MgS growth

Cell temperatures of 375ºC and 800ºC were used for the Mg and ZnS sources respectively. It is well known from the previous experience of our group that prolonged exposure to Mg rapidly causes the background current of an ion gauge to rise and so routine measurement of Mg flux was avoided in order to prevent contamination.

The growth temperature ranged from 160-310°C for the MgS layer. Observation of the RHEED pattern developing during growth was used to monitor the phase stability. The

MgS growth was halted when 3-D faceted growth was indicated by RHEED shown in figure 3.1. Details of the growth conditions and observations made during the initial stage of the growth are shown in Table 3.1.

For the first few growths a thin ZnS layer was grown on top of the ZnSe buffer. At this stage of the project, it was thought that the chemical composition of the surface layer might influence the success of the MgS growth, and that a thin ZnS surface layer could facilitate the chemical reaction required to form ZB MgS. This procedure was not found to be necessary and so was stopped in the early stage of the project. It can be seen from the table 3.1 that the growth temperature leading to optimum conditions is in the region of 240°C. This temperature was recorded by both low temperature pyrometer which had an emissivity setting of 0.6, and by the thermocouple. It was soon apparent that the maximum ZB material thickness decreased substantially if grown outside the 230 to 250°C temperature range.

Sample No	Substrate temperature (°C)	ZnSe Buffer Thickness (nm)	MgS Thickness (nm)	Capping Layer Thickness (nm)	RHEED Observation
HWC 603	315	10 + 2 ZnS	-	2(ZnS)	Spotty almost as soon as MgS growth starts
HWC 604	280	10 +2 ZnS	-	2(ZnS)	Spotty after 3-minute MgS growth
HWC 606	265	10 +2 ZnS	-	2(ZnS)	Spotty after 7-minute MgS growth
HWC 607	270	10 +2 ZnS	-	2(ZnS)	Spotty after 6-minute MgS growth
HWC 608	275	10 +2 ZnS	-	2(ZnS)	Spotty after 3-minute MgS growth
HWC 627	300	50	-	50 (ZnSe)	Spotty and diffuse from start of MgS growth
HWC 634	170	5	-	5 (ZnSe)	Spotty after 4-minute MgS growth
HWC 635	160	5	-	5 (ZnSe)	Spotty and diffuse amorphous rings
HWC 645	240	50	3	50 (ZnSe)	Streaky
HWC 646	240	50	5	50 (ZnSe)	Streaky
HWC 647	240	50	6	50 (ZnSe)	Streaky
HWC 648	240	50	8	50 (ZnSe)	Streaky

Table 3.1: Growth conditions and RHEED observations.

The ratio of fluxes was also found to influence the growth. Although the ion gauge current for Mg was not measured routinely, a value of 4nA was recorded for optimum growth conditions. It should be noted that the Mg cell temperature has remained constant at 375°C throughout this project and no problems attributable to the Mg source has been noted. Fluctuations in the ZnS flux, however, have been found to seriously affect the growth conditions. Optimum conditions are achieved for a ZnS ion gauge current of ~50nA and the maximum thickness that can be grown in the ZB phase falls drastically as this value

decreases. This observation is possibly due to insufficient ZnS coverage on the surface to maintain the ZB MgS growth.

Once the optimum growth conditions had been established, the material was routinely capped with a thin ZnSe layer. MgS is hygroscopic and so this step was essential in order to prevent degradation of the material due to surface oxidation.

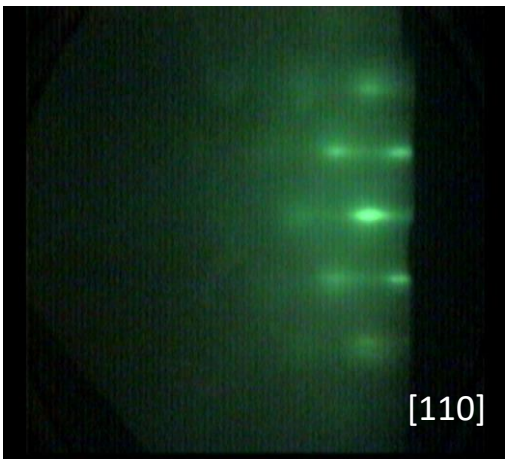

Figure 3.1: RHEED pattern of MgS surface under Mg exposure for extended time along the [110] direction.

3.6 RHEED observation during MgS growth

The interpretation of RHEED pattern leads to possible models of surface configurations, and the identification of the growth conditions. A series of identical MgS layers were grown to study the effect of Mg flux and annealing conditions on the MgS surface. A 20 nm thickness layer of ZnSe was grown before the deposition of MgS layer. A sharp (2x1) RHEED pattern was observed during the growth of ZnSe buffer layer, which indicates flat surface at the end of the growth of this layer and a c(2x2) RHEED pattern was observed during the growth of MgS layer, shown in figure 3.2. The ZnSe layer were grown on top of MgS layer and the structural characterisation studies is done using X-ray measurements.

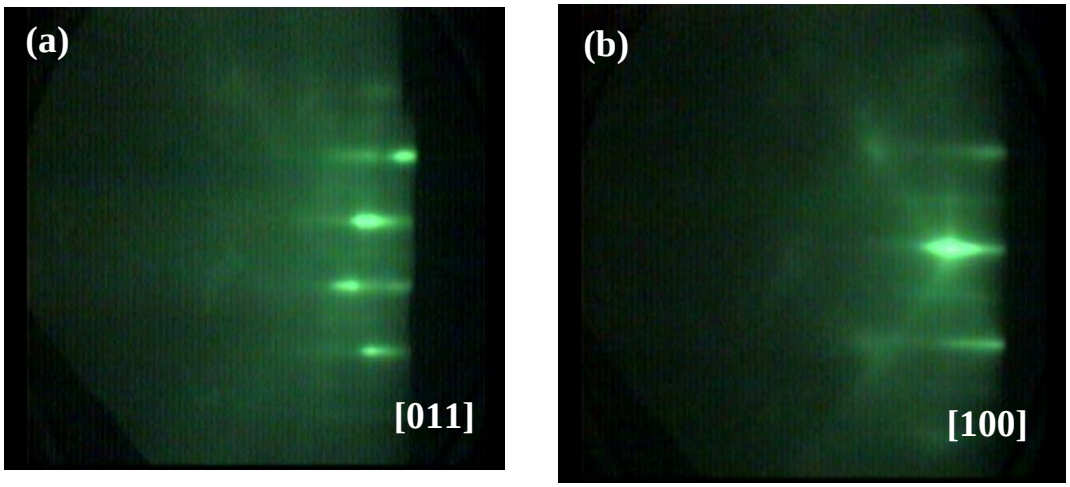

Figure 3.2: RHEED pattern observed during growth of (a) ZnSe buffer showing 2x along [011] direction and (b) ZB MgS layer showing c(2x2) pattern along [100] direction.

3.7 Growth of MgS based quantum well structure for ELO

The growth temperature was set at 240°C for all samples. Two samples were grown: first was a single ZnCdSe QW with ZnSe barriers, the second was a multi quantum well (MQW) of the same structure with x3 well repeats for the ELO technique which is detailed in chapter 4. The structural design of the single and multi QW is shown in figure 3.3.

The growth parameters remained constant for both the samples sets and were grown under the same flux ratio, growth temperature, and on the same day to allow for a direct comparison between them. The thickness of the layers was previously calibrated using a combination of a DEKTAK thickness profiler and X-Ray interference (XRI) characterisation and yielded growth rates of 0.55 Å/sec and 0.88Å/sec for the ZnSe and ZnCdSe respectively. XRI was also used to determine the QW composition as $Zn_{0.79}Cd_{0.21}Se$. All MgS growths were attempted on a thin ZnSe buffer layer to protects the GaAs substrate from sulphur contamination and provides the best surface for the growth of MgS sacrificial layer [18] [19]. The normal ZnSe (2x1) and MgS c(2x2) RHEED patterns [20] were observed during both layer growths.

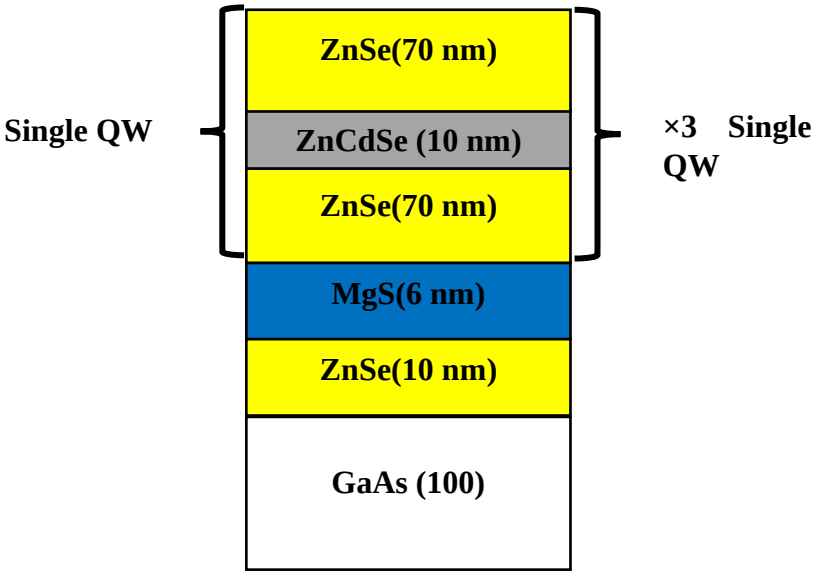

Figure 3. 3: The quantum well structure.

At this stage, the samples were characterized by XRI and Photoluminescence (PL) spectroscopy using a 375 nm GaN diode laser focussed onto the sample and emission collected by a CDD spectrometer. PL emission for single QW was measured at room temperature (RT) and low temperature (LT) at 77k results are discussed in detail in section below.

3.8 X-ray Interference measurements before ELO

Before ELO, symmetric 004 double crystal X-ray diffraction (XRD) rocking curves were obtained from all structures grown and are shown in figure 3.3. For this experiment, the MgS forms a thin spacer layer inserted between two layers of ZnSe creating a Bragg interferometer. The thin spacer layer causes phase shift in diffracted X-rays resulting in a strong modulation of the interference (Pendellösung) fringes. The modulation pattern produced is a function of both the planar spacing of the central layer and its thickness and repeats regularly with increasing thickness [19].

Three different samples, HWC 657, HWC658, HWC 659 were grown with the structure GaAs (100)/ ZnSe (50 nm)/ MgS(x)/ ZnSe (50 nm) where x, the growth time was 1 minutes, 2 minutes and 3 minutes, respectively. These samples were grown at 240ºC and the RHEED patterns indicated that the MgS growth was in the zincblende phase. Details given in Table 3.2. These sample structures were used because accurate measurements are available for both the lattice and elastic constants of ZnSe. The combined thickness of the ZnSe layers is enough to provide well defined x-ray peaks without exceeding the critical thickness of the material.

The strain between II-VI compounds is much larger than that found in the III-V system, causing the modulation pattern of the Pendellösung fringes to repeat more frequently with increasing layer thickness [21]. It was therefore necessary to use both the 400 and 115 reflections in order to obtain an unambiguous choice of layer thickness shown in figure 3.4 and 3.5 respectively. By using two reflections with different planar spacing a unique value can be obtained.

The thickness of the central layer is dependent on the growth parameters used during the MgS growth. The best fit simulation model was found, when the $Mg_xZn_{1-x}S$ contained layer to allow for the residual Zn incorporation. From the x-ray scans of three samples shows a good resolution of the modulation fringes which indicates good quality of the grown structure and growth rate calculated as ~0.36 Å/s obtained. The cell temperature of Mg was kept constant and there was no change in the flux ratio observed during long time, within experimental error (± 4%).

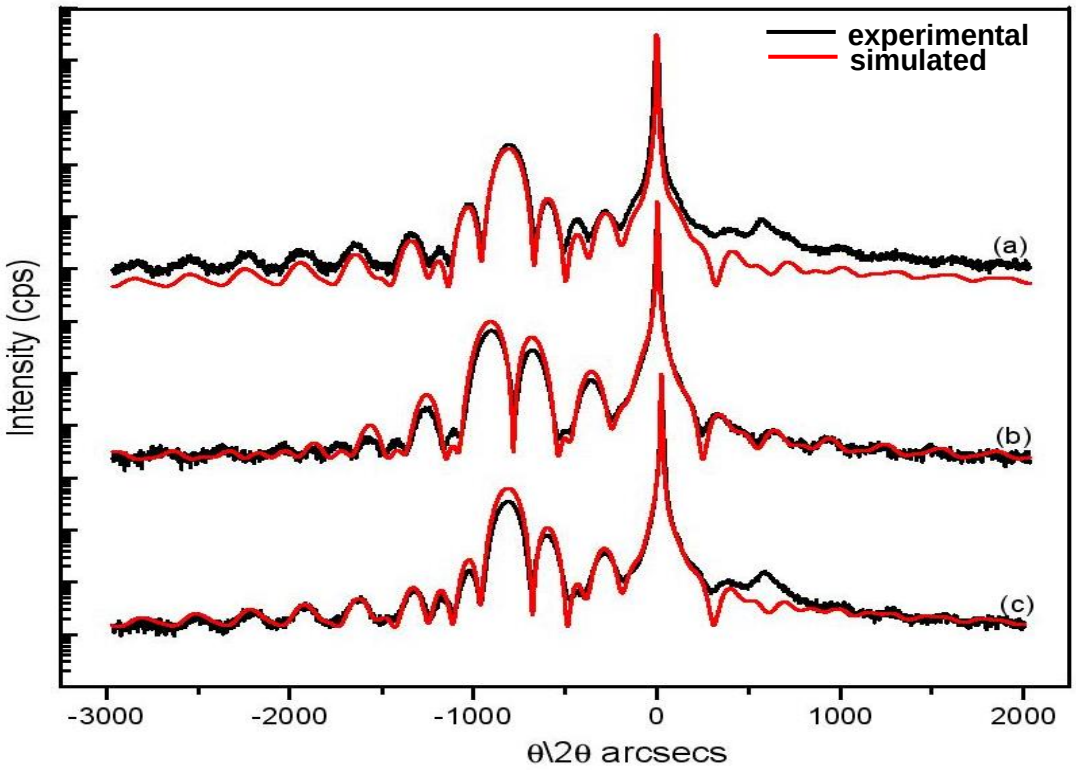

Figure 3.4: 004 reflection of experimental and simulation scans of (a) HWC 657 (b) HWC658 (c) HWC659, with a structure of GaAs (substrate)/ZnSe (50 nm)/ MgS(x)/ ZnSe (50 nm).

Sample No	MgS growth time (seconds)	MgS Thickness (nm)	Zn incorporation (%)	Growth rate (Å/s)
HWC657	60	2.05	0.8	0.35
HWC658	120	4.31	1.3	0.36
HWC659	180	6.89	0.3	0.38

Table 3.2: MgS thickness and growth rate obtained from XRI measurements from samples HWC657, HWC658and HWC659.

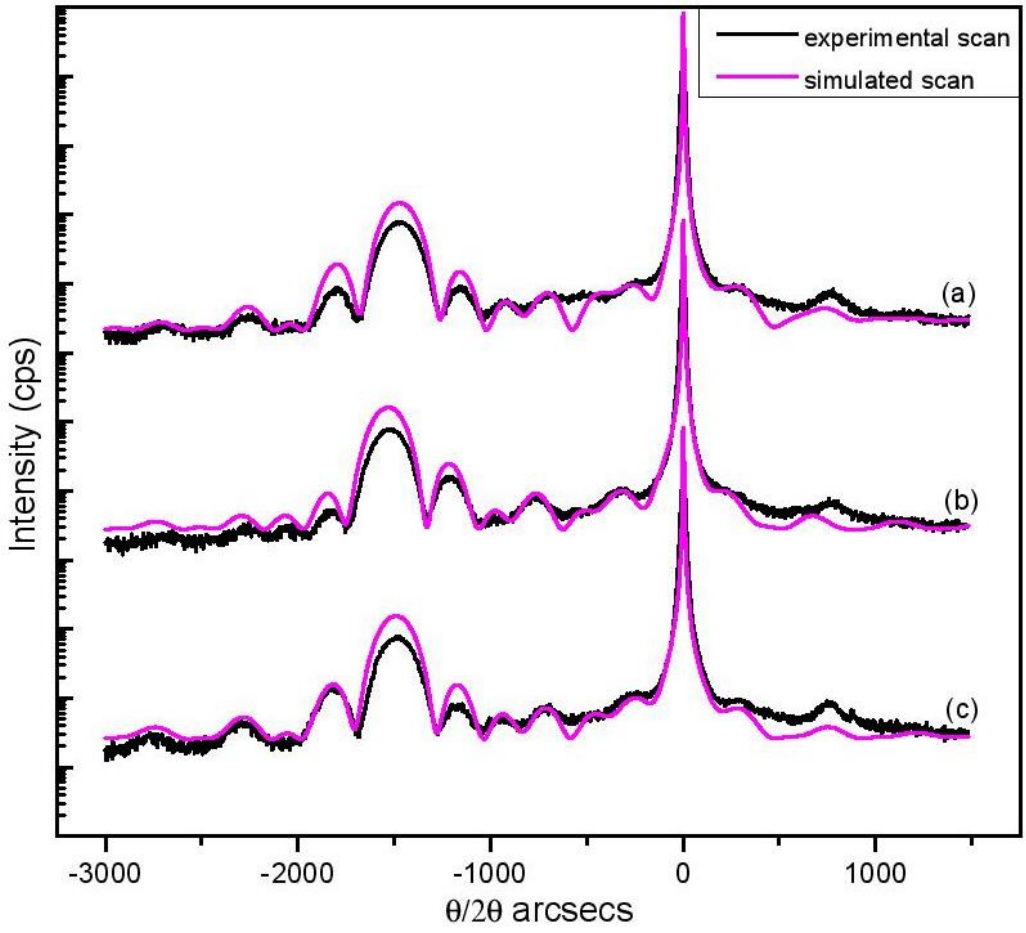

Figure 3.5: 115 reflection experimental and simulation scans from samples (a) HWC 657 (b) HWC658 (c) HWC659, with a structure of GaAs (substrate)/ZnSe (50 nm)/ MgS(x)/ ZnSe (50 nm).

Sample No	MgS growth time (seconds)	MgS Thickness (nm)	Zn incorporation (%)	Growth Rate (Å/s)
HWC657	60	2.12	1.2	0.35
HWC658	120	4.25	0.1	0.34
HWC659	180	6.83	0.5	0.38

Table 3.3:MgS thickness and growth rate obtained from XRI measurements from samples HWC657, HWC658 HWC659.

3.8.1 Initial determination of alloy composition and growth rate

In the case of a ZnCdSe spacer layer between ZnSe cladding layers, for any given cadmium composition XRI curves will give well defined interference fringes for all thicknesses below the for the formation of mismatch dislocations (as opposed to phase conversion) of the spacer. As the thickness exceeds the critical thickness, the curve will rapidly change to one with ill-defined fringes. Thus, by growing a set of samples of this structure, all with the same cadmium content in the spacer but with varying thicknesses we can find the critical thickness for a layer of this composition in such a structure.

Fig.3.6 shows the experimental rocking curves of a set of samples. The sample structure was intended to be ZnSe (70 nm)/ZnCdSe (variable width)/ZnSe (70 nm). A calibration sample of thick ZnCdSe with the same growth temperature and cell temperatures as the multilayers was grown and the cadmium mole fraction was determined by XRD to be 20±1%. For the first sample, a simulation has been fitted to the experimental rocking curve. The structure of the best fit simulation for this sample was ZnSe (50 nm)/$Zn_{0.79}Cd_{0.21}Se$ (10 nm)/ZnSe (50 nm). A stray reflection is observed around 500 arcsec which is due to multiple diffraction from the sample. The goodness of fit (GOF) is one of the key abilities of the BEDE RADS software to simulate specified models and compare them to the experimental scans.

Sample No	ZnCdSe Growth time (seconds)	ZnCdSe Thickness (nm)	Growth rate (Å/s)	Goodness of Fit (GOF)
HWC 704	60	5.1	0.85	0.18
HWC 705	120	10.2	0.85	0.20

Table 3.4: ZnCdSe thickness and growth rate obtained from XRI measurements.

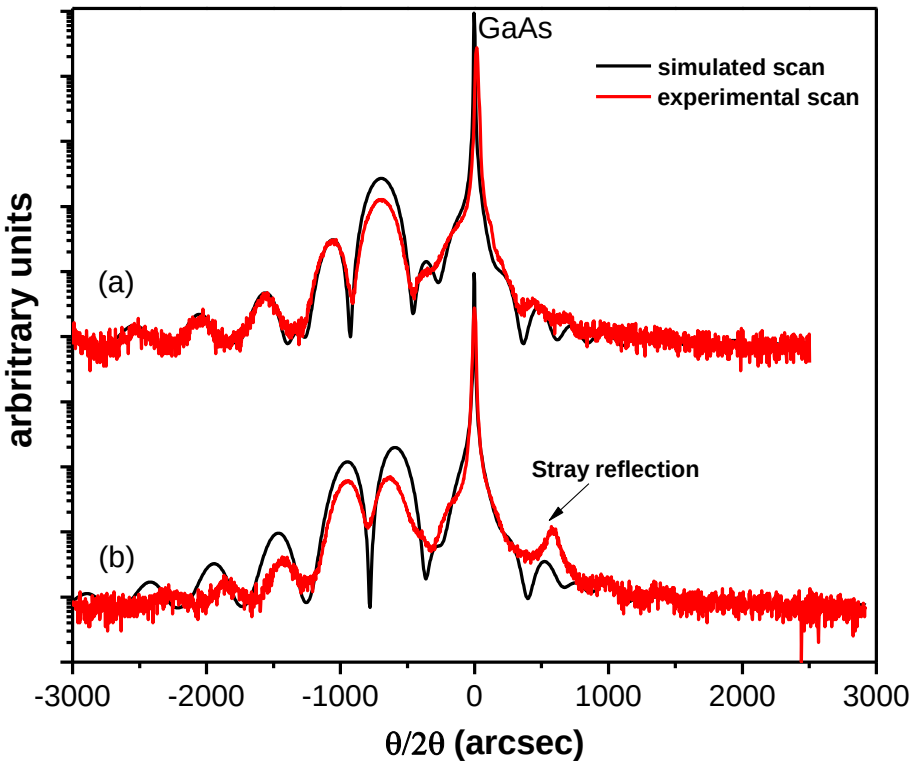

Figure 3.6: 004 reflection of experimental and simulation scans of (a) HWC 704 (b) HWC705, with a structure of GaAs (substrate)/ZnSe (70 nm)/ ZnCdSe(x)/ ZnSe (70 nm).

It is obvious that for the 12 nm and 19 nm quantum well samples the spacer layer has exceeded the critical thickness. XRI peaks of 7 nm,12 nm and 19 nm shown in figure 3.7. In the thickest quantum well, there are no subsidiary fringes whatsoever, only the substrate and quantum well are easily definable. The cladding layer peaks have smeared into each other which is to be expected for relaxed layers. However, the 12 nm quantum well layer still contains fringes. The two cladding layer peaks are just observable, indicating that little peak broadening has occurred. The cladding layer fringes are much closer together and so a small amount of peak broadening is enough for them to become merged into one another. The quantum well subsidiary fringes are present in the scan. The presence of these fringes and the absence of any from the cladding layers is probably due to the relatively large widths of these fringes. Although Pendellösung fringes are still present in the rocking curve, we can state that relaxation has taken place. This is more evidence of

the sensitivity and usefulness of the XRI technique. Therefore, the critical thickness of $Zn_{0.7}Cd_{0.3}Se$ in ZnSe is between 7 nm and 12 nm.

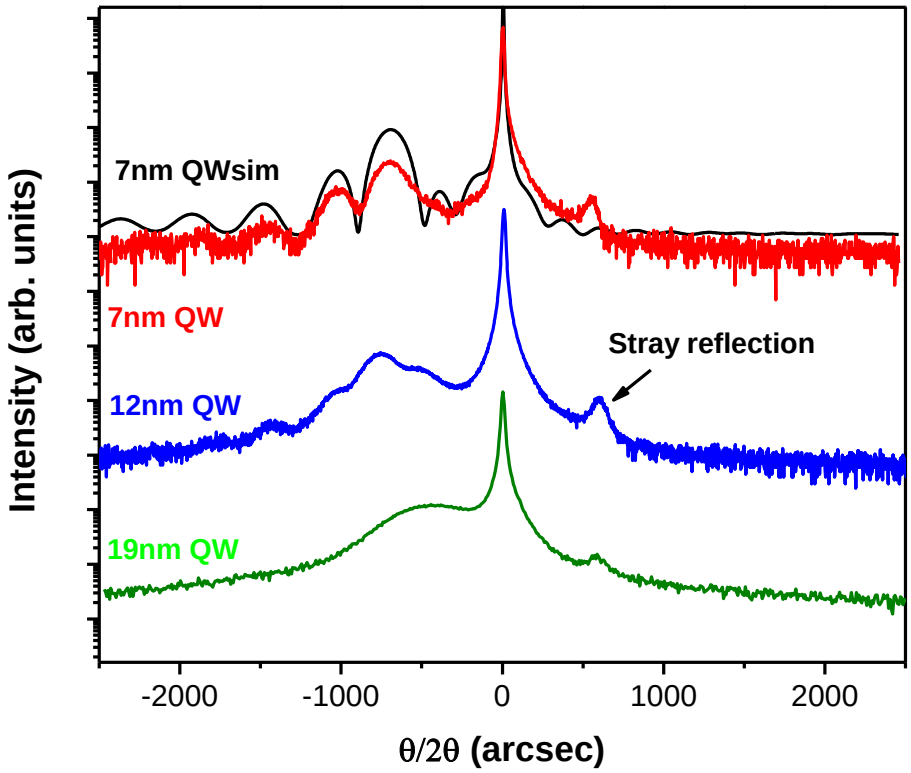

Figure 3.7: Rocking curves of ZnSe/$Zn_{0.7}Cd_{0.3}Se$/ ZnSe layers with $Zn_{0.7}Cd_{0.3}Se$ widths of 7 nm, 12 nm and 19 nm, respectively.

3.9 Optical Characterization of quantum well structure

A single QW structure with well width of 10 nm has been fabricated at a growth temperature of 240°C. A schematic of these structures is shown in figure 3.8. The spectrum of a single 10 nm wide ZnCdSe quantum well exhibits sharp and clear transitions for both the light and heavy hole excitons, confirming the good sample quality.

Figure 3.8: Schematic diagram of single QW structure of ZnSe (70 nm)/ZnCdSe (10 nm)/ ZnSe (70 nm)/ MgS (6 nm)/ZnSe (20 nm)/GaAs (100).

The PL spectra of grown sample before lift-off was investigated to determine the confinement properties of the ZnCdSe QW structure grown on MBE. The PL spectra of 10 nm well width of ZnCdSe QW before lift-off at low temperature (LT) and room temperature (RT) is shown in figure 3.9. The emission from the ZnSe layer (2.78eV) could not be observed as the QW emission is more dominant and to allow for comparison between samples we required a laser power low enough not to saturate our CCD detector. This reduced ZnSe peak such that it can't be seen in these spectra. Table 3.5 shows the values of FWHM, emission energy and thickness measured for the sample.

The ZnCdSe QW samples are strained so that the total thickness of the quantum wells was kept low to avoid relaxation in the wells. PL of these samples revealed full width half maximum (FWHM) at well width of 10 nm for RT and LT of around 38 meV and 23 meV respectively for the well exciton emission. Also, PL emission from the barrier layers of the same order of intensity as the well emission.

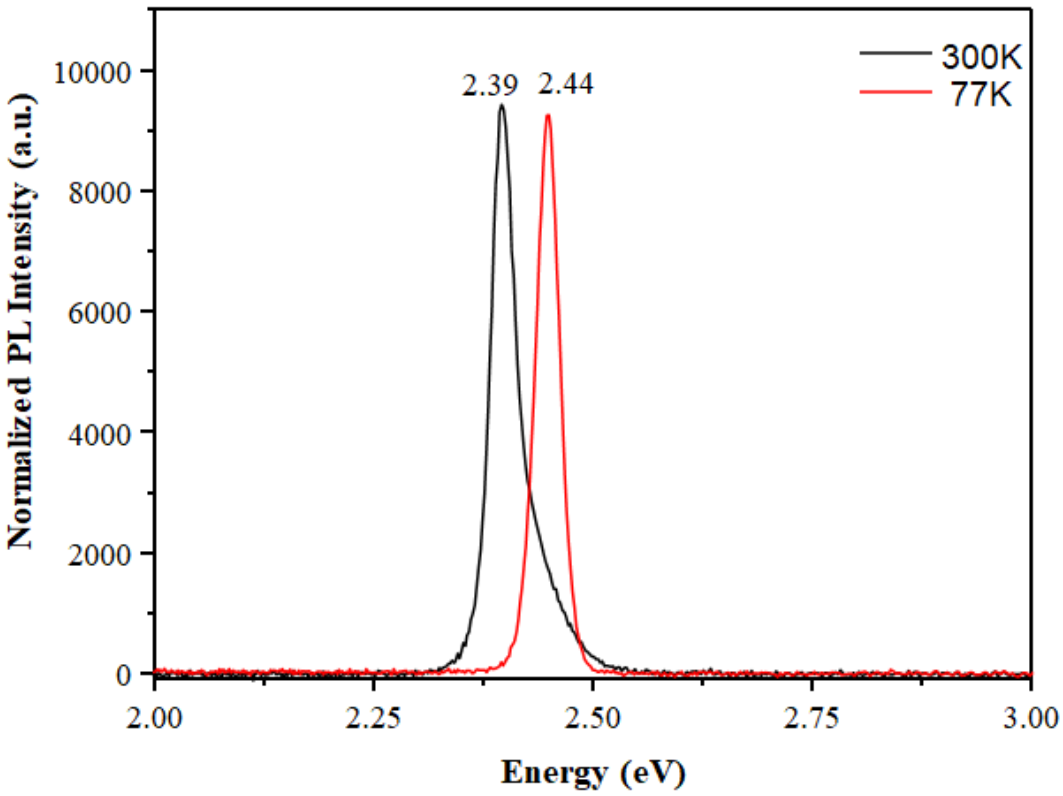

Figure 3. 9: Normalized PL spectra of ZnCdSe QW sample before lift-off at 300K and 77K.

Sample No	ZnSe Barrier Thickness (nm)	QW Thickness (nm)	FWHM (meV)		PL peak emission (eV)	
			LT	RT	LT	RT
HWC 724	70	10	23	38	2.44	2.39

Table 3. 5: Details of quantum well structure

3.10 Summary of the results

The growth of ZB MgS on GaAs (100) substrate has been obtained using MBE growth technique. It is quite difficult to grow MgS in zinc blende structure since its bulk crystal structure is rocksalt. By using MBE growth technique, it is possible to grow in ZB MgS. The main aim to grow ZB MgS is to use as sacrificial layer in ELO process explained in chapter 4. The initial attempts to grow ZB MgS layers have been studied. Pyrometer and

thermocouple measurements has monitored for the accurate substrate measurements. RHEED measurements were monitored during MgS growth for the good quality of the sample.

The growth of MgS halted when 3-D faceted RHEED shows. A small buffer layer grown before the MgS growth. A sharp (2x1) RHEED pattern indicates the flat surface at the end of the growth. During the growth of ZB MgS it changes to c (2x2). On top the MgS layer ZnSe layer was grown.

XRI measurements were done to find the thickness of MgS layer grown. A series of MgS layer with ZnSe barrier layer grown for the XRI measurements. The growth rate of MgS (~0.36Å/s), calculated using BEDE RADS simulation software. The initial composition of ZnCdSe QW samples is also identified using XRI measurements. The growth rate of ZnCdSe is found to be ~ 0.85Å/s.

Pl measurements are taken for the ZnCdSe sample. The good quality quantum well structure found in well width of 10 nm ZnCdSe. The optical characterisation of these samples gives details about crystalline quality. These samples were used for the ELO process later discussed in chapter 4

REFERENCES

[1] C. Y. Yeh, Z. W. Lu, S. Froyen and A. Zunger, "Zinc-blende–wurtzite polytypism in semiconductors," Physica Review B, vol. 46, pp. 10086-10091, 1992.

[2] Y. Kawakami, T. Taguchi and A.Hiraki, "Excitonic and edge emissions in MOCVD-grown ZnS films and ZnSe-ZnS superlattices," Journal of Crystal Growth, vol. 89, pp. 331-339, 1988.

[3] A. Navrotsky and J. C. Phillips, “Ionicity and phase transitions at negative pressures,” Physical Review B,, vol. 11, pp. 4-10, 1975.

[4] C. Bradford, C. B. O’Donnell, B. Urbaszek, C. Morhain, A. Balocchi, K. A. Prior and B. C. Cavenett, “Highly confined excitons in MgS/ZnSe quantum wells grown by molecular beam epitaxy,” Physica Review B, vol. 64, pp. 195309-195315, 2001.

[5] H. Okuyama, k. Nakano, T. Miyajima and k. Akimoto, “Epitaxial Growth of ZnMgSSe on GaAs substrate by Molecular Beam Epitaxy,” Japanese Journal of Applied Physics, vol. 30, pp. 1620-1623, 1991.

[6] N. Singh and D. R. Vij, “Luminescence and related properties of magnesium sulphide phosphors,” Journal of Material Science, vol. 29, pp. 4941- 4945, 1994.

[7] N. Teraguchi, H. Mouri, Y. Tomomura, A. Suzuki, H. Taniguchi, J. Rorison and G. Duggan, “Growth of ZnSe/MgS strained-layer superlattices by molecular beam epitaxy,” Applied Physics Letters, vol. 67, pp. 2945-2947, 1995.

[8] K. Uesugi, T. Obinata and I. Suemune, “Epitaxial growth of zinc-blende ZnSe/MgS superlattices on (001) GaAs,” Applied Physics Letters, vol. 68, pp. 844-846, 1996.

[9] C. Bradford, C. B. O'Donnell, B. Urbaszek, A. Balocchi, C. Morhain, K. A. Prior and B. C. Cavenett, “Growth of zincblend MgS/ZnSe single quantum wells by molecular beam epitaxy using ZnS as a sulphur source,” Applied Physics Letters, vol. 76, pp. 3929-3931, 2000.

[10] A. Rajan, R. T. Moug and K.A. Prior, “Control of surface defects in zinc blende MgS grown by MBE,” Journal of Crystal Growth, vol. 368, pp. 62-66, 2013.

[11] C. Bradford, C. B. O'Donnel, B. Urbaszek, A. Balocchi, C. Morhain, K. A. Prior and B.C. Cavenett, "Growth of zinc blende MgS and MgS/ZnSe quantum wells by MBE using ZnS as a sulphur source," Journal of Crystal Growth, vol. 227, pp. 634-638, 2001.

[12] J. Massies and J. P. Contour, "Substrate chemical etching prior to molecular-beam epitaxy: An x-ray photoelectron spectroscopy study of GaAs (001) surfaces etched by the H2SO4 - H2O2 - H2O solution," Journal of Applied Physics, vol. 58, pp. 806-810, 1985.

[13] S. Takatani, T. Kikawa and M. Nakazawa, "Reflection high-energy electron-diffraction and photoemission spectroscopy study of GaAs(001) surface modified by Se adsorption," Physica Review B, vol. 45, pp. 8498-8502, 1992.

[14] C. Bradford, A. Currran, A. Balocchi, B. Cavenett, K. Prior and R. Warburton, "Epitaxial lift-off of MBE grown II–VI heterostructures using a novel MgS release layer," Journal of Crystal Growth, vol. 278, pp. 325-328, 2005.

[15] C. Bradford, C. B. O'Donnell, B. Urbaszek, C. Morhain, A. Balocchi, K. A. Prior and B. C. Cavenett, "Highly confined excitons in MgSÕZnSe quantum wells grown by molecular beam epitaxy," Physica Review B, vol. 64, pp. 195309 1-8, 2001.

[16] R. T. Moug, C. Bradford, D. Thuau, A. Curran, R. J. Warburton and K. A. Prior, "MBE Growth and Characterization of MgS-Rich Zinc-Blende ZnxMg1−xS1−ySey Alloys," Journal of the Korean Physical Society, vol. 53, pp. 3004-3006, 2008.

[17] K. A. Prior, X. Tang, C. O'Donnell, C. Bradford, L. David and B. C. Cavenett, "Characterization of MBE grown II-VI semiconductor thin layers by X-ray interference," Journal of Crystal Growth, vol. 251, p. 565–570, 2003.

CHAPTER 4

Epitaxial lift-off and stacking multiple layers of II-VI structures

4.1 Introduction

The technology of combining dissimilar materials on single substrate has been studied for many years. One of the growth techniques such as Molecular Beam Epitaxy (MBE) has been used for the fabrication of good crystal quality structures. One of the main limitations in II-VI semiconductor material development is the requirement to grow on III-V materials such as GaAs, GaP, InP etc as these are readily available, of high quality and cheaper than any II-VI substrates. Typically, the substrates are one of the most expensive items in the epitaxial growth, so the ability to separate the epitaxial layer from substrate and reuse the substrate multiple times provides epitaxial lift off (ELO) technique highly beneficial.

This chapter shows that ELO layers can be stacked into new structures while maintaining their desired structural properties. Here we demonstrate, by exfoliating a quantum well (QW) structure of ZnSe/$Zn_xCd_{1-x}Se$ from its substrate, and stacking it on top of itself, we can manufacture a structure of comparable quality to that of an MBE grown multi QW (MQW) sample of the same design. Photoluminescence (PL) spectroscopy is used to compare the optical emission from a stacked QW layer and an MQW grown structure.

4.2 Overview of Epitaxial lift-off (ELO)

ELO is a post growth process used to exfoliate layers from their growth substrate allowing transfer to different functional surfaces [1]. The first use of release layer for ELO process was demonstrated in III-V materials by Konagai et al [2] and they used the term ‘Peeled Film Technology’ rather than ELO. The successful lift-off of a 30 µm thick GaAs layer has been demonstrated by using thick $Al_xGa_{1-x}As$ sacrificial layer to exploit the etching

between AlAs and GaAs in aqueous hydrofluoric acid (HF). For values of $x \geq 0.5$, the etch rate of the Al-containing alloy is many orders of magnitude faster than that of GaAs and so ELO can be achieved in these materials by growing a thin release layer of AlAs between substrate and the active layer. After growth, the wafer is etched in HF, which selectively etches through the AlAs but negligible effect on GaAs, InGaAs and low Al-content AlGaAs alloys.

In addition to the importance of the etch selectivity, another crucial factor is to stress the epitaxial layer thus causing it to bow up slightly maintaining an open channel for the etch to proceed. Although the stress can be applied by several methods, the simplest method is achieved by applying a layer of black Apiezon W wax to the top of the structure, which also helps support it after the etch. The wax, when cooled to room temperature, is under tension and the substrate under compression, so, as the release layer is etched away, the thin film curls up slightly, thus aiding the lift-off process.

However, there are other techniques to separate the epitaxial layers from their substrates:

1. Chemical or mechanically etching: This method has been developed to etch away the whole substrate for several material systems, but it has some drawbacks as well. This method can cause damage to the epilayers and substrate after etching [3] [4] [5].
2. Thermal lift-off process: In this process the substrate is chosen to have a very different thermal expansion coefficient with respect to the epilayers. When cooling, the differential contraction induces a large stress field which is released by the initiation and the propagation of a crack parallel to the surface and thus results in delamination [6]. Although, this method has an advantage that it does not require any post growth processing, it however require pattering of the

substrate before growth to control or assist the delamination process and typically causes damage to the epitaxial layers.

3. Laser lift-off process: This is another lift-off technique, the whole substrate is exposed to laser light of high intensity pulses which are absorbed by epitaxial layers, causes degradation of substrate in small volume. This process can etch the layers rapidly, but it is likely to induce damage [7] [8].

A new approach for the ELO process by annealing the substrate before applying Apezion wax could form dome shape structure which can induce strain in the epilayers on the substrate, was first demonstrated by Yablonovitch [9]. It has improved the etch rate of release layer and allowed larger areas to be lifted. Applying stress to the epilayer during etching will cause an upward force which can open up the etch the layer [9]. The handling of the ELO layers was studied to attach lifted layers onto a new substrate without an adhesive.

ELO technology has been studied before and successfully transferred the epilayer on different substrate material and also some of them have been integrated with other grown substrate devices such as GaAs light emitting diodes (LEDs) [10] [11], GaAs/AlGaAs laser diodes [12] [13] strained single quantum well in InGaAs/GaAs high electron mobility transistors (HEMTs) [14], GaAs metal-semiconductor field-effect transistors (MESFETs) [15] ,optical waveguides [16] and solar cell [17].

Even though there have been many promising results from ELO process, but still it requires improvement in the technique to increase the etching rate of the release layer, design more complex devices and make it suitable for industrial production [18] [1]. There were some attempts to improve the strain induced in epitaxial layers without cracking them to allow large areas to be lifted. This leads to other modification in the ELO

process including weight induced epitaxial lift-off process (WI-ELO) [19] and using flexible plastic carrier to aid the lift-off of a whole 2-inch wafer [18].

One of the major problems with ELO is to give special care while handling lifted epilayers as, using strain to increase the lifted area and etch rate and mechanical adhesion of the epilayers to new host substrate [19]. This can lead to the cleavage cracks in the lifted layers. For instance, in large area devices such as solar cells, there is significant risk of forming cleavage cracks. These cleavage cracks could break the circuit, increasing its resistance. The lifted layers itself is stress free layer separated from the substrate and as a result strains as low as 0.1% can introduce cracks. It has been reported that a switch from using Apiezon wax to commercially available thin film polymers for support has proved to be advantageous in producing crack-free films. Thin polymer layers can tolerate much smaller stresses, meaning there is less stretching of the lifted -off film.

Studies recently focussed on combining semiconductor structures using novel post growth processing such direct wafer bonding to overcome some inherent growth or material limitations. ELO process shows that two different semiconductor layers can be combined in one structure.

4.3: II-VI Epitaxial Lift-off

Studies focussed on combining III-V semiconductor structures using novel post growth processing such direct wafer bonding to overcome some inherent growth or material limitations. When applied to II-VI semiconductor materials, it required both III-V and II-VI MBE due to the unavailability of suitable sacrificial material.

In Heriot Watt MBE group pioneered II-VI ELO by substituting AlAs with highly reactive MgS as the sacrificial layer. MgS is easily soluble in HCl with a high etch rate compared with other II-VI materials, ~10^8:1. This allows for quick and consistent exfoliation of the II-VI layers. Our group have previously shown that the lifted layers can be transferred to

a range of alternative substrates including BO_2Si_3 glass, distributed Bragg reflectors (DBR's) and lithium niobate surfaces for a range of functional applications [20].

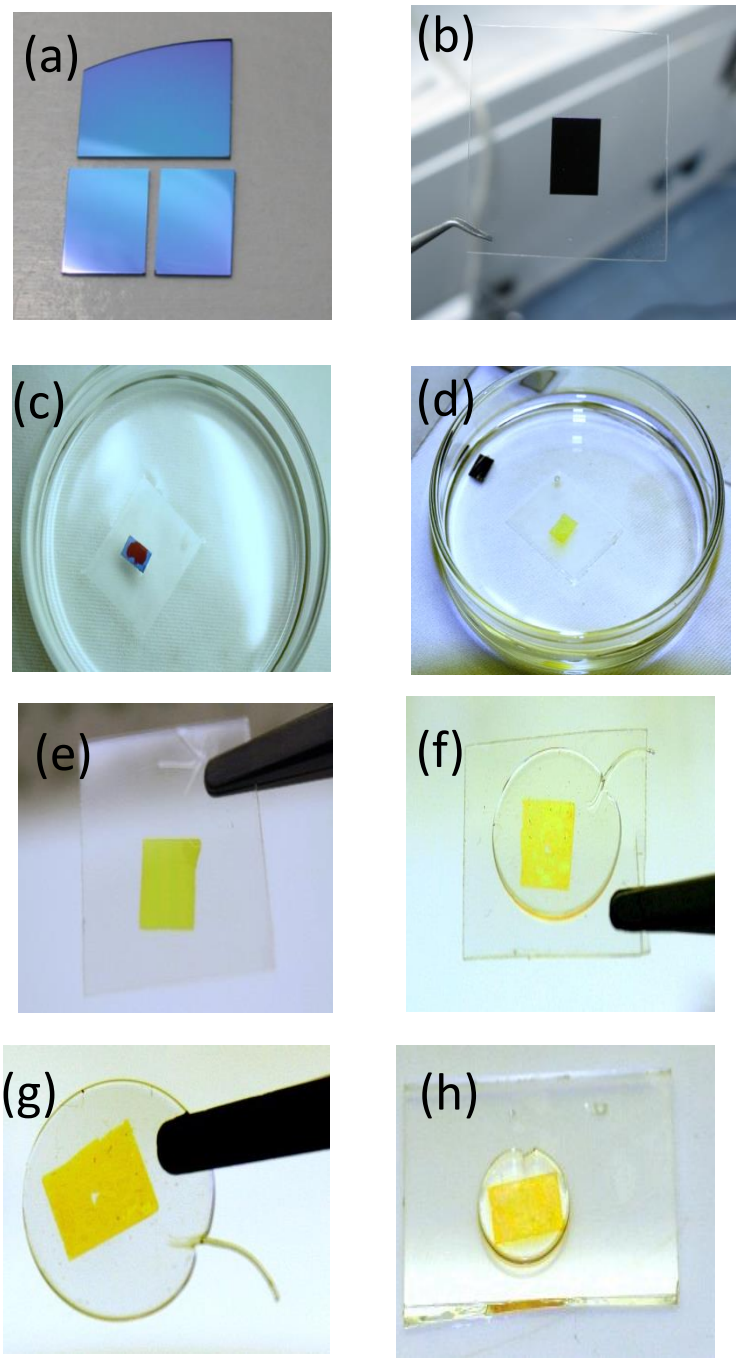

Figure 4.1: Photographic representation of various stages involved in modified version Epitaxial lift off process (a) Cleaving (b) Thin film polymer (c) Etching (d)Substrate falls to bottom (e)Transfer to thin film (e) Separated layer on polymer film (f)Applied clear wax on exposed layer (g) Separated the layer from polymer film (h) Bonding to glass plate.

4.4 Minimum release layer thickness

From the previous experimental work, the minimum MgS release layer thickness necessary for lift-off was found to be ~3 nm. This minimum thickness arises from the van der Waals (VDW) interaction between two adjacent unetched layers. This force is very short ranged, typically just a few nanometres, varying with the layer separation cubed. Here, the layer separation is simply the thickness of the MgS release layer.

The amount of VDW force from the release layer was calculated by Gusso et. al. for GaAs and silicon [21]. These show a force per unit area equivalent to a pressure>18 atm. when the layers are separated by 2 nm, decreasing to ~5 atm. at 3 nm. However, the total force acting on the layers during lift-off from substrate is unknown. By using thin polymer film can produce upward pressure of the order of 10s of atmospheres arising from its surface tension (0.065 ± 0.003 Nm^{-1}). This explains that for any thickness below 3 nm, the VDW force will match or overcome the upward force and thus stop the epilayers from lifting.

4.5 MgS based Epitaxial Lift-off process

The epitaxial lift-off process in II-VI material is six stage process and shown pictorially in Figure 4.1.

a) **Substrate cleaving**: Samples were cleaved into the size of 5x5 mm^2 pieces. We have also expanded the cleaving to 1 inch per square size for successful lift-off.
b) **Flexible carrier**: The cleaved samples were stuck onto thin polymer film. This film provides an upward force helping lift the layer while providing structural support while in etch. The polymer is easily available and cheap which is one of the advantages.
c) **Chemical Etching**: The sample is placed in solution of 30% dilute HCl at room temperature. Once etched the substrate falls to bottom, leaving lifted layer and thin film on surface. The etch rate of MgS is around 3mm/hour.

d) **Transfer**: The lifted layer is carefully removed from the solution and rinsed in deionised water. The clear wax is heated around 125°C to melt and forms a smooth liquid. This melted wax is then dropped onto the exposed surface of II-VI semiconductor layer and then coated with clear wax, to remove the film and transfer to glass plate.

e) **Bonding**: The layer is then transferred to glass plate using Hydrogen Peroxide (30% of water). No glue is used during deposition of the layer to glass plate. Hydrogen peroxide is used as medium between II-VI layer and glass plate. The samples placed under tension of 6-12 hours. Since there is medium of Hydrogen peroxide, surface produced in aqueous environment have some oxygen linkage to the bonded layer to both Se – OH and Zn – OH. This probably comes from water in H_2O_2. Also adding an extra link means there is an extra degree of freedom which can cope with misalignment in x, y and z direction.

f) **Wax removal**: Wax is then removed by dissolving it in acetone. The wax will completely dissolve in two minutes and the sample is then cleaned using IPA and deionised water.

g) **Stacking of lift-off layer**: This process is repeated for each lifted layer stacking each new layer on top of the previous.

Figure 4.2 shows the flow diagram of the ELO process and stacking of multiple layers on top of each other.

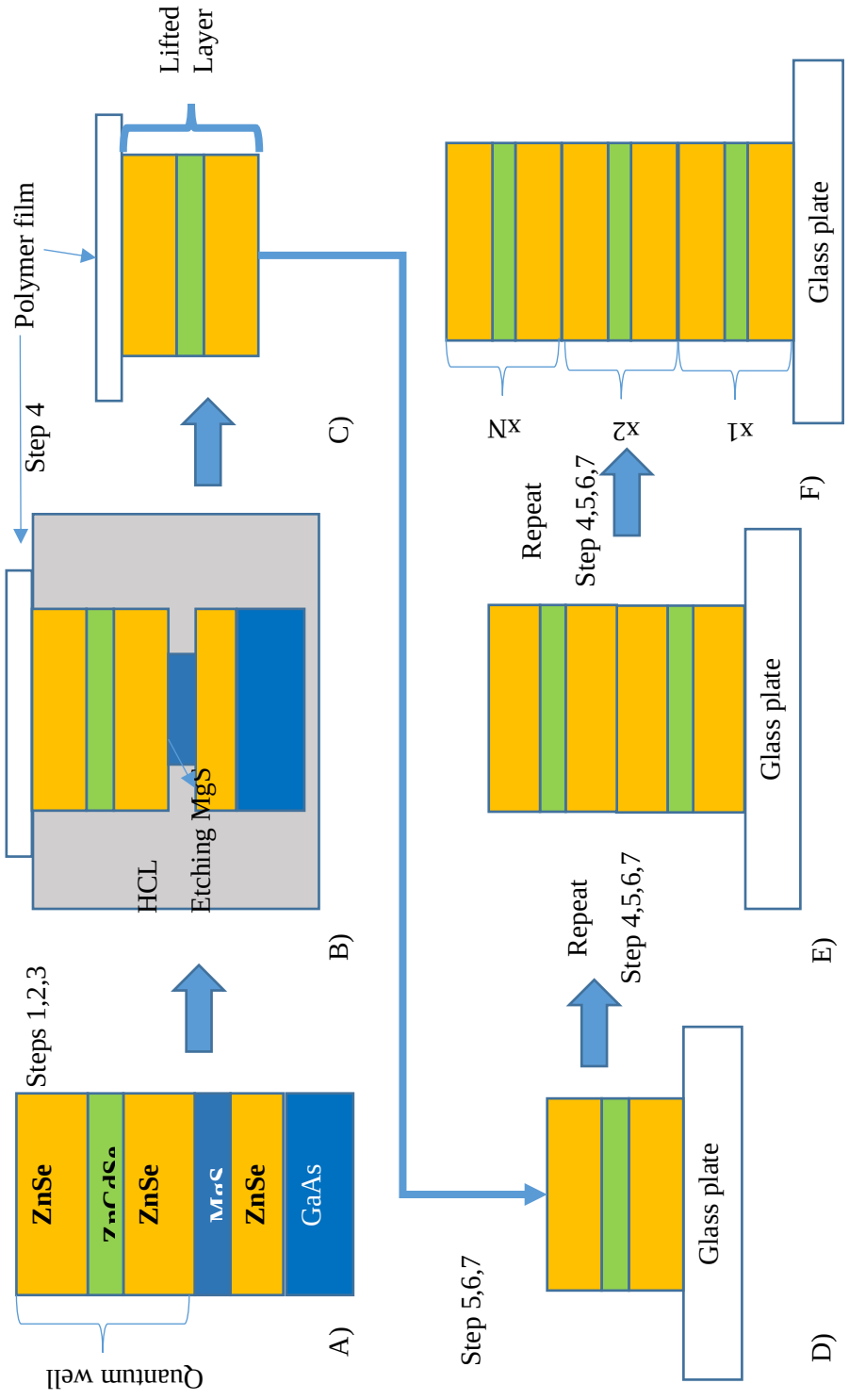

Figure 4.2: Flow diagram showing how layers are stacked on top of each layer after lift-off.

4.6: MgS Etch Mechanism

A 30% (~ 12 mol) HCl etch solution is used for all the lift-off process in this thesis. When the MgS reacts with etch solution to form Mg^{2+} and Cl^- ions along with hydrogen sulphide (H_2S). The reaction gives in equation 3.1.

$$MgS + 2HCl \Longrightarrow Mg^{2+} + 2\,Cl^- + 2H_2S \qquad \text{Equation (4.1)}$$

Both the Mg^{2+} and Cl^- are highly soluble in water up to high concentrations, whereas etch rates of ZnSe and ZnCdSe layers are very slow in HCl. The etch rate of MgS on GaAs (100) is approximately 3 mm/hour, much faster compared to the etch rate of AlAs 0.5mm/hour release layer which is used in comparable GaAs/AlGaAs devices [9].

4.7: Cracking of lift-off layers

While the grown sample is deposited onto a new surface, considerable care should be given as the epilayer structure is in nanometre scale, and the layer can be possibly damaged if handled carelessly. When applying pressure on top of the sample during bonding with glass plate, too much pressure was found to crack the sample which is shown in Figure 4.3. The surface morphology of the lifted layer was checked under ultra-violet microscope.

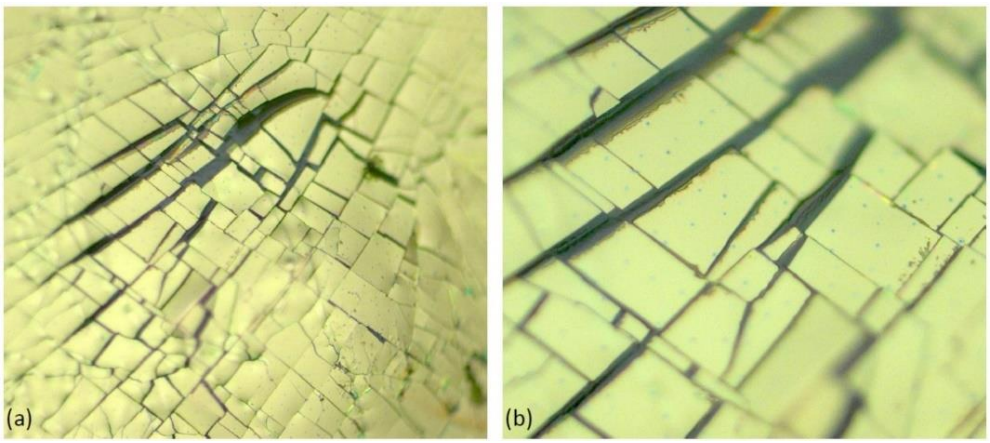

Figure 4.3: (a) 50x and (b)200x magnification image of the crack formed on the lifted epilayer by applying more pressure during bonding onto a glass plate.

In some cases when the surface is not properly cleaned can also cause cracks due to dust or particulates between the epilayer and the new surface, which leaves an area of epilayer not bonded to the new surface. Figure 4.4 shows crack due to trapped particle in the glass plate.

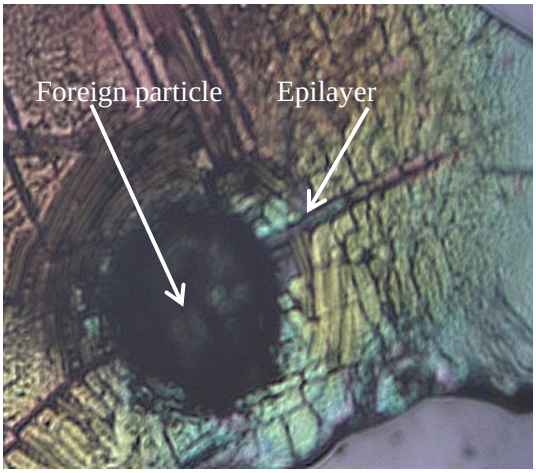

Figure 4.4: Microscopic image of the crack in the lift off layer while sticking on a glass plate with particle trapped in it.

This problem can be avoided by cleaning the substrates before use and remove the epilayers from their final rinse using the new substrate. Also, microscopic glass plates were used which had rough surfaces, it was found that there were defects on the epilayer, the amount of which can be reduced by using glove box.

The thickness of each ELO layer on the glass plate was measured by DEKTAK thickness profiler and shown in Figure 4.5. The linear increase in the thickness of each layer has an error of ±10% and as such is not overly accurate, however demonstrates that the layers have stacked successfully. The comparison of 3x stacked QW on a glass plate and triple QW grown on GaAs substrate shows roughly the same thickness within the error of ±10%. The layers were stacked staggered to each other to create steps for the thickness measurement.

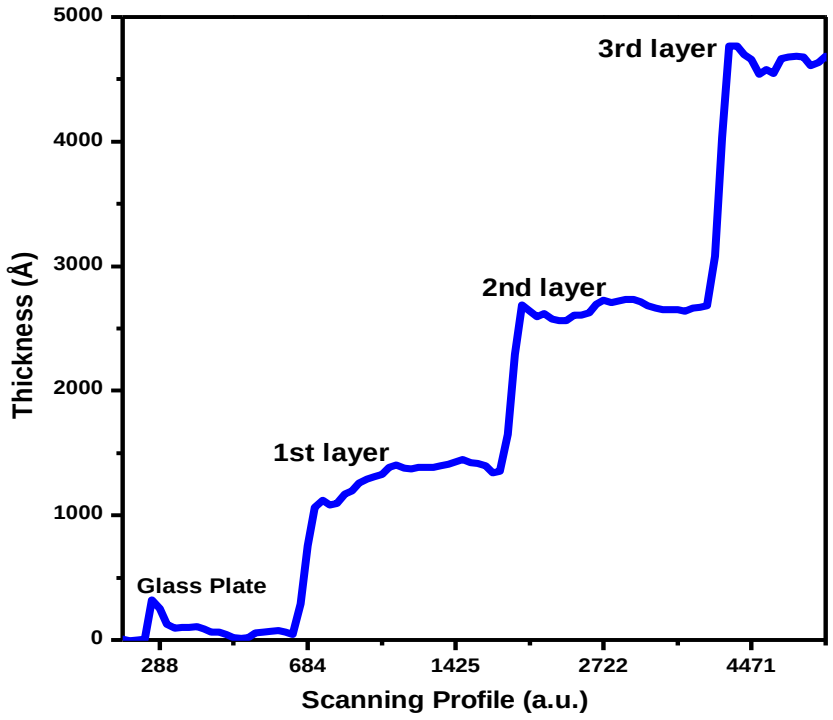

Figure 4.5: Thickness measurement taken by DEKTAK thickness profiler. Blue line indicates total structural thickness after each additional layer. The stacked layers were positioned staggered to each other to allow for a step to be made specifically for this measurement.

4.8 Analysis of PL spectra for stacked layers

To examine the quality of the stacked layer, PL measurements of both single and triple QWs on GaAs substrates were taken and compared to the 3 stacked single QW on the glass plate. All samples were measured at both 77K, with the same excitation power (25mW) and integration time (10s), and RT, with excitation power (65mW) and integration time (10s). The resultant spectra are shown in Figure 4.6. Table 4.1 shows the values of FWHM, emission energy and sample thickness measured for all samples.

From the results there is negligible shift in PL peak position (~2meV) of stacked layer compared with that of the ‘as grown’ structure. This shows there is little strain induced during the ELO and stacking procedure. The ZnSe peak at 2.78eV is not visible in these spectra as the QW emission dominates, and to allow for comparison between samples we

required a laser power low enough not to saturate our CCD detector. This reduced the ZnSe peak such that it cannot be seen in these spectra. What is of great interest is the large increase in PL emission intensity of the stacked well.

The increase in the PL emission intensity of the 3x stacked layer compared to its 'as grown' comparison is of great interest and completely unexpected. I suspect that non radiative recombination effects, due to defects, increases in the grown layer once it has fully relaxed and limits the emission intensity. The single well structure is below the critical thickness for relaxation (~150 nm) and therefore the radiative recombination rate for each stacked layer remains the same. This provides an additive effect to the emission intensity for each additional layer, unhindered by defect generation. Therefore, the PL intensity emission of these stacked structures can be increased further by stacking more layers. Limited only by absorption effects within the structure. The intensity of the 3 stacked layers on glass plate is ~200% larger compared to the triple QW grown on GaAs, this was seen to be true for both LT and RT measurements.

Quantum Well Structure (QW)	**FWHM (meV)**		**Peak Energy (eV)**		**Thickness (nm)**	**Peak height (a.u.)**	
	77K	**RT**	**77K**	**RT**		**77K**	**RT**
Single QW	33.65	43.06	2.456	2.392	150	1842	6623
Triple QW	33.52	46.75	2.458	2.385	450	5899	9421
3xStacking single QW	35.01	81.35	2.458	2.387	465	9855	11592

Table 4.1: The change in the peak position, FWHM, peak height and thickness of single QW, triple QW and 3 stacking single QW at 77K and RT.

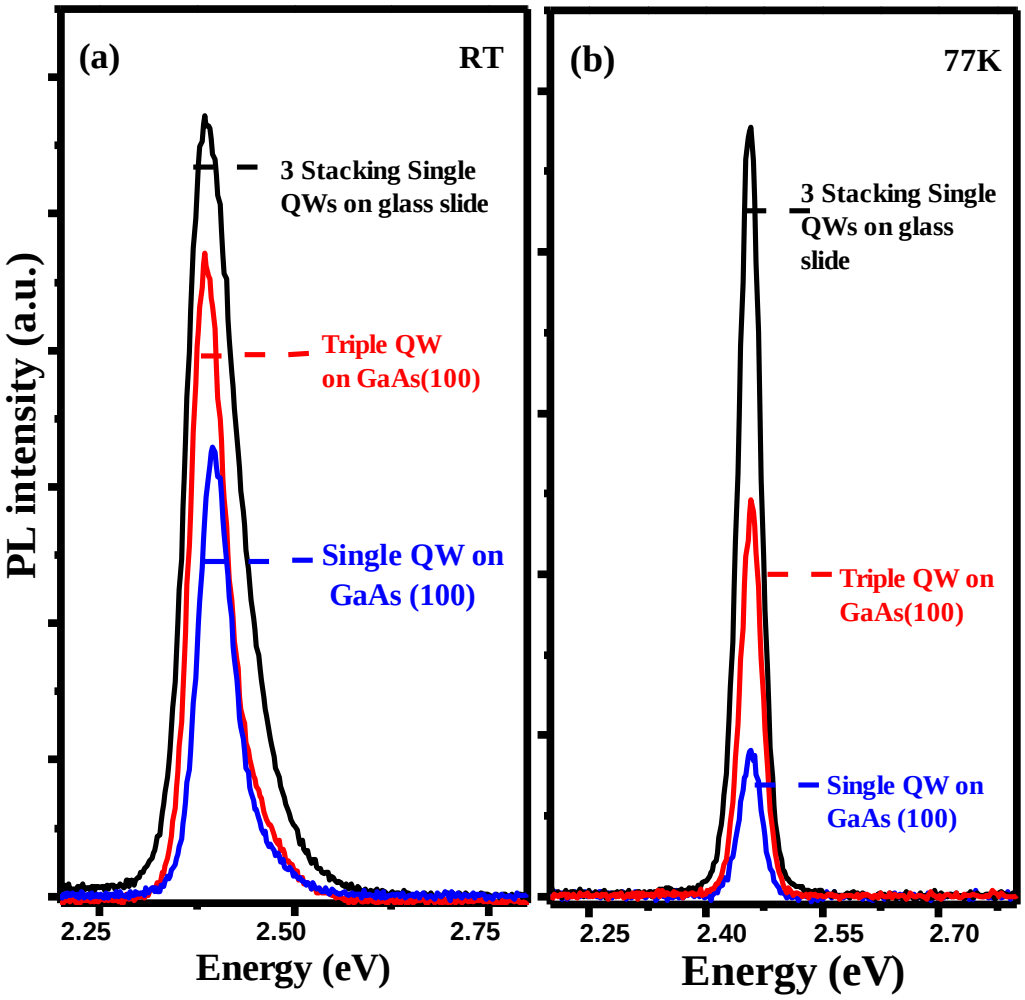

Figure 4.6: PL Spectra of single, triple QW and 3 x stacked QW at 77K and RT. All measurements were taken under same conditions so a relative intensity comparison can be made.

4.9 Stacking of lift-off layers on GaAs (100) substrate

We have repeatedly done the ZnCdSe QW growth and stack the lifted layers on GaAs (100) substrate. Two types of structures were grown,

HWC803: ZnCdSe (10 nm)/ZnSe (70 nm)/MgS (6 nm)/ZnSe (10 nm)/GaAs (100)

HWC 804: ZnSe (70 nm)/MgS (6 nm)/ZnSe (10 nm)/GaAs (100)

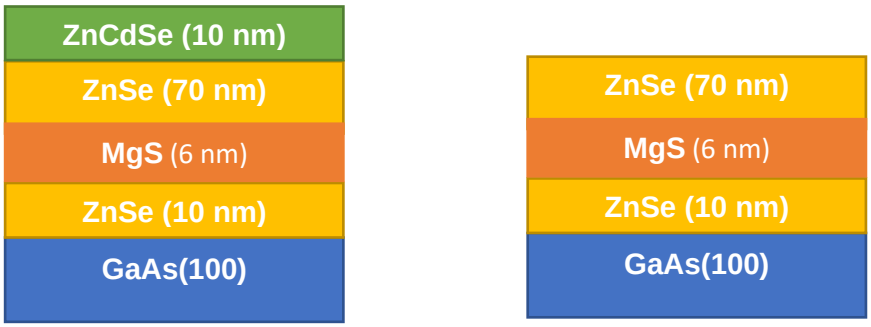

(a) (b)

Figure 4.7: Schematic diagram of samples (a) HWC 803 and (b) HWC 804 with structures ZnCdSe (10 nm)/ZnSe (70 nm)/MgS (6 nm)/ZnSe (10 nm)/GaAs (100) and ZnSe (70 nm)/MgS (6 nm)/ZnSe (10 nm)/GaAs (100) respectively.

The growth parameters remained constant for both the samples HWC 803 and HWC 804, were grown under the same flux ratio, growth temperature, and on the same day to allow for a direct comparison between them. After lift-off process, both samples were measured at 77K, with the same excitation power (25 mW) and integration time (10 s). The epitaxial layer from HWC 803 was lifted by using ELO process and stacked on top of GaAs (100) substrate. PL spectra of stacking ZnSe barrier layer on top of lifted layer ZnCdSe/ZnSe stacked on GaAs (100) substrate at 77K shown in Figure 4.8.

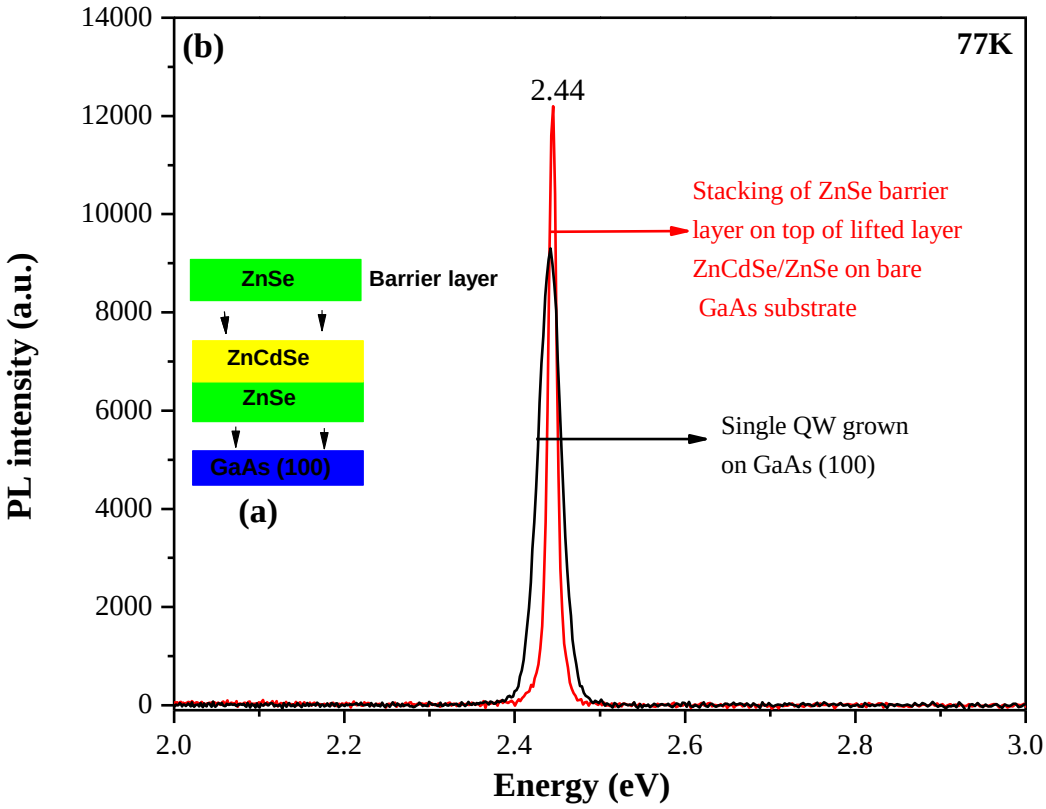

Figure 4.8: (a) Schematic diagram showing stacking of HWC 804 after lift-off of ZnSe barrier layer on top ZnCdSe/ZnSe/GaAs (100) and (b) PL spectra of stacking ZnSe barrier layer on top of lifted layer ZnCdSe/ZnSe QW at 77K.

PL spectra of one and two-layer stacking of HWC 803 (ZnCdSe/ZnSe) on top of bare GaAs (100) substrate is shown in figure 4.9. The FWHM of both stacked layers were remain constant around 16meV at 77K and there was no significant change in the PL peak position. There is no peak from ZnSe layer (2.78eV), shows quantum well emission is more dominant compared to ZnSe barrier layer. Also, the strain induced during stacking of multiple layers can be reduced in bare GaAs (100) substrate or polished glass plate. The roughness of the glass plate was determined to be ~11 nm compared to ~0.4 nm for a bare GaAs wafer.

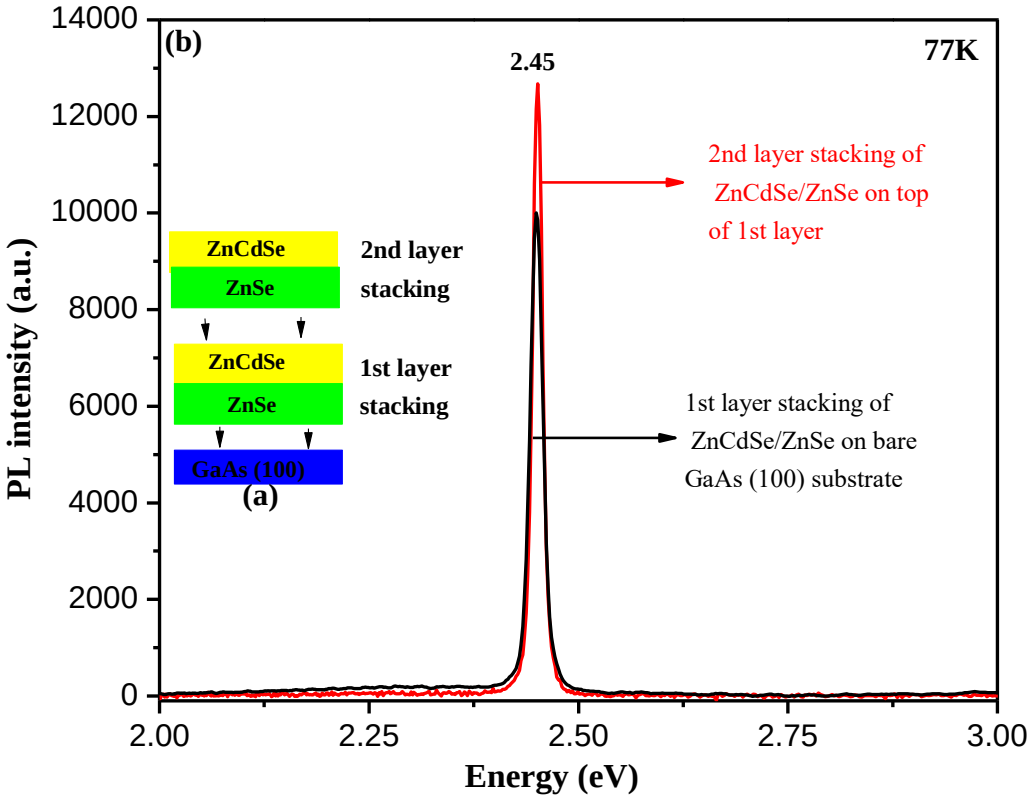

Figure 4.9: (a) Schematic diagram showing lift-off layer from HWC 803 ZnCdSe/ZnSe QW structure stacked one layer and second layer on top of bare GaAs (100) substrate and (b) PL spectra of stacked one layer and two layers of ZnCdSe/ZnSe QW layer on bare GaAs (100) substrate at 77K.

Figure 4.10 shows the corresponding temperature dependence of the PL emission of ZnSe barrier layer on top ZnCdSe/ZnSe/GaAs (100). The PL intensity remains constant at temperatures <100K, and as the temperature rises gradually, intensity decreases steadily to RT, see figure 4.10. This shows for temperature <100K, the radiative recombination is more dominant. In this regime the single exponential nature of the decay is consistent with linear excitonic recombination while the second component observe at the lowest temperature is probably due to localized or impurity bound exciton recombination. For temperature >100K, the PL intensity decrease with increasing temperature, and thus the

corresponding reduction of the PL decay time is consistent with increasing nonradiative recombination.

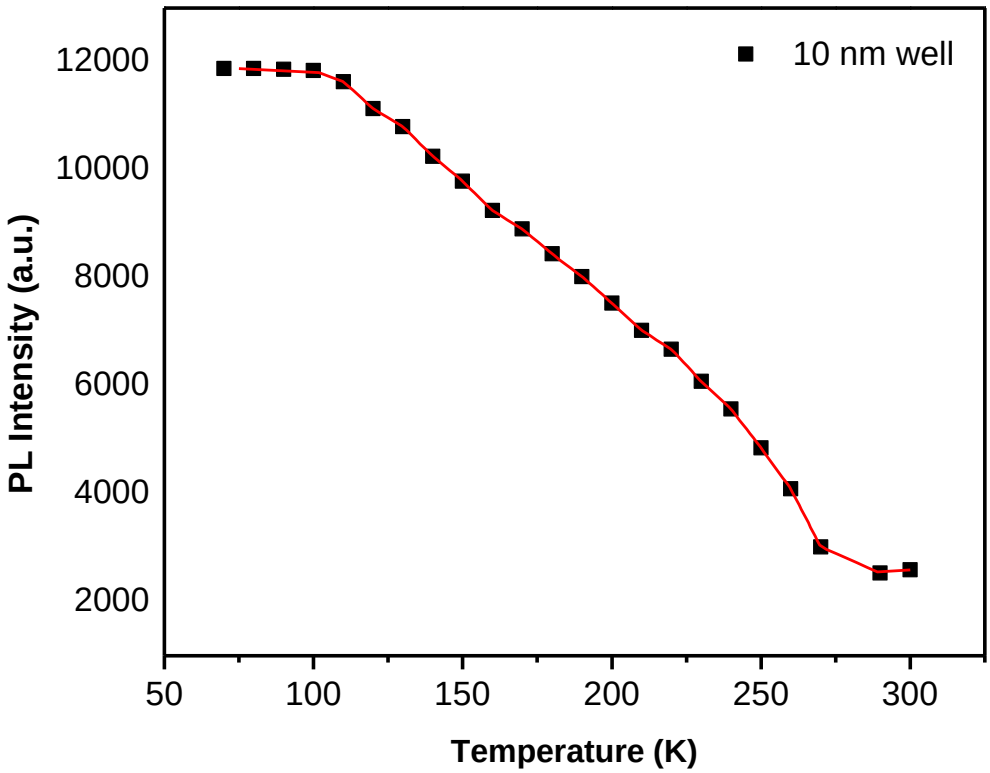

Figure 4. 10: PL emission vs temperature for single quantum well structures with 7 nm and 10 nm wells stacked on GaAs (100) substrate.

4.10 Multiple stacking of QW layers

Figure 4.11 shows the PL spectra of 15-layer stacking of QW layers on glass plate at 77K. During each stacking of lifted layers, the stacked layers were gone under several temperature cycles and stress effect during new stacked layer. Even though the PL peak position has negligible shift of ~2-3meV. A linear increase in FWHM shows after stacking multiple layers can cause additional stress while handling nanometer regime layers.

There might be another situation where total internal reflection occurred between the stacked layers. When incident laser is travelling from a medium with high refractive index

toward a medium with lower index, if the angle of incidence on the interface between two media is above critical angle which can be calculated using Snell's law. For instance, air-glass interface is ~43 degrees, it is being reflected into optically dense medium. But there is still electro-magnetic field in the second medium, that is not propagating and exponentially decays from the interface. This decay distance (penetration depth) depends on refractive index of both media, angle of incidence and wavelength.

The penetration depth of the incident laser is depending on focal spot size and wavelength of incident wave, shown in equation 3.8.

Penetration depth = $k.w^2$ where $k = \frac{2x3.14}{\lambda} * n$ Equation (3.8)

n is the refractive index

λ is the wavelength of the incident wave and

w is the width of spot size

From the above equation 3.8 the penetration depth of GaN diode laser is calculated around ~2.25 µm, which is the thickness of 15 stacked layers on glass plate. The incident laser cannot penetrate beyond the penetration depth which could be the reason for the saturation after 15 stacked layers.

The adhesion properties of ZnSe to ZnSe layer and ZnSe to glass slide has been studied [22]. The result indicates that the bonding at the interface between ZnSe and ZnSe or glass is predominately chemical instead of van der Waals. This shows, linear increase in the PL emission shows the emission from each stacked layer is between the epitaxial layers. Figure 4.12 shows PL intensity vs number of stacked layers on glass plate.

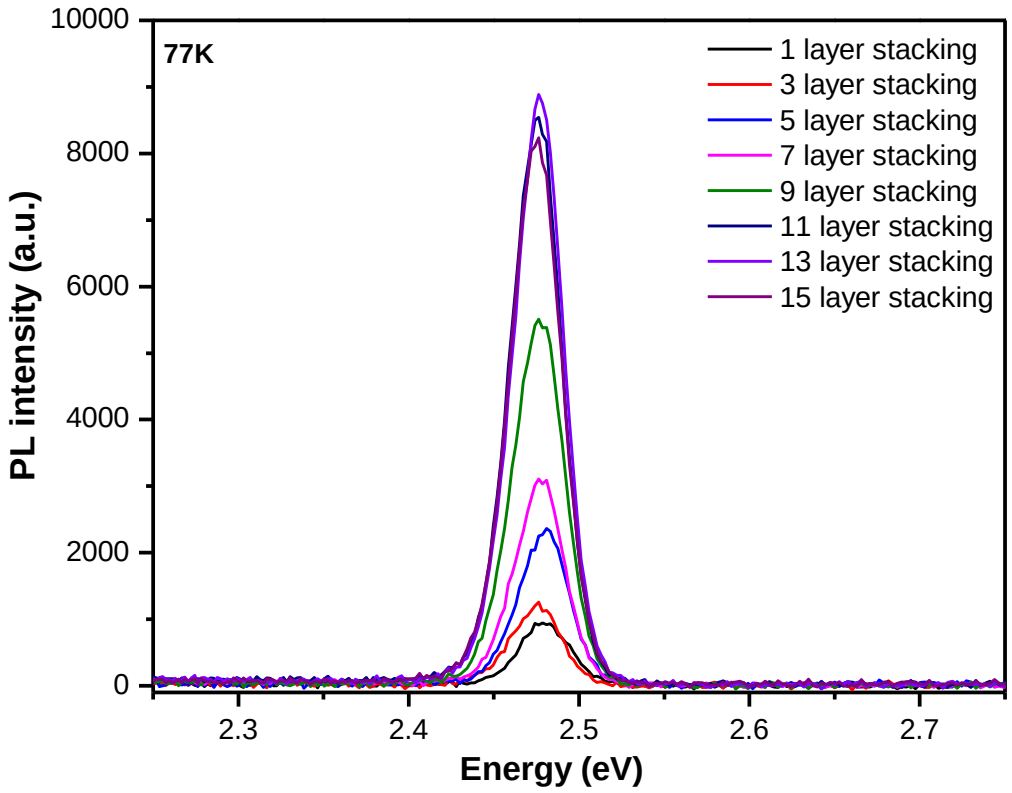

Figure 4.11: PL spectra of 15-layer stacking of ZnSe/ZnCdSe/ZnSe lifted layer on glass plate after ELO process.

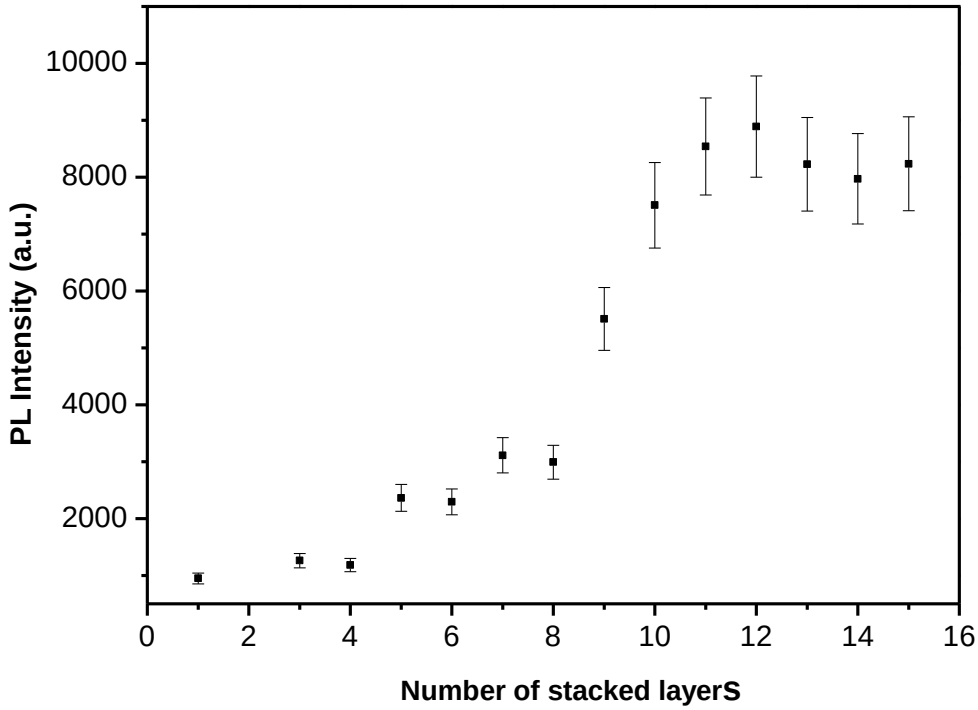

Figure 4. 12: PL intensity vs number of stacked layers for single quantum well structures with ZnSe/ZnCdSe/ZnSe stacked in glass plate.

The comparison of different quantum well layers grown in MBE with stacked layers to find out the difference in optical properties shown in figure 4.13. For this experiment we have grown 3, 6 and 9QWs ZnCdSe/ZnSe structures on GaAs (100). All these samples were measured with same excitation power (55mW), integration time (10s) and 77K temperature. The increase in the QW shows decrease in PL emission from the sample grown in MBE machine. This result proves the importance of ELO process in complex devices which cannot grow physically in growth chamber.

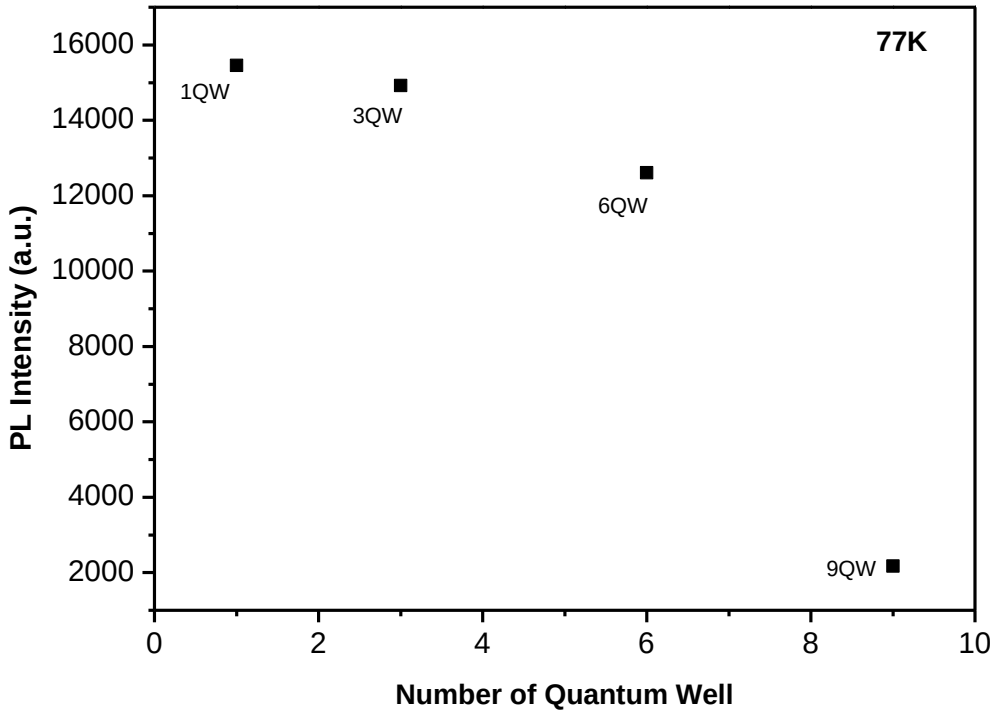

Figure 4.13: PL emission vs number of quantum well grown in GaAs (100) substrate before lift-off.

4.11 Discussion of stacked layers

There is a slight increase in the FWHM between the triple well and the stacked well at both 77K and RT, we suspect this is due to the surface roughness of the glass plate, compare with the GaAs substrate. As the layer is adhered to the glass plate, we propose that the layer adopts the profile of the glass and generates pinch points in the layer, this in turn generates a variation in the QW emission and broadens the FWHM. The roughness of the glass plate was determined to be ~11 nm compared to ~0.4 nm for a bare GaAs wafer. This could easy be resolved with a higher polish of glass. It would be advantageous at this stage to measure the roughness of the final stacked layer to investigate how this roughness propagates through successive layers and this will the topic of future work. More structural characterisation is required for this technique and in the future, we plan to attempt to obtain some XRD measurements of the stacked layer. In this study, as the

layers were stacked on glass this was not feasible, but the process can be repeated on GaAs to demonstrate structural integrity of each stacked layer. Alternatively, ellipsometry can be used to examine the layers optically. This will also give us more accurate thickness profiles and can be used to quantify surface roughness. This will be the focus of future work also.

4.12 Conclusion:

We have presented here for the first time that ELO layers can be stacked into new structures while maintaining structural and optical quality. It was seen that the stacked layers provided larger PL intensities in comparison to as grown structures of the same design. There was little or no shift in energy between stacked layers indicating that little or no strain was being introduced during the stacking process. The samples underwent many temperature cycles during the test and still strong PL was observed. This process demonstrates that ELO has the potential for creating previously unobtainable structures.

REFERENCES

[1] P Demeester, I Pollentier, P De Dobbelaere, C Brys and P Van Daele, "Epitaxial lift-off and its applications," Semiconductor Science and Technology, vol. 8, pp. 1124-1135, 1993.

[2] Konagai M, Sugimoto M and Takahashi T, "High efficiency GaAs thin film solar cells by peeled film technology," Journal of Crystal Growth, vol. 45, pp. 277-280, 1978.

[3] L. M. Liu, G. Lindauer, W. B. Alexander and P. H. Holloway, "Surface preparation of ZnSe by chemical methods," Journal of Vacuum Science and Technology B: Microelectronics and Nanometer Structures, vol. 13, pp. 2238-2244, 1995.

[4] M. Rei Vilar, J. El Beghdadi, F. Debontridder, R. Artzi, R. Naaman, A. M. Ferraria and A. M. Botelho do Rego, “Characterization of wet-etched GaAs (100) surfaces,” Surface and Interface Analysis, vol. 37, pp. 673-682, 2005.

[5] S. Pinel, J. Tasselli, J. P. Bailbe´, A. Marty, P. Puech and D. Este`ve, “Mechanical lapping, handling and transfer of ultra-thin wafers,” Journal of Micromechanics and Microengineering, vol. 8, pp. 338-342, 1998.

[6] F. Dross, J. Robbelein, B. Vandevelde, E. Van Kerschaver, I. Gordon, G. Beaucarne and J. Poortmans, “Stress-induced large-area lift-off of crystalline Si films,” Applied Physics A, vol. 89, pp. 149-152, 2007.

[7] W. S. Wong, T. Sands, M. Kneissl, N. W. Cheung, D. P. Bour, P. Mei, L. T. Romano and N. M. Johns, “Fabrication of thin-film InGaN light-emitting diode membranes by laser lift-off,” Applied Physics Letters, vol. 75, pp. 1360-1362, 1999.

[8] M. K. Kelly, O. Ambacher, R. Dimitrov, R. Handschuh and M. Stutzmann, “Optical Process for Liftoff of Group III-Nitride Films,” Physica status solidi (a), vol. 159, pp. R3-R4, 1997.

[9] E. Yablonovitch, T. Gmitter, J. P. Harbison and R. Bhat, “Extreme selectivity in the lift-off of epitaxial GaAs films,” Applied Physics Letters, vol. 51, pp. 2222-2224, 1987.

[10] I. Pollentier, P. Demeester, A. Ackaert, L. Buydens, P. Van Daele and R. Baets, “Epitaxial lift-off GaAs LEDs to Si for fabrication of opto-electronic integrated circuits,” Electronics Letters , vol. 26, pp. 193-194, 1990.

[11] I. Schnitzer and E. Yablonovitch, “30% external quantum efficiency from surface textured, thin-film light-emitting diodes,” Applied Physics Letters, vol. 63, pp. 2174-2178, 1993.

[12] I. Pollentier, L. Buydens, P. Van Daele and P. Demeester, “Fabrication of a GaAs-AlGaAs GRIN-SCH SQW laser diode on silicon by epitaxial lift-off,” IEEE Photonics Technology Letters, vol. 3, pp. 115-117, 1991.

[13] M. Yanagisawa, H. Terui, K. Shuto, T. Miya and M. Kobayashi, “Film-level hybrid integration of AlGaAs laser diode with glass waveguide on Si substrate,” IEEE Photonic Technology Letters, vol. 4, pp. 21-23, 1992.

[14] J. F. Klem, E. D. Jones, D. R. Myers and J. A. Lo, “Characterization of thin AlGaAs/InGaAs/GaAs quantum-well structures bonded directly to SiO2/Si and glass substrates,” Journal of Applied Physics , vol. 66, pp. 459-462, 1989.

[15] I. Polentier, L. Buydens, A. Ackaert, P. Demeester, P. van Daele , F. Depestel, D. Lootens and R. Baets, “Monolithic integration of an InGaAs/GaAs/AlGaAs strained layer SQW LED and GaAs MESFET using epitaxial lift-off,” Electronic Letters, vol. 26, pp. 925-927, 1990.

[16] J. C. Fan, C. P. Lee, C. M. Tsai, S. Y. Wang and J. S. Tsang, “Optical and structural properties of epitaxially lifted-off GaAs films,” Journal of Applied Physics, vol. 83, pp. 466-469, 1998.

[17] A. v. Geelen, P. Hageman, G. Bauhuis, P. v. Rijsingen, P. Schmidt and L. J. Giling, “Epitaxial lift-off GaAs solar cell from a reusable GaAs substrate,” Materials Science and Engineering: B, vol. 45, pp. 162-171, 1997.

[18] J. J. Schermer, P. Mulder, G. J. Bauhuis, M. M. A. J. Voncken, J. van Deelen, E. Haverkamp and P. K. Larsen, “Epitaxial Lift-Off for large area thin film III/V devices,” Physica status solid (a), vol. 202, pp. 75-80, 2005.

[19] M. M. A. Voncken, J. J. Schermer, G. Maduro, G. J. Bauhuis, P. Mulder and P. K. Larsen, “Influence of radius of curvature on the lateral etch rate of the weight induced epitaxial lift-off process.pdf,” Materials Science and Engineering: B, vol. 95, pp. 242-248, 2002.

[20] C. Bradford, A. Currran, A. Balocchi, B.C. Cavenett, K.A. Prior and R.J. Warburton, “Epitaxial lift-off of MBE grown II–VI heterostructures using a novel MgS release layer,” Journal of Crystal Growth, vol. 278, pp. 325-328, 2005.

[21] A. Gusso and G. J. Delben, “Dispersion force for materials relevant for micro- and nanodevices fabrication,” Journal of Physics D: Applied Physics, vol. 41, p. 175405, 2008.

[22] N. Mavridi, J. Zhu, N. Eldose and K. Prior, “Adhesion Measurements of Epitaxially Lifted MBE-Grown ZnSe,” Journal of Electronic materials, vol. 47, pp. 4394-4398, 2018.

This page intentionally left blank

CHAPTER 5

Growth of Zinc Blende (ZB) MgS on GaAs (211) B

5.1 Introduction

The growth of II-VI heterostructures on GaAs (211) B substrate has been previously studied [1]. When strained layers are grown on low symmetry surfaces such as (211), there is a large polarization field due to the internal piezoelectric effect [2] and this has opened the way to applications in electro-optic and non-linear optics such as the self electro-optical effect devices (SEED) which used for optical switching. Also, there is a refractive index dependence for transmitted light related to the surface orientation of the epilayer which is the focus of the current work on (211) oriented layers. If a II-VI epitaxial layer can be removed from the GaAs (211) B substrate, by techniques such as epitaxial lift off (ELO), discussed in chapter 6 and stacked in different crystal orientations, then these (h11) oriented layers (or any surface other than (100)) allows devices to be constructed which optimize second harmonic generation [3].

The following chapter details the growth of zinc blende (ZB) magnesium sulphide (MgS) on GaAs (211) B substrate. The structural characterisation is done by using *in situ* RHEED monitoring during growth, x-ray measurements and Photoluminescence (PL) spectroscopy of the grown sample discussed below.

5.2 GaAs (211) B substrate

Crystal facets are classified into three groups:

1. Singular surfaces: which are formed by planes of high symmetry i.e., all the surface atoms with cut bonds or nearest missing neighbours lie in a single plane such as the (100), (111), and (110) planes. They are low Miller index surfaces that correspond to local minima in surface energy.

2. Vicinal surfaces: lie near singular surfaces, where the surface atoms with cut bonds do not lie in one plane. They are normally a few degrees off singular surfaces.
3. Non-singular surfaces: the surface atoms with cut bonds do not lie in one plane, but these surfaces are formed by combinations of singular surfaces for example (100) and (111). They normally are high Miller index surfaces.

The (211) surface is a non-singular surface and can be considered to have either of two surface configurations, which are formed by the termination of the bulk crystal [4] and are shown in Figure 5.1 and Figure 5.2.

The first configuration shows that the surface is formed by a (111) terrace and (100) step, where the A atoms marked 1 and 7 have been removed. In the second configuration, A atoms 1 and 7 have been left and the surface is formed by a (111) terrace, (211) plane and a riser. Several planes have been shown for comparison in Figure 5.2.

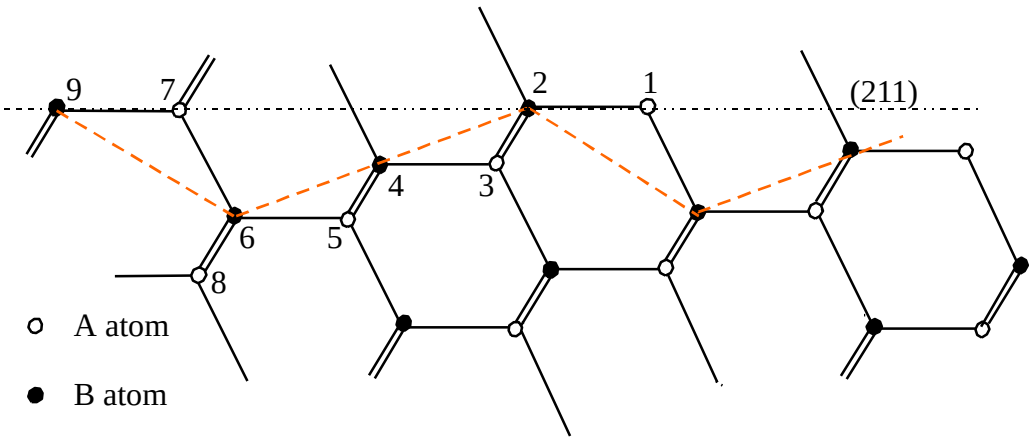

Figure 5.1: Surface Configuration One of GaAs (211) B.

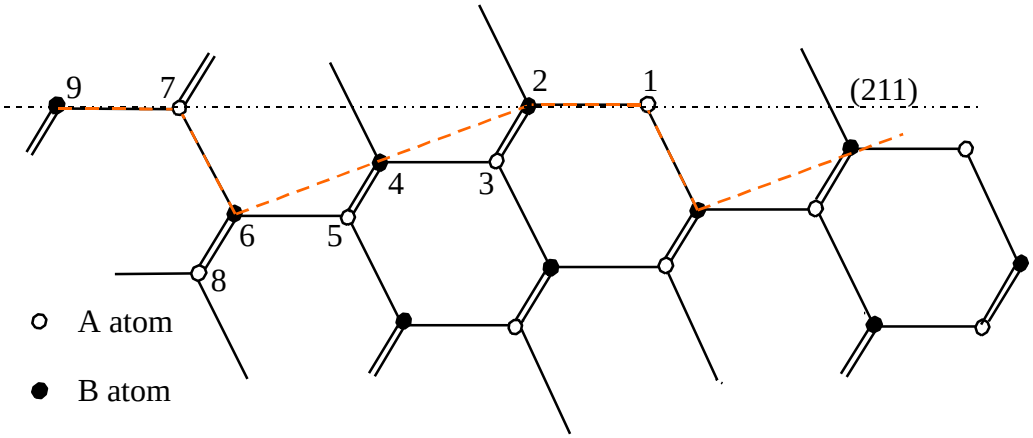

Figure 5. 2: Surface Configuration Two of GaAs (211) B

The surfaces of semiconductor crystals can be polar or non-polar; the polarity of a surface is important although electrically the interface between a substrate and epilayer is neutral. It can determine the crystal structure (zincblende or wurtzite) of II-VI epitaxial layers [5], generally the polarity of the substrate is continued in the epilayer. The polarity of a surface depends upon where the covalent bonds are cut to form the surface since the bonds are polar. Sign convention is defined by placing A atoms on the origin of the basis and B atoms at the other sites in the unit cell, e.g. the (¼, ¼,¼) lattice sites. The [111] a direction is from the A atom to the B atom. The polarity, P may be determined by using the following relation [shown in equation 5.1:

$$P = \frac{(n_A - n_B)}{n_T} \qquad \text{Equation (5. 1)}$$

Where n_A and n_B are the number of A and B atoms in a surface unit mesh and $n_T = n_A + n_B$.

When P = -1 and P = 1, represent the polarities of fully polar surfaces like (111) B and (111) A respectively. A value of zero indicates a neutral surface e.g. (011). When $-1 < P < 0$, the surface is predominately covered by B atoms, so it is the B face and $0 < P < 1$, the surface is covered predominately by A atoms, the A face. The (211) surface is polar, therefore it is predominately terminated by non-metal atoms, the (211) B surface or metal

atoms, the (211) A surface, where $0 < |P| < 1$, depending on the surface configuration, e.g. configuration one has $P = -1$ for the (211)B surface. In this project, (211) B GaAs substrates have been used and therefore the surface is predominately terminated by arsenic for GaAs and selenium for (Zn, Cd) Se epilayers.

The (211) surface unit cell is rectangular with $a_o/\sqrt{2}$ width along $[0\,1\,\bar{1}]$ and $\sqrt{3}\,a_o$ length along $[\bar{1}\,1\,1]$ (atoms 2 to 9 in Figure 5.1 and Figure 5.2, [6] and it is shown in Figure 5.4

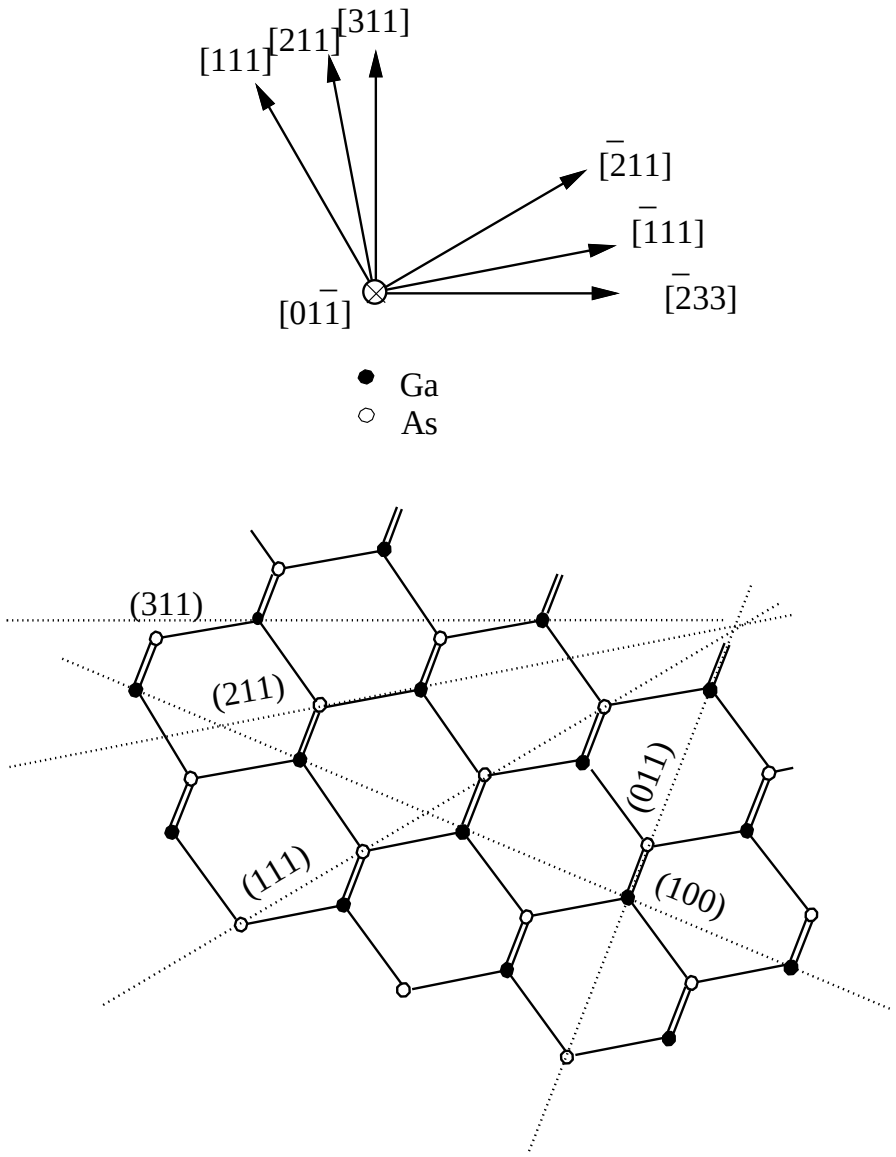

Figure 5. 3: Cross Section of GaAs Showing Several Planes and Directions

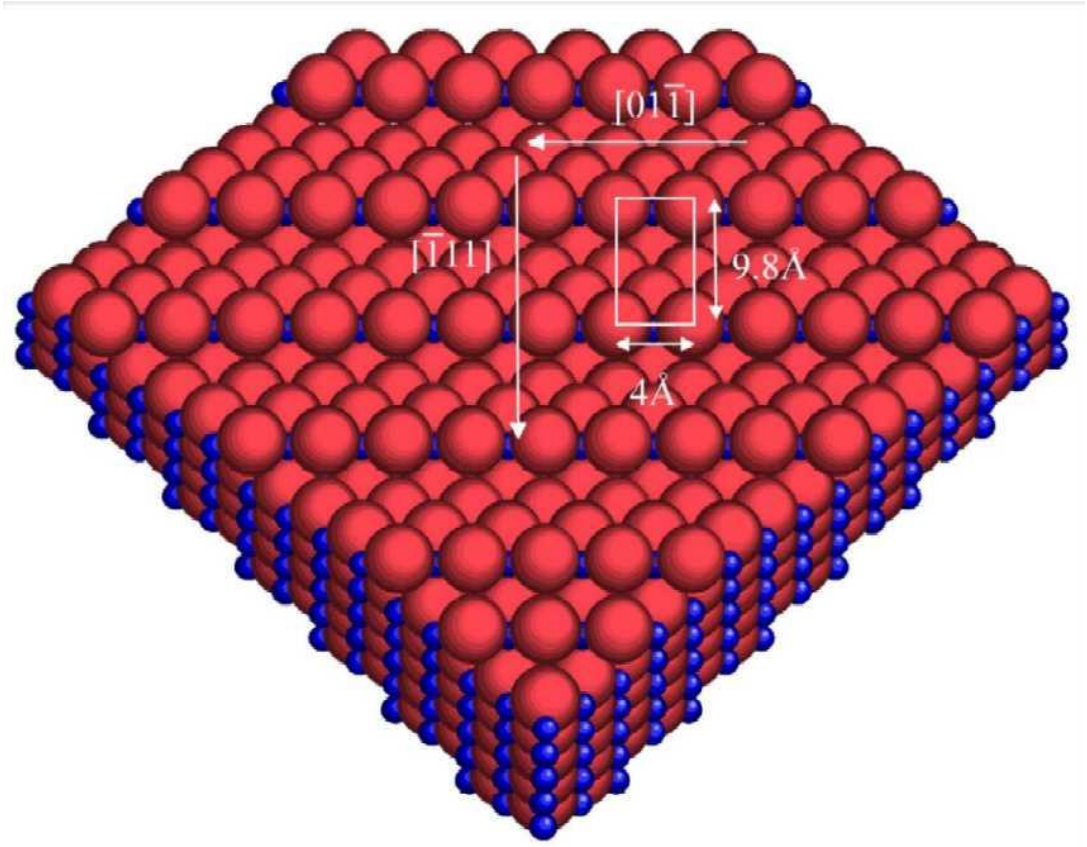

Figure 5. 4: The (211) B Surface with Surface Unit Cell Marked

5.3 GaAs (211) B substrate preparation

The MgS structures were grown on GaAs (100) and GaAs (211) B substrates from American Crystal Technology (AXT) were used to grow ZB MgS. Before transfer into the MBE system the substrate was etched as outlined by Bousquet *et al.* [7] in a 15:2:2 solution of H_2SO_4: H_2O_2: H_2O at 90 seconds. The substrates were then rinsed in 18MΩ deionised water and quickly dried with a jet of dry nitrogen gas. The wafers were then bonded to a molybdenum block using molten indium as a bonding agent. It has been shown by Massies et al [8] that the bonding process produces a surface that is highly oxidised. The oxide layer thickness is typically 2-3 nm and is strongly dependent on the temperature and time taken during bonding.

Once mounted the sample is transferred via fast entry lock to the preparation chamber. It is then placed in the substrate heater and heated to a temperature of approximately 200°C for 10 minutes, which helps to dry the sample before it is transferred to the growth chamber.

The substrates were then cooled down to growth temperature under Zn flux. Previously (211) B ZnSe was deposited with growth temperature ~320-370°C [9], however, it has been shown that for good (100) MgS the substrate temperature should be kept low [10], so for this study we grew both sample sets at the nominal temperature of 240°C, discussed in chapter 3. During the growth of ZnSe, RHEED pattern developed from chevrons along the [11] direction to short streaks, as expected for Se stabilized surface. The orthogonal direction remained similar throughout growth.

On exposure to MgS there appeared to be little change in the RHEED in both azimuths. For (100) MgS growth there is a noticeable change from (2×1) non-metal, to c (2×2) metal growth conditions. This is not due to a change in the flux ratio but the nature of our growth technique where Mg and ZnS fluxes react at surface forming ZB MgS and liberating Zn, which does not then incorporate substantially into the lattice. This gives the appearance of metal rich conditions despite the beam equivalent pressure (BEP) ratio of ZnS:Mg being approximately 500:1. On Zn only exposure there was a very slight change in [11] RHEED pattern to show fractional order streaks that corresponded to a metal stabilized surface. However, it was so subtle there may be other factors such as the low growth temperature that impinge the clarity, therefore further study is required to clearly determine the growth mode for (211) B MgS. Subsequent ZnSe, and ZnCdSe layers described in results section were then grown. It should be noted that during the remainder of the growth there was no change in RHEED. This implies that the MgS had grown in the ZB crystal structure.

5.4 GaAs (211) B oxide desorption – Heriot Watt RHEED observation

RHEED pattern	Figure number	Azimuth	Description
GaAs- Nα	Figure 5.6	$[\bar{1}11]$	Contains no chevrons or fractional orders
GaAs-Nβ	Figure 5.7	$[\bar{1}11]$	Contains chevrons
GaAs-Nγ	Figure 5.8	$[\bar{1}11]$	Integral order streaks are very short, contains chevrons
GaAs-Mα	Figure 5.9	$[01\bar{1}]$	Regular step array pattern

Table 5. 1:Table of RHEED patterns observed for GaAs (211) B in Heriot Watt System**.**

In the Heriot Watt system, the (211) B RHEED patterns observed during oxide desorption below 590°C are like those seen during GaAs (100) deoxidisation where a broad (discussed detail in chapter 2), diffuse arc is observed along with the occasional appearance of streaks in the RHEED patterns. Between 590 to 600°C, the RHEED patterns of the underlying (211) B GaAs surface start to appear and simultaneously the pattern due to the oxide layer disappears, see Figure 5.5. Above 600°C, the intensity of the streaks in the RHEED patterns increases so that the GaAs surface displays the GaAs-Nα and GaAs-Mα RHEED patterns along the $[\bar{1}11]$ and $[01\bar{1}]$ azimuths respectively, see Figure 5.6 and 5.9.

Upon further heating to 640°C, the GaAs surface reconstructs along $[\bar{1}11]$, and the RHEED patterns GaAs-Nβ or GaAs-Nγ are observed, see Figure 5.7 and Figure 5.8, but there is no change in the RHEED pattern observed along $[01\bar{1}]$. The RHEED pattern GaAs- Nγ is generally observed if the temperature can increase after high intensity, sharp chevrons have been observed in the RHEED patterns. If the oxide desorption process is stopped after the surface has displayed the RHEED patterns GaAs-Nα GaAs-Nβ or GaAs-Nγ, then the patterns are maintained to growth temperature. No further changes are

observed along the [$01\bar{1}$] azimuth during cooling to T_G (the temperature at which growth is performed).

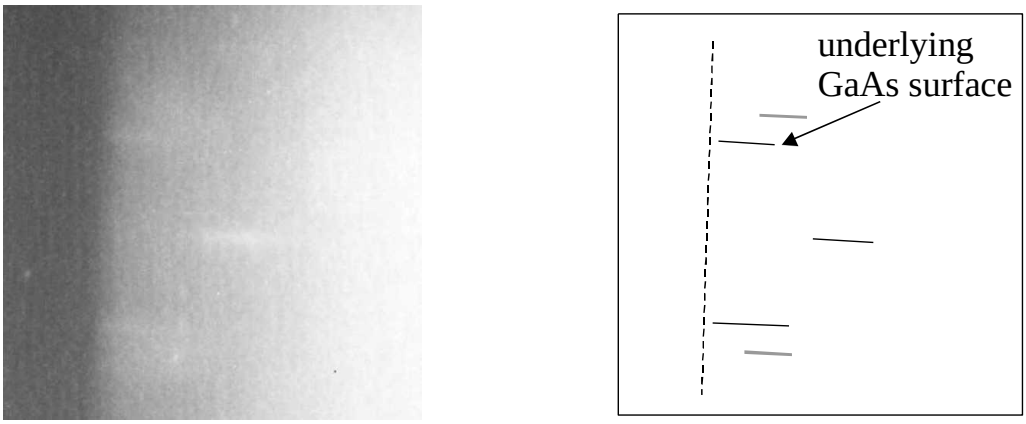

Figure 5.5: RHEED pattern observed along the azimuth as the oxide is removed from the surface. The high intensity sharp streaks are due to the underlying GaAs surface while the pattern due to the oxide layer displays diffuse, less intense streaks.

The description of the patterns observed during cool down to growth temperatures also applies when the surface is not exposed to zinc. Zinc pre-treatment is applied to the (211) surface as it is assumed that it will reduce the number of defects in the epilayers as has been observed for (100) growth [11]. Different patterns were observed though when the GaAs surface was accidentally exposed only to selenium at growth temperature (240°C). Along [$\bar{1}11$] the surface reconstructs over a period of minutes after the start of exposure to selenium.

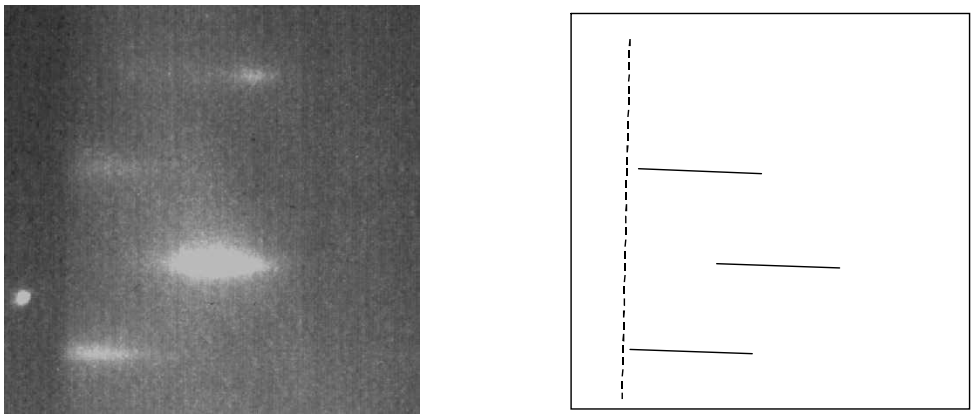

Figure 5.6: GaAs-Nα RHEED patterns of GaAs (211) B surface along [$\bar{1}11$].

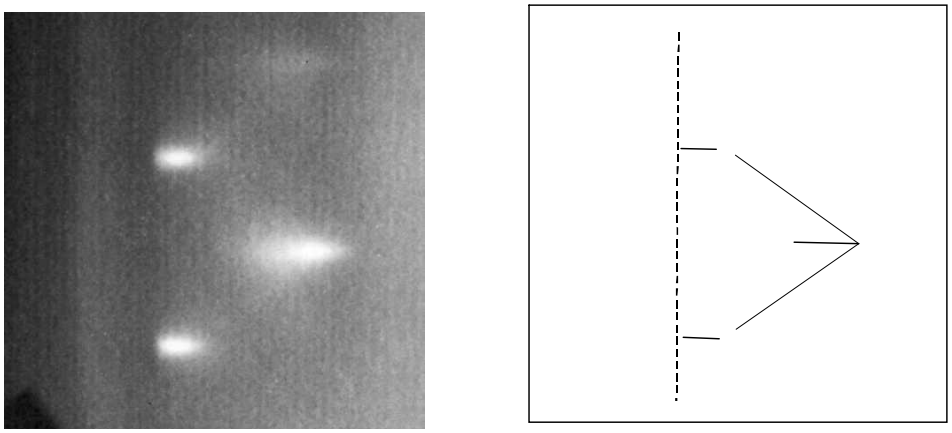

Figure 5.7: GaAs-Nβ RHEED patterns of GaAs (211) B surface along $[\bar{1}11]$.

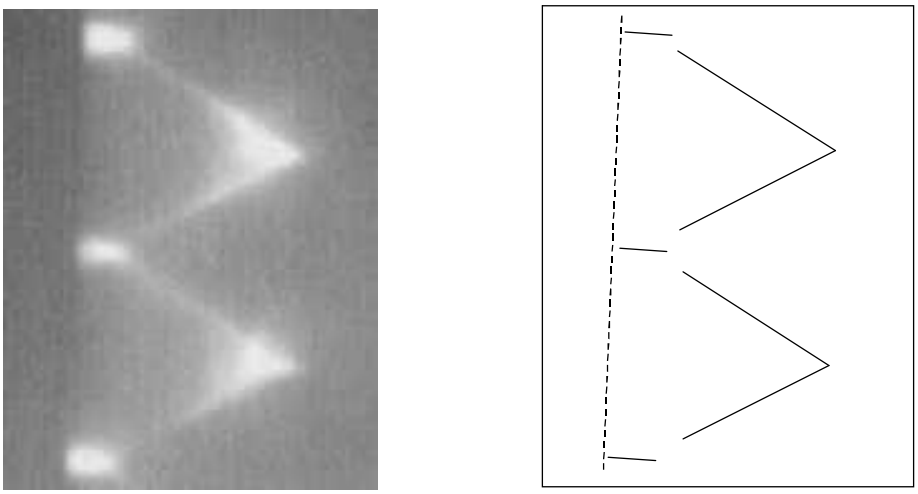

Figure 5.8: GaAs-Nγ RHEED patterns of GaAs (211) B surface along $[\bar{1}11]$.

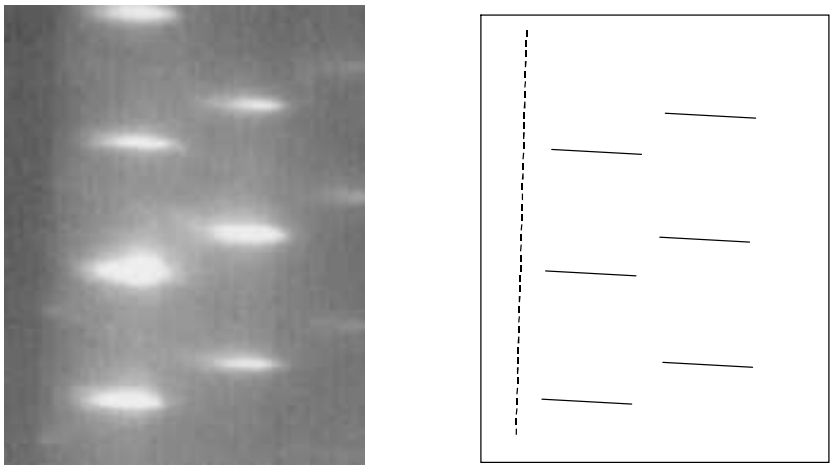

Figure 5.9: GaAs-Mα RHEED pattern observed along the azimuth $[01\bar{1}]$.

5.5 Challenges in Initial growth of ZB MgS

The growth modes of ZnSe and MgS are quite different. ZnSe and ZnCdSe are typical in that the growth is performed under slightly group VI rich conditions and this is reflected in the RHEED patterns. On (100) the typical Se-stabilised 2x1 surface is seen which is detailed in chapter 3, while on (211) B, during ZnSe growth the RHEED pattern changed from chevrons along the [11] direction to short streaks, which is also to be expected for a Se stabilized surface. The orthogonal direction stayed unchanged throughout growth.

In the case of (100) MgS, although the ZnS: Mg BEP ratio is approximately 500:1, the very low incorporation coefficient of S, together with the near-unity coefficient for Mg, means that the surface is actually metal-rich. For (100) MgS the typical c (2×2) RHEED pattern is observed. As (211) MgS growth is not well studied, the RHEED pattern of optimal growth is unknown, however as we are growing the MgS under identical conditions to that of 100 samples a metal stabilised surface should be visible. A metal stabilised ZnSe (211) B surface at the lower growth temperature was examined so we could compare with MgS later. On Zn only exposure there was only a very slight change in [11] RHEED pattern producing fractional order streaks corresponding to a metal stabilized surface. However, the fractional order streaks were faint and other factors such as the low growth temperature may be contributing, therefore further study is required to clearly determine the growth mode for a metal rich surface at this lower growth temperature.

As there was no clear difference in the RHEED between the group VI and group II stabilised surfaces on 211samples, all MgS structures were grown simultaneously on both 100 and 211 GaAs/ZnSe buffers to confirm our growth conditions were optimal. This was essential as the initial growths of MgS, although grew well, demonstrated no change in the RHEED from the ZnSe buffer below. It should be noted that during the remainder of the growth of MgS there was no change in RHEED, and in particular, no formation of

spots indicative of 3D growth. This implies continuity of the ZB crystal structure throughout the growth.

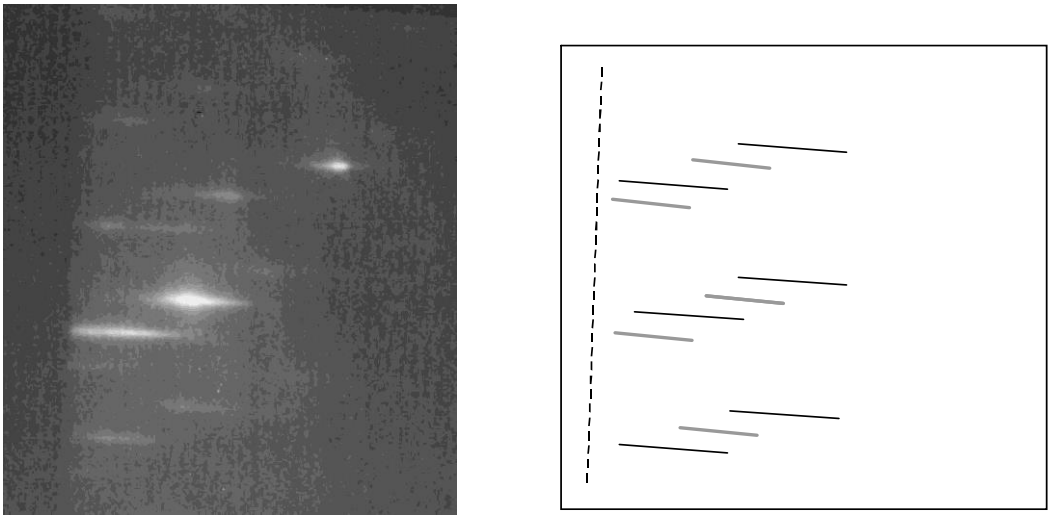

Figure 5.10: Regular asymmetric step array RHEED pattern during the growth ZB MgS on GaAs (211) B substrate along [$\bar{1}11$].

5.6 Growth of ZB MgS/ZnSe on GaAs (211) B substrate

5.6.1: Samples

Two Sets of samples were grown for this study; one set was grown using standard procedure on (100) GaAs and repeat of the first using the same conditions but on (211) B GaAs. A schematic diagram of grown samples shown in figure 5.11. In both sets two samples were grown: firstly, a sample of GaAs/ZnSe (15 nm)/MgS (6 nm)/ZnSe (1 µm) for characterisation *via* double crystal X-ray diffraction (XRD), and secondly, a quantum well sample of GaAs/ZnSe (15 nm)/MgS (6 nm)/ZnSe (70 nm)/ZnCdSe (10 nm)/ZnSe (70 nm). Due to the metastable nature of MgS, it is difficult to grow in thick layers, however our group has extensively used X-Ray interference in order to study the material properties. However, in the case of 211B substrates the XRI method will not work due to the polar surfaces associated with (211) growths. Therefore, indirect measurement of the

ZB MgS is required. Here we use the structural quality of ZnSe grown on MgS, and the PL quality of a QW on MgS. We then compare these to the 100 samples.

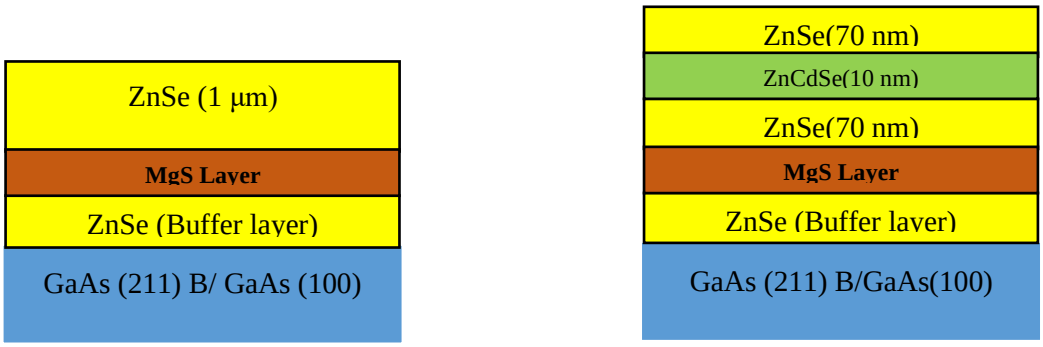

(a) (b)

Figure 5.11: Schematic diagram of the growth of (a) ZnSe (1µm) and (b) ZnCdSe quantum well structure on GaAs (211) B and GaAs (100) substrates.

5.7 X-ray measurements

X-Ray Diffraction scans were obtained on both (100) and (211) B samples of GaAs/ZnSe/MgS/ZnSe. 1 µm of ZnSe was chosen for these samples so that the layers are fully relaxed. As the ZnSe buffer and MgS layer combined are below 20 nm thickness their contribution to the XRD is minimal compared to the layer above. For the (100) XRD a standard 400 scan was taken while for the (211) B sample, 224 scans were taken. For this study only glancing exit 224 scans were taken for the (211) B ZnSe.

It has been shown in previous studies that under non-optimal growth conditions there is a phase transition in MgS from the metastable ZB structure to the stable rocksalt [12]. This leads to a mixed phase layer with domains of both ZB and RS material. When this occurs, any subsequent ZnSe growth becomes domain oriented and does not generate an XRD peak at the expected Bragg angle for ZB ZnSe [13]. Comparing the XRD peak position with that expected for ZB ZnSe we can confirm the presence of ZB ZnSe.

Figure 5.12 shows the experimental XRD (224) rocking curves for the 211B sample. The measured ZnSe peak is observed at 532 arc seconds, whilst the calculated peak position is at 534 arc seconds, well within experimental error. This was then compared to the identical structure grown on the (100) surface shown in figure 5.13. Table 4.4 shows the XRD results from 1 µm ZnSe layers grown on GaAs (100) and (211) B substrates. The FWHM of the ZnSe peak is larger on (211) B than (100), possibly due to the dislocation density difference between the two samples [14].

Sample	ZnSe peak position (arc seconds)	FWHM of ZnSe peak (arc seconds)	FWHM of substrate peak (arc seconds)
211B	532	332	55.79
100	352	267	32.57

Table 5. 2: XRD results for 1 µm ZnSe grown on GaAs (211) B and (100) substrates**.**

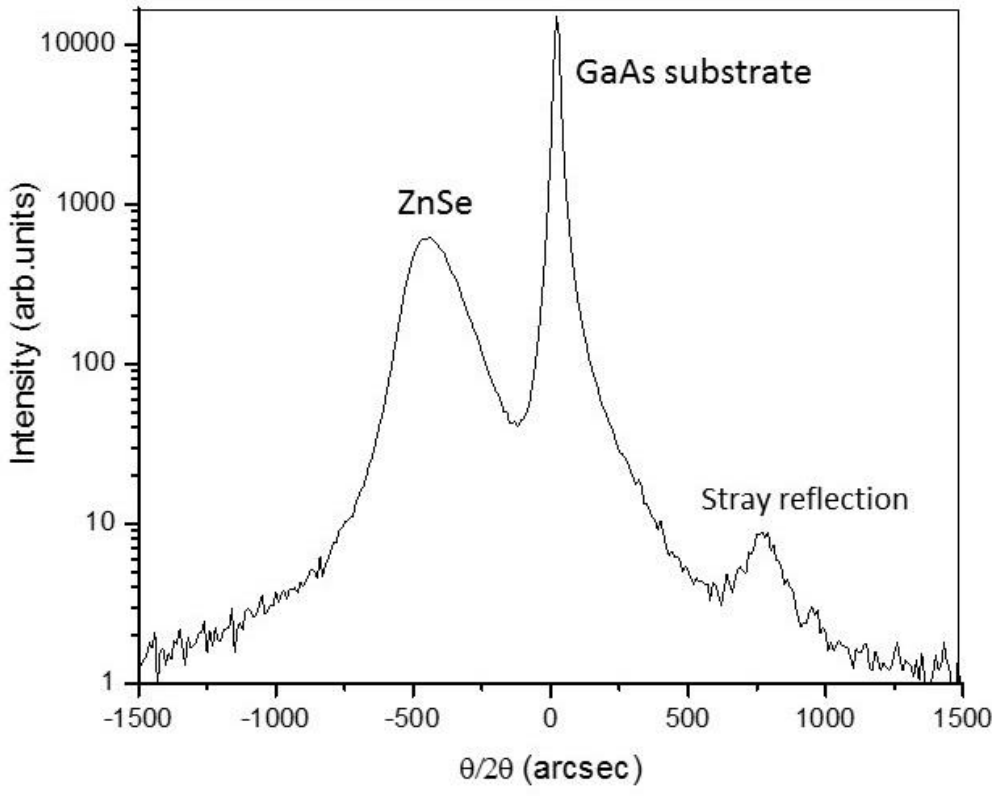

Figure 5. 12: X ray scan of ZnSe (1µm) layer on GaAs (211) B.

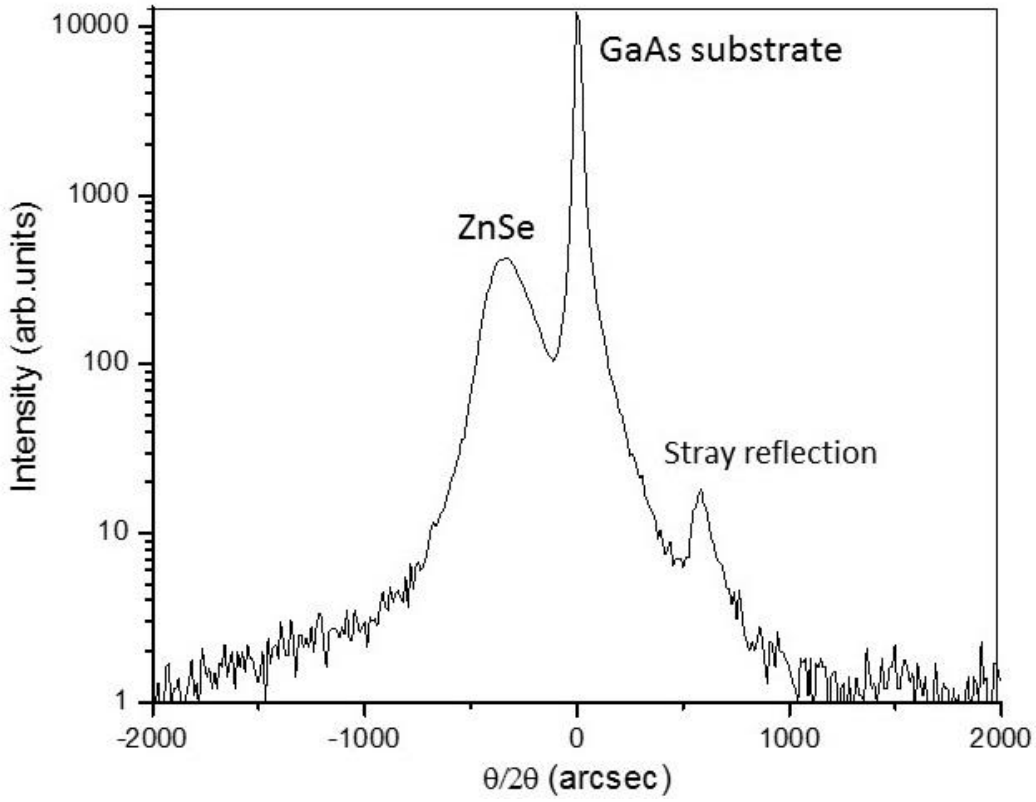

Figure 5. 13: X ray scan of ZnSe (1μm) layer on GaAs (100).

The FWHM of (211) B ZnSe was compared to the (100) ZnSe sample. It was observed that, the FWHM of the (211) B ZnSe peak is larger at 324 arc seconds compared to the (100) ZnSe at 218 arcsec [15]. As before, this is likely due to the scattering vector for the dislocations on this reflection. Both samples have narrower peak widths when grown on MgS surfaces. This further confirms that the (211) B MgS is of comparable quality to the (100) and has grown in the ZB structure.

5.8 Photoluminescence measurements

Photoluminescence spectroscopy (PL) is an established technique for assessing the quality of epitaxially grown semiconductors [16]. Using this method, optical transitions from excited electronic states to lower states can be investigated. A transition that is detected can provide the following information, which can used to improve material quality:

- It can indicate the presence of crystal imperfections such as impurities, and native crystal defects, however, there are defects that do not interact radiatively.

- The fundamental bandgap of alloys can be measured, from which the composition of an alloy such as ZnCdSe can be determined.

Changes in the growth conditions of a sample will alter the structure of the crystal, which can be detected in the PL spectrum of the sample. The PL spectrum can then be used as feedback, so that the quality can be improved by altering one growth variable and observing the resulting effect. This method was used to improve the structural quality of ZnSe and ZnCdSe (211) samples, where typical ZnSe and ZnCdSe (100) growth conditions were used as a starting point [17].

5.8.1 ZnSe PL Spectrum

An example of a nominally undoped ZnSe spectrum is shown in Figure 4.14 for sample HWA 415 grown by another grower. Some of the main transitions that can be observed for ZnSe have been marked and their assignments are shown in Table 5.3. The relative intensities of these peaks can be used to qualitatively determine the crystalline quality of a ZnSe sample. When a sample is considered to be of high quality, the spectrum is dominated by the free and bound exciton transitions with no or little luminescence for energies less than approximately 2.7eV. Poor quality ZnSe can still show the presence of excitonic emissions, but the Y_o, and deep level emissions have intensities comparable to or larger than the excitonic transitions.

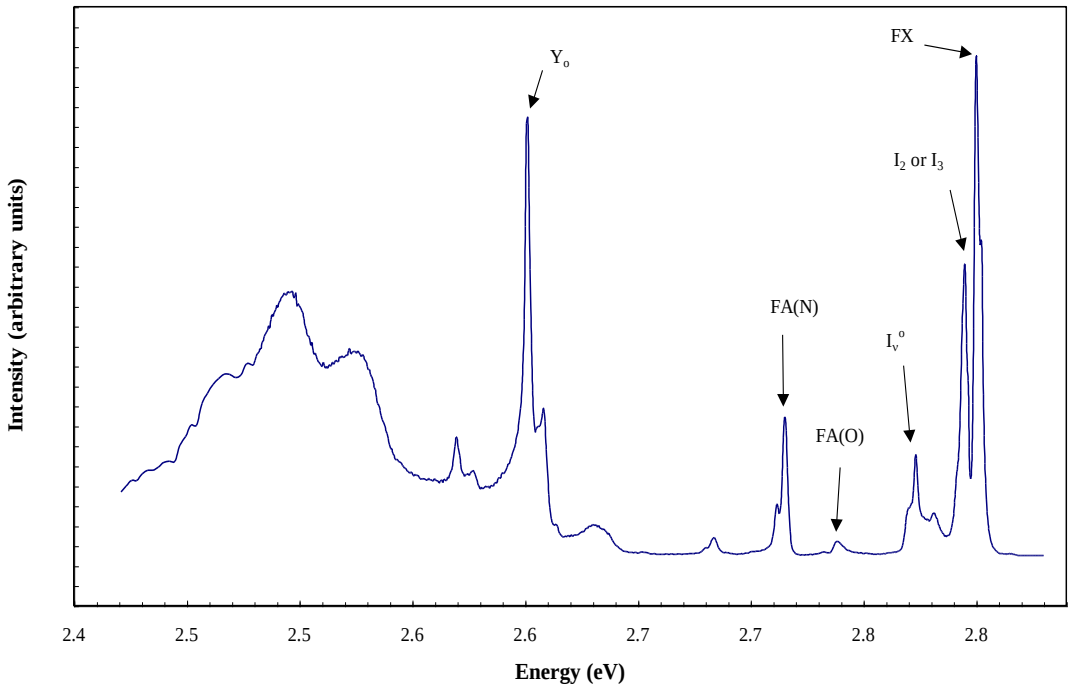

Figure 5. 14: Example of nominally undoped ZnSe spectrum at 4K.

Name of emission peak	Assignment of transition	Energy /eV
Y_o	Dislocation related	2.600
FA	Free electron to acceptor (nitrogen)	2.710
FA	Free electron to acceptor (oxygen)	2.735
I_v^o	Selenium site related defects	2.773
I_1	Exciton bound to neutral acceptor	2.790
I_3	Exciton bound to ionised donor	2.794
I_2	Exciton bound to neutral donor	2.798
FX	Free exciton	2.802
FX_{2s}	Excited state of free exciton	2.815

Table 5.3: Emission peaks observed in nominally undoped ZnSe

5.8.2 Determination of high quality ZnSe and ZnCdSe (211) epilayers

The typical growth conditions that are used to produce high quality ZnSe and ZnCdSe epilayers on GaAs (100) are listed below in Table 5.4. The growth temperatures listed are those that are normally used, since improved incorporation of impurities for doping occurs at these temperatures. However, high quality growth of both ZnSe and ZnCdSe epilayers is achieved the temperature range of 240 ±5°C [18]. The GaAs oxide desorption temperature is not included in the table as it was performed at similar temperatures to those recorded for (100) desorption and was not varied purposely discussed in chapter 3.

Epilayer material	GaAs RHEED pattern	T_{GaAs} (clean up) (°C)	T_G (°C)	Se/Zn BEP ratio	Growth rate (μm/hr)
ZnSe	(4×3)	~ 600	240	2 – 4	0.25 – 0.50
ZnCdSe	(4×3)	~ 600	240	2 – 4	0.25 – 0.50

Table 5. 4: Growth conditions for ZnSe and ZnCdSe (100) samples.

Table 5.5 shows the range of growth temperatures and Se/Zn BEP ratios that were used where one condition was fixed, while the other was altered to see the effect on the quality of the ZnSe and ZnCdSe (211) epilayers. The GaAs oxide desorption temperature is not included in the table as it was performed at similar temperatures to those recorded for (100) desorption and was not varied purposely. The changes in the intensity of the RHEED patterns observed during oxide removal on the (211) surface are the same as those seen for GaAs (100). The intensity of the RHEED patterns increases as the temperature approaches 590 to 600°C during the oxide desorption. Heating of the sample is stopped for GaAs (100) when the (4×3) RHEED pattern is observed, approximately 590 to 610°C and at these temperatures, the RHEED patterns GaAs-Nα and GaAs-Mα are seen for GaAs (211). The heat clean was stopped at this point for all the samples in sets 1 to 3.

The PL spectra recorded from ZnSe samples grown in set one was not good, see figure 5.16. They showed virtually no excitonic peaks; instead, they were dominated by deep level emission, while a strong Y_o peak was observed, indicating that quality of the ZnSe epilayers was very poor.

Similar spectra were recorded for the samples in set two grown with temperatures below 240°C, while those that were grown with temperatures above 240°C showed an improvement with the bound exciton peak appearing, see Figure 5.16 (b). However, the Y_o peak and deep level emission were still observed and their intensity was larger than that of the excitonic peak, showing that the structural quality was still poor. An extra peak at approximately 2.71 eV was observed in the spectra of these samples grown above 240°C, which was not identified at that time. This peak has since been identified as being due to a donor-acceptor transition, but it has the value of that due to a nitrogen acceptor, see Table 5.3. Since there is no possibility of nitrogen within the growth system, it has been attributed to oxygen as the acceptor, which has emission energy similar to nitrogen [19]. This has been confirmed with its disappearance after improvements in the heat clean procedure. It therefore related to incomplete removal of the GaAs oxide.

Sample set	Material	Growth condition varied	T_G (± 5°C)	Se/Zn BEP ratio (± 0.5)	Cd/Zn BEP ratio (± 0.5)
One	ZnSe	Se/Zn BEP ratio	250	1.2 – 15.3	N/A
Two	ZnSe	Growth temperature	220 – 260	2.0 – 3.0	N/A
Three	ZnCdSe	Cadmium flux	265	3.5	0.3 – 0.1
Three	ZnCdSe	Cadmium flux	240	1.5 – 2.5	0.3 – 0.1
Four	ZnCdSe	Growth temperature	220 – 260	2.0	0.2
Five	ZnCdSe	Growth temperature	210 - 250	3.5	0.3
Six	ZnCdSe	Growth temperature	240 – 280	3.0 – 4.0	5.0

Table 5. 5: Growth Conditions Used for ZnSe and ZnCdSe (211) Growth

Confirmation of the importance of oxide removal from the GaAs (211) surface came from a set of ZnCdSe samples that were grown, after the growth of a ZnCdSe (211) sample HWC 754 shown in figure 5.15. The PL spectrum of this sample displayed a sharp excitonic peak and virtually no deep levels. It had been accidentally overheated during the heat clean, but its growth temperature had also been difficult to control and so it was unclear whether the high growth temperature or the high deoxidisation temperature, was the cause. Therefore, in the set of samples grown subsequently, either the growth or the deoxidisation temperature was altered to determine the cause, see table 5.6.

Sample number	Substrate clean–up temperature (± 5°C)	GaAs RHEED pattern	T_G (± 5°C)	Epilayer thickness (μm ±5%)
HWC 754	625	GaAs-Nβ	240	0.76
HWC 755	596	GaAs-Nα	235	1.33
HWC 756	599	GaAs-Nα	240	0.76
HWC 757	612	GaAs-Nβ	230	1.33
HWC 758	609	GaAs-Nβ	230	0.76
HWC 759	620	GaAs-Nβ	240	0.76
HWC 760	620	GaAs-Nβ	260	0.76

Table 5. 6: Growth of ZnCdSe samples HWC 754 to 760

Samples HWC 754 and 760 had oxide desorption performed at the normal temperatures that had been used previously, i.e., the heat clean was stopped when the RHEED pattern GaAs-Nβ was observed. HWC 756 was grown with the same thickness, as HWC 754 to check that strain in the epilayer was not affecting the quality. The PL spectra recorded for these samples are shown in figure 5.15. HWC 755 showed an excitonic peak, but its size was comparable to that of the deep level emission indicating that the sample had poor structural quality, while the excitonic peak in HWC 756 was very broad and low.

During the oxide desorption of HWC 757, the temperature was increased, but no improvement in the PL spectrum was recorded and sample HWC 758 was a repeat of HWC 757 to check that result. However, both samples had displayed the GaAs-Nβ RHEED pattern that had been observed during the deoxidisation of HWC 754. The heat clean temperature was further increased during the growth of HWC 759, which resulted in the PL spectrum displaying a sharp excitonic peak that was larger than the other emission peaks. This sample demonstrated that the heat clean temperature higher than previously used was responsible for the change in quality.

Sample HWC 760 had a similar oxide desorption temperature to HWC 759, but the growth temperature was reduced to 240°C to see if this affected the quality, even when the higher heat clean temperature was used. The PL spectrum indicated that the structural quality was poor, as it was dominated by deep level emission. Therefore, a combination of high growth temperature and oxide desorption temperature had improved the structural quality of ZnCdSe epilayers.

The spectrum of sample HWC 759 was not as good as that of sample HWC 754, which is due to the difference of ±20°C in the heat clean temperature. However, it is assumed that the oxide desorption temperature of HWC 759 is lower than that of HWC 754. It must also be considered that HWC 759 had displayed the GaAs-Nβ RHEED pattern, but both HWC 757 and 758 had shown the same pattern. Their heat clean temperature was 10°C lower than HWC 754 and their PL spectra had been poor.

These growth conditions, i.e., Se/Zn BEP ratio, oxide desorption temperature and growth temperature, were applied to the growth of ZnSe (211) epilayers and the PL spectrum of the first ZnSe sample grown is shown in Figure 5.16. Deep level emission is still observed, but the intensities of the free and bound excitons peaks compared to that of the deep levels are larger than previously observed for similar growth temperatures. The PL spectrum also shows that the Y_o and FA peaks have virtually disappeared showing that the substrate preparation is vital to the quality of epilayers grown on GaAs (211) B. The ZnCdSe samples (HWC 754 to 760) demonstrate that oxide removal temperature >600°C is important.

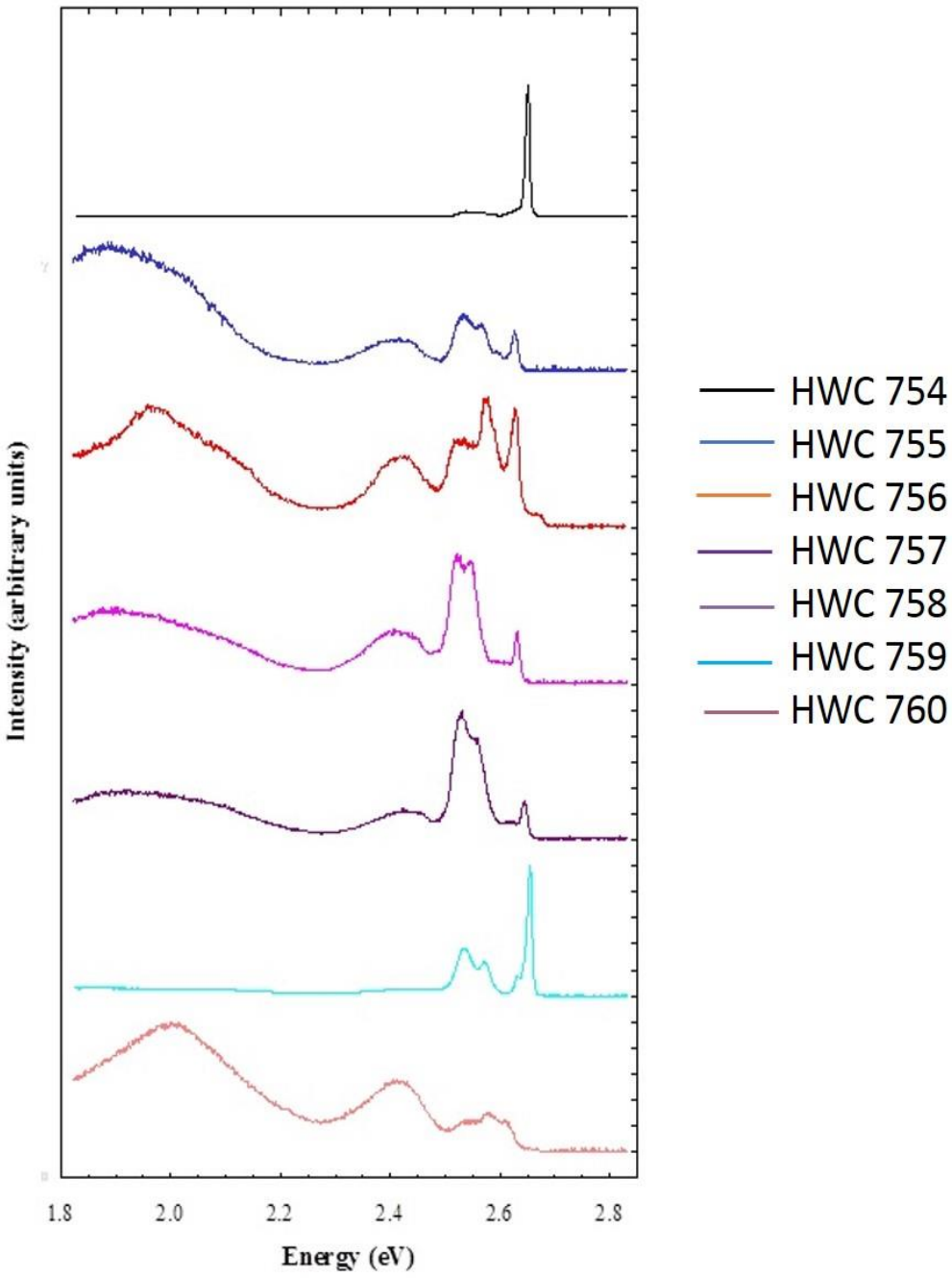

Figure 5. 15: PL Spectra of ZnCdSe Samples HWC 754 to 760 at 77K

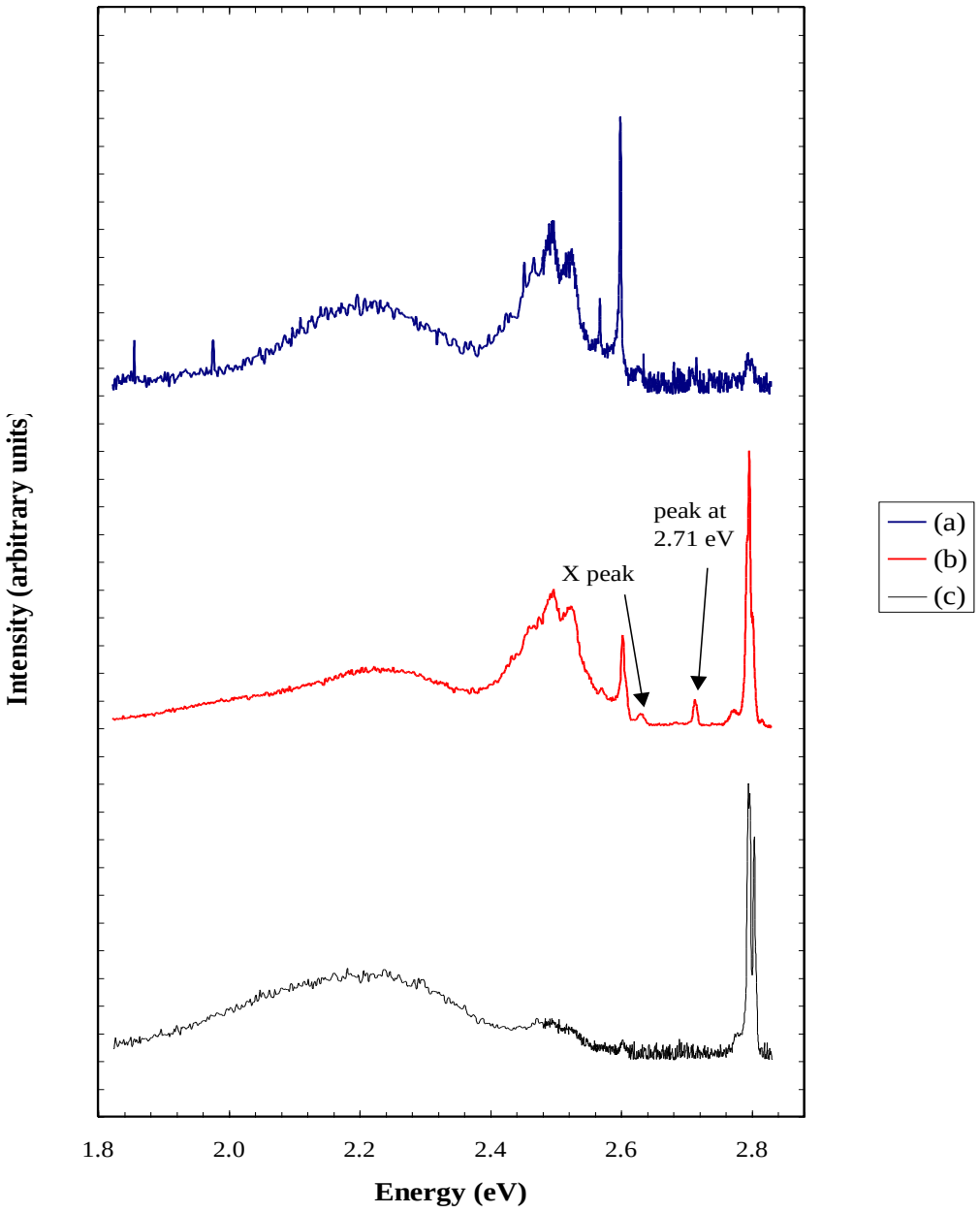

Figure 5. 16: PL Spectra of ZnSe (211) B sample at 77K

(a) PL spectrum from ZnSe sample – HWC 770 grown at T_G = 240 ± 5°C.

(b) PL spectrum from ZnSe sample – HWC 773 grown at T_G = 240 ± 5°C.

(c) PL spectrum from ZnSe sample - HWA 789 grown with growth conditions determined from ZnCdSe samples HWC 754 to 760, T_G = 240 ± 5°C.

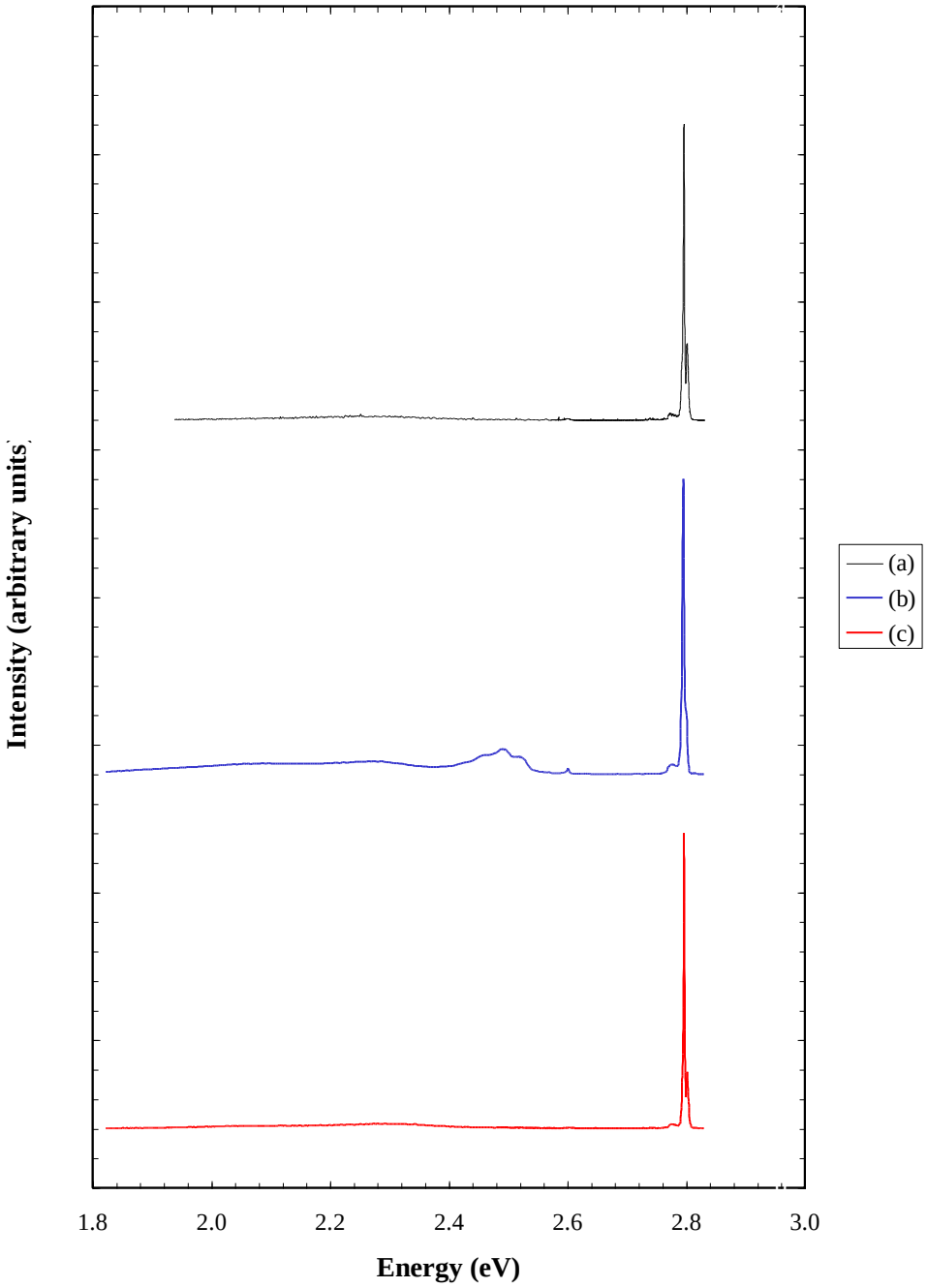

Figure 5. 17: PL Spectra of ZnSe (211) B and (100) samples at 77K

(a)High quality ZnSe (100) – HWC 667 sample grown under optimum conditions, T_G = 260 ± 5°C.

(b)Best quality ZnSe (211) B sample – HWC 689, grown at T_G = 240 ± 5°C.

(c)High quality ZnSe (100) sample – HWC 695, grown at T_G = 240 ± 5°C

5.9 Discussion and comparison of ZnSe and ZnCdSe (211) and (100) epilayers

The investigation of different growth conditions for (211) ZnSe and ZnCdSe epilayers have shown that substrate preparation and growth temperature are vital to ensure that the structural quality is good. Since the investigation, the quality of ZnSe and ZnCdSe epilayers has been improved and Table 5.7 shows the range of growth conditions that have produced the best optical quality epilayers on (211) B GaAs.

Epilayer material	GaAs RHEED pattern	Oxide desorption temperature T_{GaAs} (^oC)	Growth Temperature T_G (^oC)	Growth rate (µm/hr)
ZnSe	GaAs-Nβ	> 610	230 – 250	.25-.50
ZnCdSe	GaAs-Nβ	> 610	230 – 250	.25-.50

Table 5. 7: Growth of ZnSe and ZnCdSe epilayers on GaAs (211) B.

5.9.1 ZnSe Epilayers

Figure 5.17 shows the PL spectra of (a) a high quality ZnSe (100) sample grown under optimum growth conditions (b) which is the best ZnSe sample grown on GaAs (211) B and for comparison, (c) a ZnSe (100) sample, grown at a similar temperature to (b). Although, the PL spectrum of the (211) sample displayed in Figure 5.17(b) is displaying bound exciton emission only, the majority of ZnSe (211) samples display both bound and free exciton emissions similar to ZnSe (100) samples. However, it should be remembered that the process of bound exciton emission is more efficient than free exciton emission and the ratio is a function of the excitation power.

Deep level emission is always observed in the PL spectra of ZnSe (211) samples, while high quality ZnSe (100) samples have virtually no deep level emission. It has been reduced to the minimum level shown in Figure 5.17(b) where the ratio of deep level

emission to excitonic emission is approximately. The deep level emission has the highest intensity in the energy range 2.4 to 2.6 eV, which is called the S band emission and it is believed to be due to transitions between donor-acceptor pairs. Similar spectra have been observed for (100) ZnSe samples, but the cause of the higher intensity in (100) is unknown, as the growth conditions, are the similar to those samples that have virtually no S band emission.

A possible cause of the higher deep level emission in the (211) samples may lie in the fact that it has been found for similar growth conditions, i.e. Se/Zn BEP ratios and growth temperatures, that the growth rate of ZnSe on GaAs (211) B is higher that on GaAs (100).

5.9.2 ZnCdSe epilayers

Figure 5.18 shows the PL spectra of (a) the best ZnCdSe (211) B sample, (b) a typical ZnCdSe (211) B sample and (c) for comparison, a high quality ZnCdSe (100) sample, grown with a similar temperature in the same growth chamber. The samples have similar quality since all three-show large excitonic peaks and low deep level emission, indicating the high structural quality of the epilayers.

An energy difference of 202 meV corresponds to the difference between the excitonic and Y_o transitions, while 165 meV corresponds to a peak that is sometimes observed in ZnSe (100) and (211) PL spectra, see Figure 5.18 (b). The peak is unidentified, but it is always accompanied by the higher intensity Y_o peak, which suggests that it be related to that transition and will be designated Y_1 in this thesis.

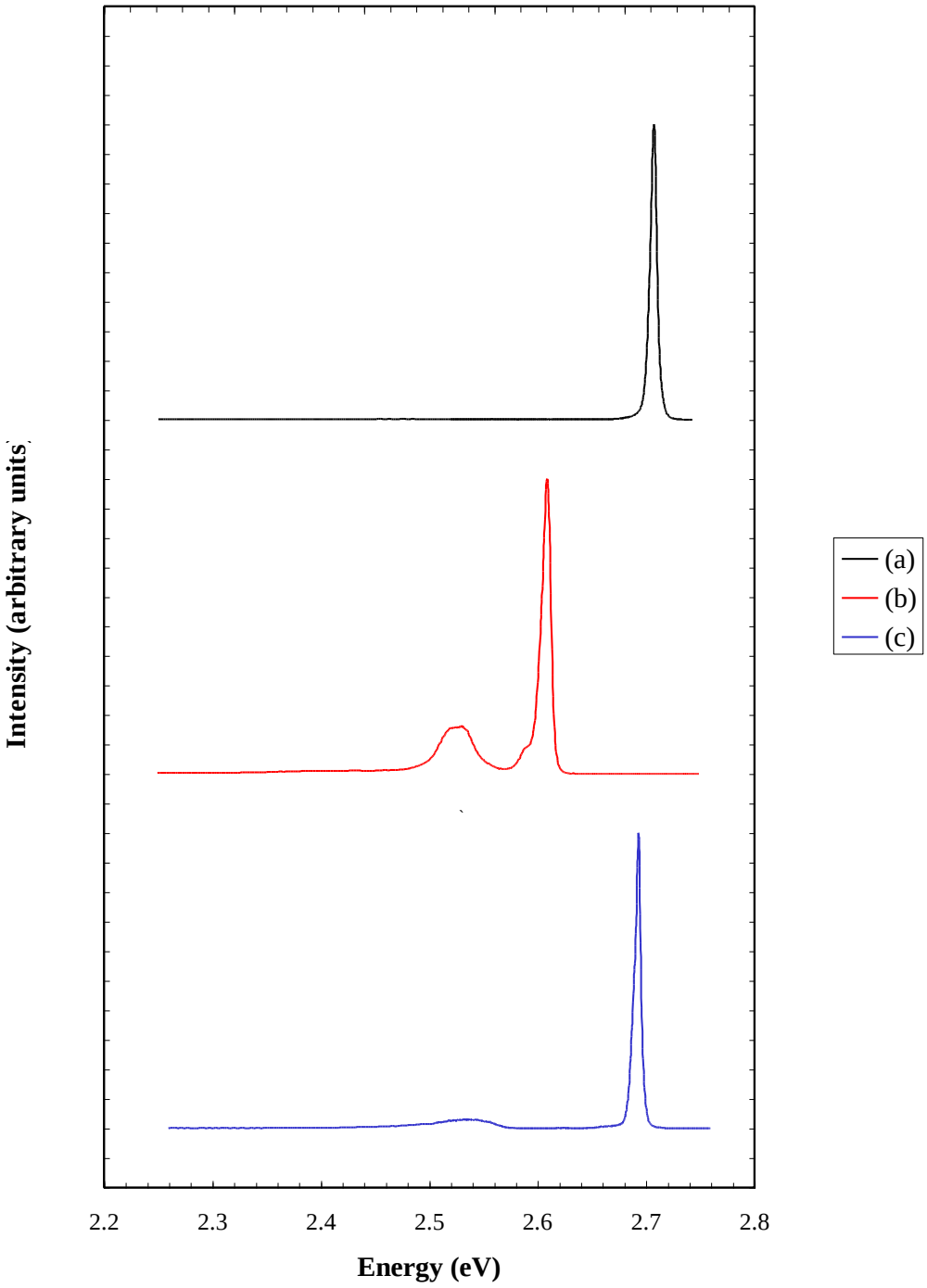

Figure 5. 18:PL Spectra of ZnCdSe (211) B and (100) samples at 77K

(a) The best quality ZnCdSe (211) B sample - HWA 809, $T_G = 240 \pm 5°C$

(b) A typical ZnCdSe (211) B sample - HWA 829, TG = 235 ± 5°C.

(c) A high quality ZnCdSe (100) sample - HWA 810 grown with $T_G = 240 \pm 5°C$

It was also suggested earlier in this section that the transition observed for ZnCdSe (100) and (211) samples with similar energy-difference values be due to an overlap of the two separate transitions. An overlap is perhaps more likely to occur if the two transitions are related. The Y_o transition has the higher intensity on the (100) orientation, while the Y_1 transition is larger on the (211) orientation. The Y_o transition is due to dislocations, which generate local strain fields that result in an electric field. A similar field might be generated by the defect responsible for the Y_1 transition and this field could then interact with the electric field due to the different strain components in the (211) epilayer. Such an interaction may explain the higher intensity of the Y_1 transition in the (211) ZnCdSe epilayers.

5.10 Conclusion

In conclusion, we have shown that ZB MgS layers can be grown on GaAs (211) B substrates and characterisation by RHEED, XRD and PL indicates the good quality of the grown ZnSe layers. The crystal structure of the MgS grown was demonstrated to be ZB from the RHEED patterns during growth and from the XRD peak of the ZnSe capping layer.

- The GaAs (211) surface achieves complete oxide removal more than 20ºC higher than the (100) GaAs surface. It is probably due to the different number of gallium and arsenic bonds on the surface.
- During oxide removal, the (211) surface displays the (1×1) reconstruction below 620ºC.
- In the Heriot Watt system, the GaAs (211) surface does not display reversible faceting, which is due to the lack of an overpressure of arsenic in the system.
- Selenium is absorbed on the GaAs (211) surface filling in the facets and forming irregular domains.

- Photoluminescence spectroscopy was used to identify the growth conditions that produce high quality ZnCdSe and good quality ZnSe epilayers have been grown on GaAs (211) B.
- The growth rate of ZnSe on GaAs (211) B is higher than that on GaAs (100), which is due to the zinc rich growth conditions of the (211) epilayers. These conditions result in the ZnSe (211) epilayers always displaying deep level emission in the PL spectra.

REFERENCES

[1] S. Y. Wang, P. J. Thompson, G. Horsburgh, T. A. Steele, G. D. Brownlie, K. A. Prior and B. C. Cavenett, "Piezoelectric effect in ZnSe/ZnCdSe quantum wells grown on (211) B GaAs," Journal of Crystal Growth, vol. 159, pp. 459-462, 1996.

[2] J. S. Milnes, C. Morhain, S. A. Telfer, W. Meridith, T. A. Steele, K. A. Prior and B. C. Cavenett, "A spectroscopic study of the piezoelectric effect in ZnSe/ZnCdSe single quantum wells grown on (2 1 1)B GaAs," Journal of Crystal Growth, vol. 184, pp. 714-717, 1998.

[3] R. Haidar, P. Kupecek, E. Rosencher, R. Triboulet and P. Lemasson, "New mid-infrared optical sources based on isotropic semiconductors (zinc selenide and gallium arsenide) using total internal reflection quasi-phase-matching," Opto-electronics Review 11, vol. 2, pp. 155-160, 2003.

[4] R. Notzel, L. Daweritz and K. Ploog, "Topography of high- and low-index GaAs surfaces," Physical Review B, vol. 46, p. 8, 1992.

[5] D. B. Holt, “Surface polarity and symmetry in semiconducting compounds,” Journal of Materials Sciecne, vol. 23, pp. 1131-1136, 1988.

[6] P. Hren, D.W. Tu and A. Kahn, “Surface structure of GaAs(211),” Surface Science, vol. 146, pp. 69-79, 1984.

[7] V. Bousquet, C. Ongaretto, M. Laügt, M. Behringer, E. Tournié and J.-P. Faurie, “(001) GaAs substrate preparation for direct ZnSe heteroepitaxy,” Journal of Applied Physics, vol. 81, pp. 7012-7017, 1997.

[8] J. Massies and J. P. Contour, “Substrate chemical etching prior to molecular-beam epitaxy: An x-ray photoelectron spectroscopy study of GaAs {001} surfaces etched by the H2SO4-H2O2-H2O solution,” Journal of Applied Physics, vol. 58, pp. 806-810, 1985.

[9] S. A. Telfer, G. Horsburgh, J. S. Milnes, C. Morhain, P. J. Thompson, K. A. Prior and B. C. Cavenett, “Growth of ZnSe and ZnCdSe on (211)B GaAs substrates,” Journal of Crystal Growth, vol. 184/185, pp. 51-56, 1998.

[10] A. Rajan, R. T. Moug and K. A. Prior, “Epitaxial growth of zinc blend MgS directly on GaAs (001) substrates,” Semiconductor Science and Technology, vol. 29, 2014.

[11] L. H. Kuo, K. Kimura, T. Yasuda, S. Miwa, C. G. Jin, K. Tanaka and T. Yao, “Effects of interfacial chemistry on the formation of interfacial layers and faulted defects in ZnSe/GaAs,” Applied Physics Letters, vol. 68, pp. 2413-2416, 1996.

[12] Akhil Rajan, Richard T. Moug and Kevin A. Prior, “Growth and stability of zinc blende MgS on GaAs, GaP, and InP substrates,” Applied Physics Letters, vol. 102, pp. 032102-032105, 2013.

[13] C. Bradford, C. B. O'Donnell, B. Urbaszek, A. Balocchi, C. Morhain, K. A. Prior and B. C. Cavenett, “Growth of zincblend MgS/ZnSe single quantum wells by molecular beam epitaxy using ZnS as a sulphur source,” Applied Physics Letters, vol. 76, pp. 3929-3931, 2000.

[14] B. Yarlagadda, A. Rodriguez, P. Li, R. Velampati, J. F. Ocampo, E. N. Suarez, P. B. Rago, D. Shah, J. E. Ayers and F. C. Jain, “X-ray characterization of dislocation density asymmetries in heteroepitaxial semiconductors,” Applied Physics Letters, vol. 92, p. 202103, 2008.

[15] J. Zhu, N. M. Eldose, N. Mavridi, K. A. Prior and R. T. Moug, “Molecular beam epitaxial growth of zinc blende MgS on GaAs (2 1 1)B substrates,” Journal of Crystal Growth, vol. 485, pp. 86-89, 2018.

[16] B.P. Chandra, V.K. Chandra and Piyush Jha, “Nanomaterials,” Luminescence of II-VI Semiconductor Nanoparticles, pp. 1-65, 2015.

[17] S. Telfer, G. Horsburgh, J. Milnes, C. Morhain, P. Thompson, K. Prior and B. Cavenet, “Growth of ZnSe and ZnCdSe on (2 1 1)B GaAs substrates,” Journal of crystal growth, vol. 184, pp. 51-54, 1998.

[18] C. Bradford, A. Currran, A. Balocchi, B.C. Cavenett, K.A. Prior and R.J. Warburton, “Epitaxial lift-off of MBE grown II–VI heterostructures using a novel MgS release layer,” Journal of Crystal Growth, vol. 278, pp. 325-328, 2005.

[19] J. Gutowski, N. Presser and G. Kudlek, “Optical Properties of ZnSe Epilayers and Films,” Physica status solidi (a), vol. 120, pp. 11-15, 1990.

[20] S. Telfer, C. Morhain, B. Urbaszek, C. O'Donnell, P. Tomasini, A. Balocchi and K. A. Prior, "MBE growth of ZnS and ZnCdS layers on GaP," Journal of Crystal Growth, vol. 215, pp. 197-201, 2000.

This page intentionally left blank

CHAPTER 6

Epitaxial lift-off and stacking multiple layers of II-VI layers grown on GaAs (211) B substrate

6.1 Introduction

Epitaxial lift off (ELO) is a post growth process which allows an epitaxial layer to be removed from its original substrate and transferred to a new one. Due to the problems encountered during the hetero-epitaxial growth directly on lattice mismatched substrates, such as the large dislocation densities and thermal stress, difference in material properties, and the incompatibility of different process steps, it has been difficult to demonstrate more sophisticated semiconductor devices [1]. ELO technique allows the combination of lattice mismatched materials and therefore can create new devices which cannot be grown epitaxially.

Previously, our group demonstrated growth of ZB ZnSe and $Zn_xCd_{1-x}Se$ ($x<0.8$) layers lattice matched to GaAs (211) B substrates. The surface reconstructions during growth were reported by S. A. Telfer [2]. The growth of ZB MgS has been extensively studied by our group on GaAs (100) substrates, leading to the development of a novel II-VI ELO. However, ZB MgS growth on GaAs (211) B was explained in chapter 5 and is key in transferring the ELO technique to GaAs (211) B substrates. Due to the advantages of ELO in developing sophisticated devices [3] [4], the investigation of ELO on GaAs (211) B substrate becomes necessary.

ELO can be used to create completely new structures from stacked ELO layers by changing the relative orientations of adjacent layers, by using layers grown on GaAs (211) B substrate with different orientations or rotating the ELO layers about the surface normal. This method can produce frequency doubling using the second order susceptibility in ZB semiconductors by quasi phase matching (QPM). ZnSe is particular of interest as it is

transparency over the infra-red (IR) and most of the visible range and has higher second-order nonlinear optical susceptibility than most commonly used NLO materials [5].

In this chapter, ELO of ZB ZnSe layers on GaAs (211) B substrates will be described. ZB MgS is used as a sacrificial layer for the ELO process. The lifted layers were transferred to a glass plate and stacked on top of each layer up to 20 μm thickness. The stacked structure was characterized by Photoluminescence (PL) to study the optical quality and the thickness was measured by using thickness profiler (DEKTAK).

6.2 Sample growth

Two sets of samples shown in chapter 5 were used for ELO process. One set of samples was GaAs/ZnSe (15 nm)/MgS (6 nm)/ZnSe (1 μm) for stacking multiple lifted layers and secondly a quantum well sample of GaAs/ZnSe (15 nm)/MgS (6 nm)/ZnSe (70 nm)/ ZnCdSe (8 nm)/ZnSe (70 nm) for Photoluminescence spectroscopy (PL). The RHEED measurements of ZB MgS in GaAs (211) B and the structural quality was measured using X-ray Interference method before lift-off are explained detail in chapter 5. After lift-off, the samples were stacked on to 5x5 square millimetre glass plate and the thickness measurements are obtained using DEKTAK thickness profiler. PL measurements are obtained from after lift-off of quantum well samples.

6.3 ELO and Sample stacking

The samples were cleaved into 5x5 mm sizes and adhered onto polymer film which is modified version of our ELO procedure, discussed in chapter 4. The thin polymer film was used as replacing standard wax carrier method used before. By using the thin polymer film provide upward force to lift the layer during etching. A solution of 30% HCl were used for etching the layer from substrate. The substrate will fall down when the etching is completed, and the thin film sticks onto the polymer film floated on the solution. The lifted layer is carefully taken from the etching solution and rinsed in deionised (DI) water

and dried by using compressed nitrogen gas. A clear wax is used to coat the exposed semiconductor layer. The clear wax is easier to see the structure on the film and when transferred to glass plate with structural rigidity. The layer was transferred to glass plate using water as medium to stick by giving a small pressure on top of the wax for 6-12 hours. Wax is removed by dipping in acetone for 5 minutes. Same steps were repeated for each lifted layer and layers stacked on top of each other. Figure 6.1 shows the pictorial representation of ELO process in GaAs (211) B substrate.

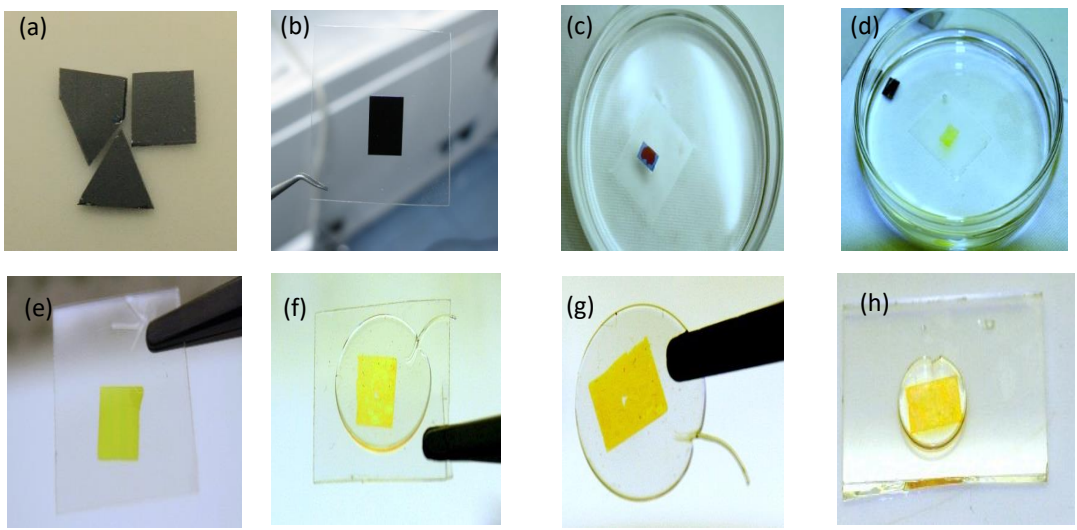

Figure 6. 1: Pictures of Epitaxial lift off process (a) Cleaving (b) Thin film polymer (c) Etching (d)Substrate falls to bottom (e)Transfer to thin film (e) Separated layer on polymer film (f)Applied clear wax on exposed layer (g) Separated the layer from polymer film (h) Bonding to glass plate

ZB MgS reacts with HCl to form $MgCl_2$ and H_2S, both of which are water soluble up to high concentrations, whereas etch rates of ZnSe and ZnCdSe layers are very slow in HCl [8]. The etch rate of MgS on GaAs (100) is approximately 3 mm/hour, much faster compared to the etch rate of AlAs 0.5mm/hour release layer which is used in comparable GaAs/AlGaAs devices [9]. Figure 6.2 shows the microscopic view of ELO lifted-off layers from GaAs (100) and (211) B substrates bonded onto glass plates after etching the

MgS sacrificial layer. The lifted layers were crack free for a square millimetre area shown in Figure 6.2.

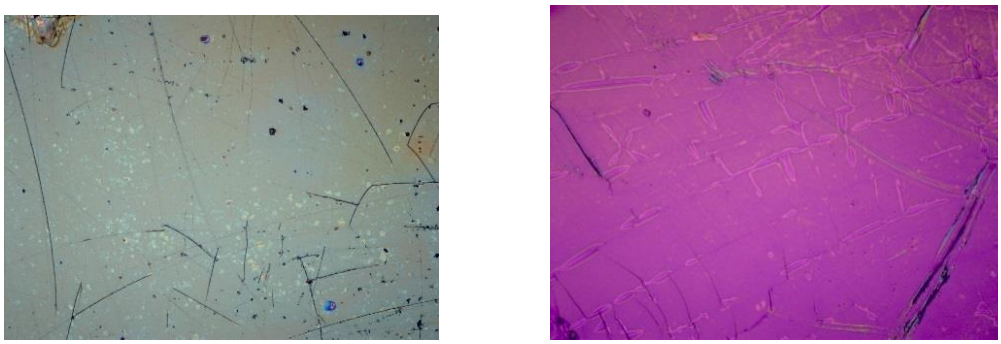

(a) (b)

Figure 6. 2: Microscope image of ELO layers transferred onto glass plates from (a) GaAs (100) and (b) (211) B substrate.

The thickness of each ELO layer on the glass plate was measured by DEKTAK thickness profiler and shown in Figure 6.3. The linear increase in the thickness of each layer has an error of ±10% and as such is not overly accurate, however demonstrates that the layers have stacked successfully. Thickness of 4 stacked 5µm ZnSe layer on glass plate were measured by using a DETAK thickness profiler. A linear increase in thickness was seen with each stacked layer with error of ±10%. The layers were stacked staggered to each other to create steps for the thickness measurement.

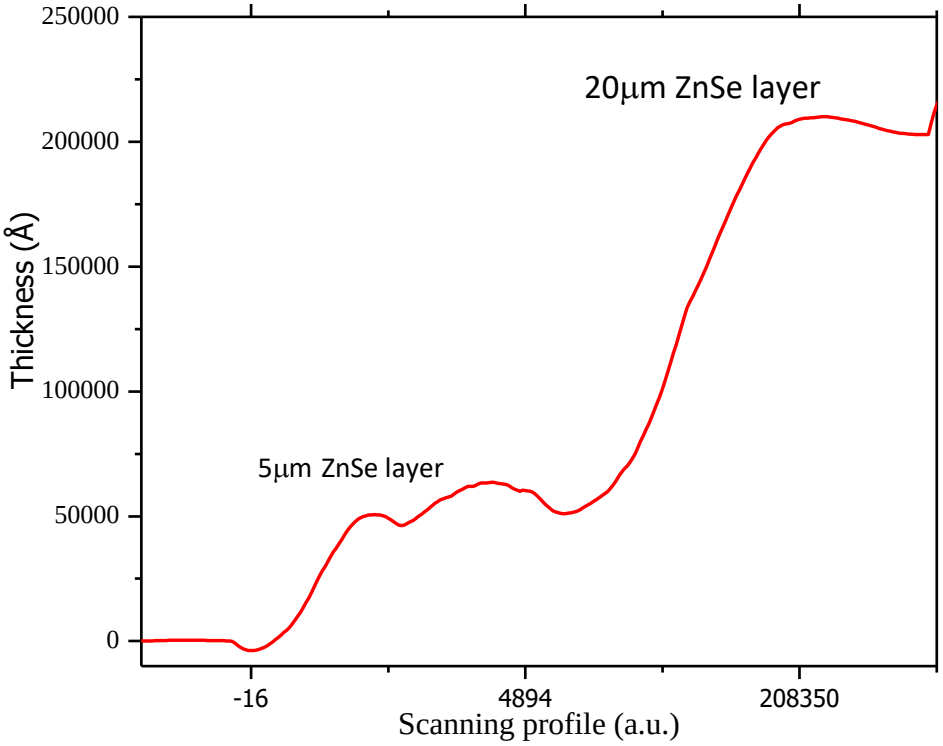

Figure 6.3: Thickness measurement taken by DEKTAK thickness profiler. Red line indicates total structural thickness after each additional layer. The stacked layers were positioned off axis to each other to allow for a step to be made specifically for this measurement.

6.4 Epitaxial lift-off PL results

Figure 6.4 and 6.5 show the typical PL spectra at 77 K of a GaAs (100) and (211) B sample containing 1 µm thick ZnSe before and after lift-off and being bonded onto a glass plate. For 100 sample, the PL peak emission is at 2.79 eV before lift-off and 2.77 eV after lift-off. For 211B sample, the PL peak emission of 2.78 eV has been obtained before lift-off, whilst after lift-off, the peak emission shifted to 2.79 eV. The full width half maximum (FWHM) has been calculated for both samples before and after lift-off. Before lift-off, FWHM was 20 meV for 100 and 25 meV for 211B, whilst after lift-off it was 32 meV for 100 and 34 meV for 211B. More detailed PL results of ZnSe/ZnCdSe/ZnSe QW and bulk ZnSe layers grown on (100) and (211) B substrates are shown in Table 6.1. PL peak

positions shift before and after lift-off, indicating the change in strain within the layer, possibly caused by the wax, the lift-off process or bonding, which requires further investigation. The broadening of FWHMs after ELO can be due to the damage during ELO process. However, FWHMs for 100 and 211B samples with the same structure are comparable to each other suggests no obvious degradation in optical quality after ELO.

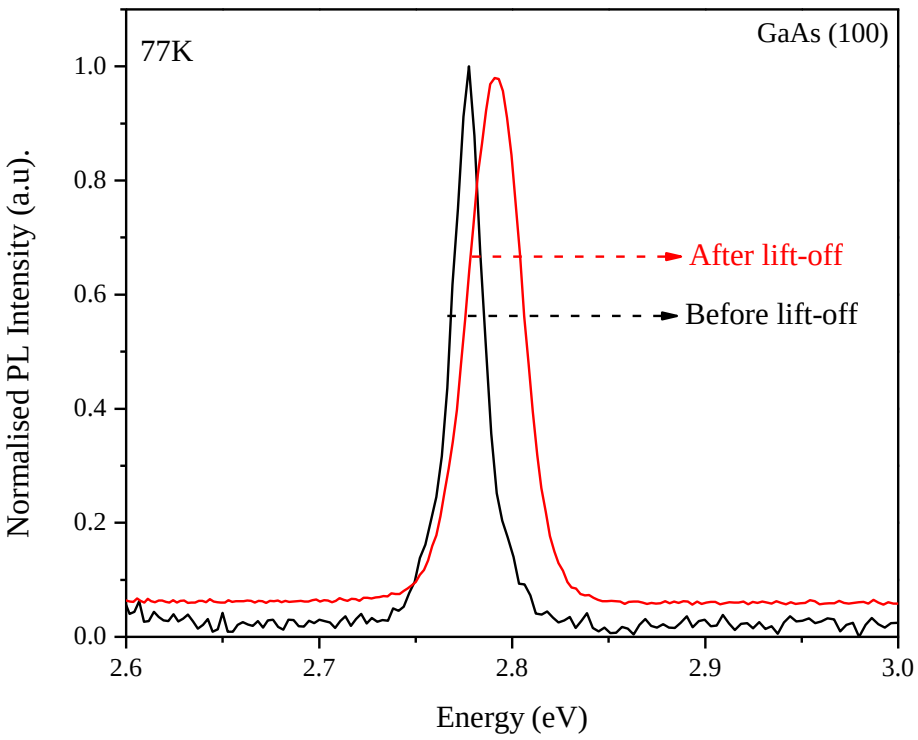

Figure 6. 4: Normalised PL intensity as a function of energy of a 1 µm ZnSe layer grown on GaAs (100) substrate at 77 K before and after ELO.

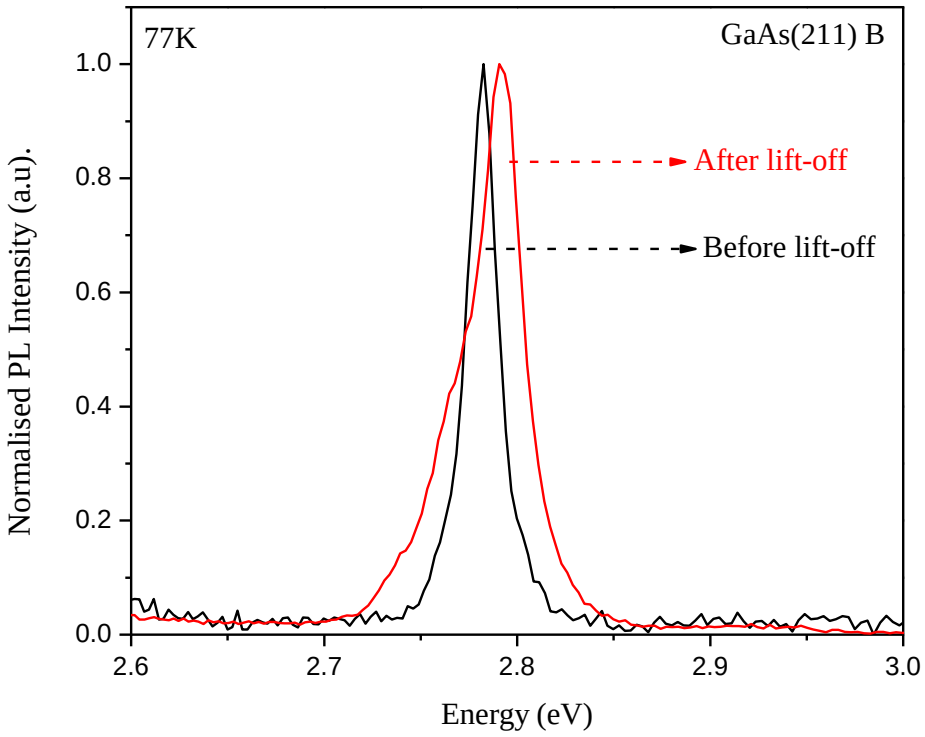

Figure 6.5: Normalised PL intensity as a function of energy of a 1 µm ZnSe layer grown on GaAs (211) B substrate at 77 K before and after ELO.

Sample	Orientation	Structure	PL peak position before ELO (eV)	PL peak position after ELO (eV)	FWHM of PL before ELO (meV)	FWHM of PL after ELO (meV)
HWC 672	(100)	QW	2.35	2.41	38	36
HWC 673	(211) B		2.46	2.49	64	100
HWC 733	(100)	ZnSe bulk layer	2.77	2.79	20	32
HWC 689	(211) B		2.78	2.79	25	34

Table 6. 1: PL results for 1 µm ZnSe and single QW grown on GaAs (211) B and (100) substrates.

6.5 ELO of ZnCdSe PL spectrum

Figure 6.6 and 6.7 show the typical PL spectra at 77 K of a GaAs (100) and (211) B sample containing ZnCdSe QW before and after lift-off and being bonded onto a glass plate. The increase in the FWHM for the (211) QW structures compared to the (100) can arise from a number of differing effects such as fluctuations in well thickness arising from interlayer roughness, alloy broadening and the inbuilt piezo field in (211) layers.

PL peak positions shift after lift-off, indicating a small change in strain within the layer, possibly caused by the wax used during the lift-off process or strain introduced during bonding, which requires further investigation. By measuring the QW emission peak shift that arises after lift-off we can estimate any change in strain attributed to the lift-off process. For the (100) sample we found the strain to be 2.2×10^{-2} after the sample was lifted, whilst for (211) B sample, the strain was 1.13×10^{-2} The broadening of FWHMs after ELO may arise from strains introduced during the ELO process. The emission intensity from the (211) B samples were an order of magnitude lower than for the 100 samples, however these layers are not intended for light emission, so photon generation or recombination is not a crucial issue, while being single crystal ZB is the aim. The large increase in FWHM in the (211) B QW sample between the un-lifted and lifted layers is most likely due to an increase in dislocation density after lifting. It is seen that there is less strain after ELO of (211) B compared to 100 for identical systems this would imply that the strain energy has gone into generating more dislocations.

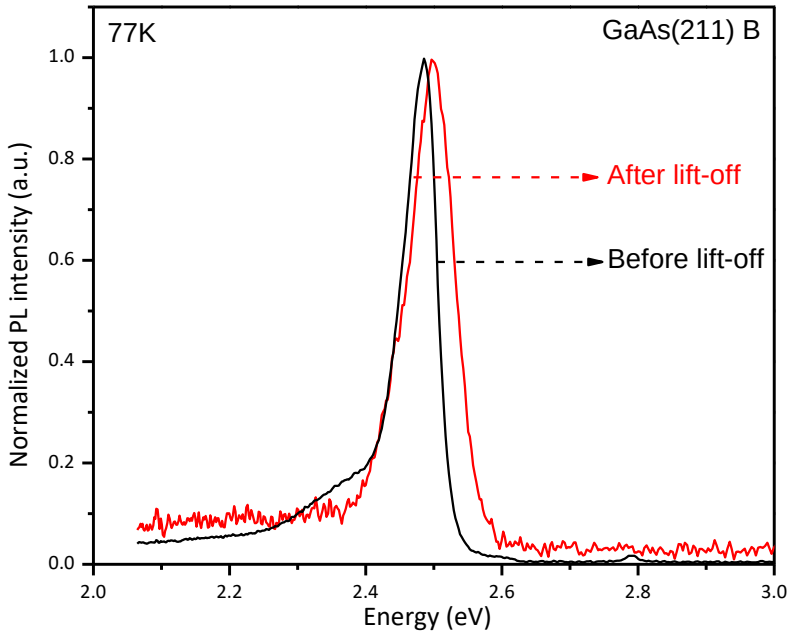

Figure 6. 6: Normalized PL intensity as a function of energy of ZnCdSe layer grown on GaAs (211) B substrate at 77 K before and after ELO.

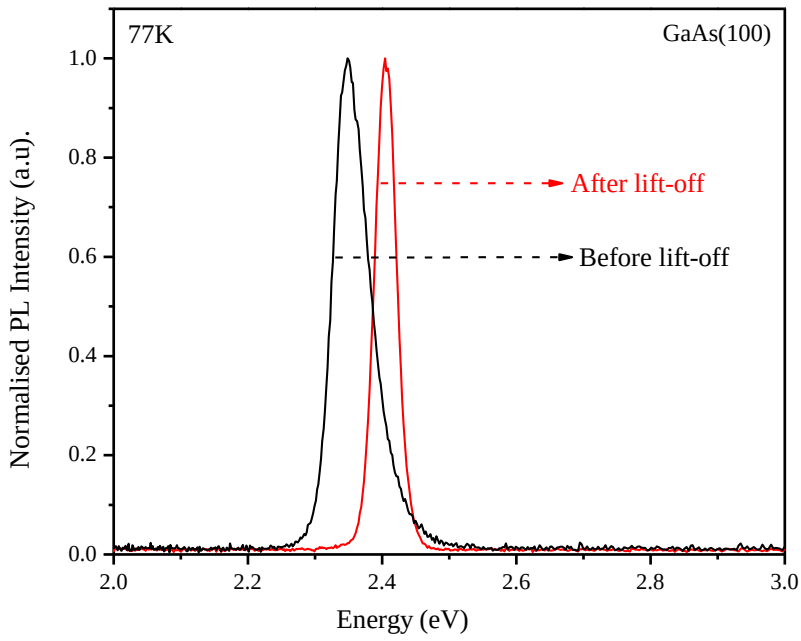

Figure 6. 7: Normalized PL intensity as a function of energy of ZnCdSe layer grown on GaAs (100) substrate at 77 K before and after ELO.

6.6 PL of stacking multiple ZnSe layers

PL measurements were taken at 77k before and after stacking multiple lift-off layers of 1µm ZnSe layer grown on 211 B substrate with same excitation power (95mW) and integration time (10s) shown in Figure 6.8. There is shift in the peak position of x5 stacked layer compared with the peak position of before lift-off which can be arise due to differing effects such as change in small degree during stacking of lifted layer, stress caused during the lift off and inbuilt piezo field in (211) layers. FWHM of x5 stacked layer was found 27 meV and before lift-off was found 23 meV which arise due to the stress obtained from wax during the lift- off process. FWHMs of 5x stacked layer and before lift-off are comparable to each other. The main aim of the stacked layers is to show single crystal ZB structure, not intended for light emission, so photon recombination is not a crucial issue.

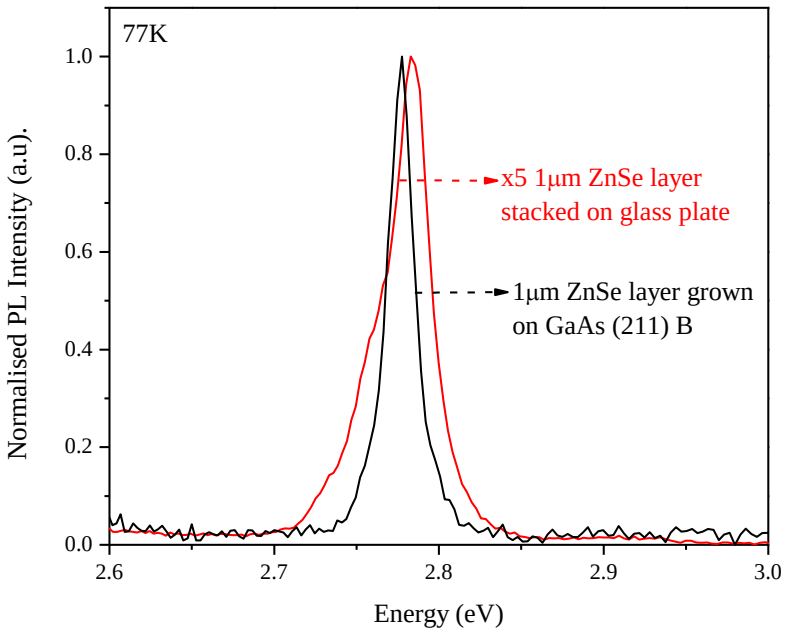

Figure 6. 8: PL spectra of x5 ZnSe (1 µm) layer stacked on glass plate compared with PL of ZnSe (1 µm) layer in GaAs (211) B substrate. FWHM of stacked layer is large due to the strain effect during lift off**.**

6.7 Discussion

The increase in the FWHM for the (211) QW structures compared to the (100) can arise from a number of differing effects such as fluctuations in well thickness arising from interlayer roughness, alloy broadening and the inbuilt piezo field in (211) layers. The PL emission intensity from the 211B samples were an order of magnitude lower than for the 100 samples, however these layers are not intended for light emission, so photon generation or recombination is not a crucial issue, while being single crystal ZB. The large increase in FWHM in the 211B QW sample between the un-lifted and lifted layers is most likely due to an increase in dislocation density after lifting. It is seen that there is less strain after ELO of 211B compared to 100 for identical systems this would imply that the strain energy has gone into generating more dislocations. This however would require further study to determine.

6.8 Conclusion

In conclusion, we have presented here for the first time that ELO layers of bulk (211) ZnSe layers can be stacked into new structures while maintaining its crystal quality. When strained layers are grown on low symmetry surfaces such as (211), there is a large polarization field due to the internal piezoelectric effect. Also, there is a refractive index dependence for transmitted light related to the surface orientation of the epilayer which is the focus of the current work on (211) oriented layers. This process demonstrates that ELO has the potential for creating previously unobtainable structures. As we have demonstrated that these layers can be effectively stacked upon each other, future work will involve optical studies to examine this technique's viability to create NLO structures.

REFERENCES

[1] A. Balocchi, A. Curran, T. Graham, C. Bradford, K. A. Prior and R. J. Warburton, "Epitaxial lift off of ZnSe-based heterostructures using a II-VI release layer," Applied Physics Letters, vol. 86, p. 011915, 2005.

[2] S. A. Telfer, G. Horsburgh, J. S. Milnes, C. Morhain, P. J. Thompson, K. A. Prior and B. C. Cavenett, "Growth of ZnSe and ZnCdSe on (211)B GaAs substrates," Journal of Crystal Growth, vol. 184/185, pp. 51-56, 1998.

[3] P. Demeester, I. Pollentier, P. D. Dobbelaere, C. Brys and P. V. Daele, "Epitaxial lift-off and its applications," Semiconductor Science and Technology, 1993.

[4] C. Bradford, A. Curran, A. Balocchi, B. C. Cavenett, K. A. Prior and R. J. Warburton, "Epitaxial lift-off of MBE grown II–VI heterostructures using a novel MgS release layer," Journal of Crystal Growth, pp. 325-328, 2005.

[5] R. Haidar, P. Kupecek, E. Rosencher, R. Triboulet and P. Lemasson, "New mid-infrared optical sources based on isotropic semiconductors (zinc selenide and gallium arsenide) using total internal reflection quasi-phase-matching," Opto-electronics Review 11, vol. 2, pp. 155-160, 2003.

[6] J.-i. Maeda, Y. Sasaki, N. Dietz, K. Shibahara, S. Yokoyama, S. Miyazaki and M. Hirose, "High-rate GaAs epitaxial lift-off technique for optoelectronic integrated circuits," Japanese Journal of Applied Physics, vol. 36, pp. 1554-1557, 1997.

[7] S. Y. Wang, P. J. Thompson, G. Horsburgh, T. A. Steele, G. D. Brownlie, K. A. Prior and B. C. Cavenett, "Piezoelectric effect in ZnSe/ZnCdSe quantum wells grown on (211) B GaAs," Journal of Crystal Growth, vol. 159, pp. 459-462, 1996.

[8] S. Subbanna, H. Kroemer and J. L. Merz, "Molecular-beam-epitaxial growth and selected properties of GaAs layers and GaAs/(Al,Ga)As superlattices with the (211) orientation," Journal of Applied Physics, vol. 59, no. 2, pp. 488-494, 1986.

[9] J. S. Milnes, C. Morhain, S. A. Telfer, W. Meridith, T. A. Steele, K. A. Prior and B. C. Cavenett, "A spectroscopic study of the piezoelectric effect in ZnSe/ZnCdSe single quantum wells grown on (211) B GaAs," Journal of Crystal Growth, 1998.

[10] A. Balocchi, A. Curran, T. C. Graham, C. Bradford, K. A. Prior and R. J. Warburton, "Epitaxial lift off of ZnSe-based heterostructures using a II-VI release layer," Applied Physics Letters, vol. 86, p. 011915, 2005.

[11] R. T. Moug, C. Bradford, F. Izdebski, A. Curran, J. Warburton, K. A. Prior, A. Aouni, F. M. Morales and S. I. Molina, "A comparison of ZnMgSSe and MgS wide bandgap semiconductors used as barriers: Growth, structure and luminescence properties," Journal of Crystal Growth, Vols. F. M. Morales, S. I. Molina, pp. 2099-2101, 2009.

[12] A. Rajan, R. T. Moug and K. A. Prior, "Epitaxial growth of zinc blend MgS directly on GaAs (001) substrates," Semiconductor Science and Technology, vol. 29, 2014.

[13] A. Rajan, R. T. Moug and K. A. Prior, "Growth and stability of zinc blend MgS on GaAs, GaP, and InP substrates," Applied Physics Letters, vol. 102, p. 032102, 2013.

[14] C. Bradford, C. B. O'Donnell, B. Urbaszek, A. Balocchi, C. Morhain, K. A. Prior and B. C. Cavenett, "Growth of zincblend MgS/ZnSe single quantum wells by

molecular beam epitaxy using ZnS as a sulphur source," Applied Physics Letters, vol. 76, pp. 3929-3931, 2000.

[15] B. Yarlagadda, A. Rodriguez, P. Li, R. Velampati, J. F. Ocampo, E. N. Suarez, P. B. Rago, D. Shah, J. E. Ayers and F. C. Jain, "X-ray characterization of dislocation density asymmetries in heteroepitaxial semiconductors," Applied Physics Letters, vol. 92, p. 202103, 2008.

This page intentionally left blank

CHAPTER 7

7.1 Conclusions

In the previous chapters, details of the growth, stability and processing of zinc blende (ZB) MgS based structure has been presented. Each chapter ended with a summary and detailed future work section. In this chapter collective results will be summarised and discussed. Despite having some very interesting properties such as ultra-wide bandgap and the lattice match to GaAs, the metastable ZB MgS has not found any attention-grabbing applications. Although the use of MgS as an efficient release layer in epitaxial lift off (ELO) has been demonstrated previously, this application is also limited largely with the fundamental research community. The main limiting factor for MgS not being used widely in real life structures was the inability to grow the ZB phase of MgS directly on a substrate. Similarly, the growth was limited to GaAs substrate-based structures because of the lattice match.

The main motivation for the experimental work detailed in this thesis was the potential advantages of ZB MgS in ELO. As explained earlier the main limiting factor was the restricted range of growth parameters. Most of this growth range has been exploited by various research groups resulting in failed attempts to grow the ZB phase either directly on GaAs substrate or any buffer layer other than ZnSe. Accordingly, growth of MgS was never attempted on lattice mismatched substrates, which was mainly due to the impression that the metastable phase is very sensitive to growth conditions.

The initial work on this project started with the growth of ZB MgS on GaAs (100) substrate. MgS has very large bandgap of ~5eV and so can form an excellent barrier material for wide band gap quantum structure. Unfortunately, its stable crystal structure is rocksalt and previous attempts to grow it in the ZB phase had met with limited success. A ZnSe buffer layer of 10 nm was grown before the deposition of MgS layer. The growth

of ZB MgS using a ZnS compound source as the only source of sulphur has enabled us to increase the maximum thickness grown to date by over an order of magnitude without any degradation of crystal quality.

In chapter 3, the surface analysis of ZB MgS is studied using RHEED. The RHEED measurements were taken at different growth temperature ranging from 160-310°C. From the RHEED observations shown in table 3.1, the growth temperature for MgS is identified as 240°C. All the growth parameters are kept constant during the growth of MgS layer. A (2x1) RHEED pattern observed during the growth of ZnSe buffer layer and changes to c(2x2) pattern when MgS growth starts. X-ray measurements were taken for all the samples and discussed in chapter 3. Also, the experimental scan was compared with BEDE RADS simulation software to measure the growth rate, composition and thickness of the grown structure. From the results, the growth rate of 0.36Å/s for MgS and 0.85Å/s for ZnCdSe are identified.

Following this work discussed the application of the MgS growth-based ELO of single ZnCdSe QW layers. ZB MgS was successfully performed on GaAs (100) substrate. In chapter 4, the lift-off of epitaxial layers and stacking of multiple layers top on each other is demonstrated. For this experiment single and triple QW structures were grown using MBE fabrication technique. The single QW layers were lifted off from the substrate and stacked 3x single QW layers onto a glass plate. Single QW and triple QW grown structures in MBE were then compared with 3x stacking single QW layer on glass plate. PL measurements were taken for all samples before and after lift-off at room temperature and 77K. From PL spectra, there is no emission from barrier layer which shows the exciton confinement quantum well dominant. Also, there is increase in the PL emission from 3x stacked layer compared with as grown triple QW layer in MBE. This shows ELO layers can design many layers on top of each other without any degradation of structural quality.

The stacking of ELO layers shows less shift in the PL peak position indicating less strain between the stacked layers. These stacked layers were gone through on many temperature cycles and still there is no PL peak shift, indicates this process can be used to fabricate devices which are not physically possible using fabrication technique. To explore the possibilities of ELO layers other than in GaAs (100) substrate.

The growth of ZB MgS on GaAs (211) B substrate introduced for first time. There are has been previous studies of II-VI material grown on GaAs (211) B substrate and it was found when strained layer grown on low symmetry surface such as 211 can induce internal piezo electric effect due to large polarisation field. The chapter 5 introduces the growth of ZB MgS on GaAs (211) B substrate for ELO technique. The substrate preparation and RHEED mesurement during oxide desorption were investigated before the MgS growth. It has found that oxide desorption temperature for (211) B substrate is 20°C higher than (100) substrates.

Both GaAs (100) and GaAs (211) B substrates were grown on same day to compare the quality of grown structure. For both substrates, ZnSe buffer layer of 10 nm were grown before the MgS growth. During this study, the growth conditions have been optimised such that the quality as judged by XRD and PL, is comparable to that of (100) epilayers. There is no phase transition in MgS grown on both (211) and (100) substrate. After that the successful growth of ZB MgS layer on GaAs (211) B substrate, the grown samples were done lift-off using ELO technique, explained detail in chapter 6. PL measurements were taken before and after lift-off.

For the first time that ELO layers of bulk (211) ZnSe layers can be stacked into new structures while maintaining its crystal quality. The PL measurements of the bulk layers after lift-off found increase in the FWHM which might be due to the surface roughness,

alloy broadening and the inbuilt piezo field in (211) layers. The strain induced in these layers can also results in the peak shift of the layers after lift-off.

7.2 Future work

More structural characterisation is required for this technique and in the future, to obtain some XRD measurements of the stacked layer. In this study, as the layers were stacked on glass this was not feasible, but the process can be repeated on GaAs to demonstrate structural integrity of each stacked layer.

One area we hope to investigate further in the future is the electrical properties of the stacked layers. As these appear to be chemically bonded there is the possibility that charge can flow between layers and therefore some electrically driven devices could be fabricated. Using II-VI material as a surface passivation layer is one area we hope to explore, and this will provide us with the first set of current-voltage measurements for the lifted layers.

Study the relaxed and strained properties of stacked layers by changing the design of the QW structure. Compare the different quantum well layers grown in MBE with stacked layers to find out the difference in optical and electrical properties.

ELO technique can increase productivity by scaling up to the full wafer of 2-inch substrate and stack on to different surface. A modification in the ELO technique is required to increase the sample size which can etch the layers faster and reduce the stacking time of each layer. Thus, it can stack more layers in short time and reuse the substrate. This process can be applicable in commercial production of devices.